The University of Liverpool

Faculty of Science

Department of Chemistry

THE ELECTROCHEMISTRY OF METAL NANOCLUSTERS AT THE WATER-1,2-DICHLOROETHANE INTERFACE

Thesis submitted in accordance with the requirements of the University of Liverpool for the degree of Doctor of Philosophy

by

Deirdre M. Coleman

SEPTEMBER 2002

I hereby declare that this submission is my own work and that, to the best of my knowledge and belief, it contains no material previously published or written by another person nor material which to a substantial extent has been accepted for the award of any other degree or diploma of a university or other institute of higher learning, except where due acknowledgement is made in the text.

Deirdre Coleman

TABLE OF CONTENTS

Acknowledgments

Firstly, I would like to sincerely thank both of my supervisors; David for giving me the opportunity to work in his research group and for his generous support, Riikka for many her many helpful suggestions and her motivating presence at times when my mind was on other things.

The financial support of the European Commission, ODRELLI network, is gratefully acknowledged.

Thanks to Drs. Henrik Jensen and David Fermin for their assistance with optical measurements, during a successful and highly enjoyable trip to Lausanne in August 2001. Also, to Dr. Simon Higgins for the redox couples used in Chapter 4 and for useful discussions.

I would like to thank my friends and colleagues, who made my time in Liverpool so interesting and enjoyable. In particular, I would like to acknowledge the support I have received in the last three months. I must especially thank Miss Georgina Hardy, Mrs. Frances Poole, Dr. Bernadette Quinn and Dr. Robert Wilson, for their unlimited help, advice and friendship.

Finally, I thank my mother, my father, Michelle and Brendan for everything.

The University of Liverpool

Faculty of Science

Department of Chemistry

THE ELECTROCHEMISTRY OF METAL NANOCLUSTERS AT THE WATER-1,2-DICHLOROETHANE INTERFACE

by Deirdre Coleman

ABSTRACT

The main aims of this project were to produce nanoclusters at the interface between two immiscible electrolyte solutions (ITIES) via a heterogeneous electron transfer (ET) reaction and to examine the possibility of charge transfer reactions with these clusters, in a two-phase system. In order to do this it was first necessary to gain an 7understanding of the general features associated with simple ET processes at these interfaces.

One of the problems associated with the study of ET at the ITIES is the limited number of suitable redox couples available; particularly redox couples soluble in the organic phase. This problem was addressed using 6-coordinate Ru(II) complexes. The ET reactions at the ITIES and at a metal electrode electrolyte interface were probed using electrochemical techniques. Simple, quasi-reversible, heterogeneous ET was observed between these complexes and the hexacyanoferrate couple in the aqueous phase, the rate of which was much slower than at the metal electrode-electrolyte interface. This is related to the increased distance between the redox species at the ITIES. Kinetic and thermodynamic parameters were related to the degree of accessibility of the redox centre.

The nucleation and growth of transition metal nanoclusters at the ITIES, as a consequence of ET to metal ions in the aqueous phase, was investigated using both electrochemical and spectroelectrochemical techniques. It was shown that, with careful choice of the experimental conditions, the potential controlled deposition of Hg, Au, Pt and Ag clusters at the interface is possible. The potential step and voltammetric responses obtained show behaviour characteristic of nucleation at a solid electrode. Thus, a model derived for nucleation at a solid electrode was applied to Ag and Pt nucleation at the ITIES in order to determine particle size. The dimensions of the particles deposited are in the nanometer size range. The presence of a passivating ligand in the case of Ag nucleation caused its low reaction rate.

The behaviour of these clusters at the ITIES was examined using electrochemical and spectroelectrochemical techniques. It was also shown that they can be charged via an interfacial ET reaction and are thus capable of acting as electrocatalytic centres. Also the Ag nanoclusters absorb and scatter incident light strongly in the visible region of the spectrum.

Table of symbols and abbreviations

a_i	Activity of species i
A	Geometric area of electrode
AC/DC	Alternating/Direct current
aq	Aqueous phase
C	Capacatance
c_i	Concentration of species i
CE	Counter electrode
CV	Cyclic voltammetry
D	Diffusion coefficient of the redox species
d	Diameter
DCE	1,2-dichloroethane
DCMFc	Decamethylferrocene
DCV	Differential cyclic voltasorptometry
DMFc	Dimethylferrocene
E	Electrode potential
$E^o / E^{o'}$	Formal/Standard potential
$E_{1/2}$	Half wave potential
$E_{1/4}/E_{3/4}$	One-quarter/Three-quarter wave potential
EC	Electron transfer followed by a chemical reaction
E_{eq}	Equilibrium potential
EPR	Electron paramagnetic resonance
E_s	Potential of stripping peak
ET	Electron transfer
F	Faraday constant
Fc	Ferrocene
FIT	Facilitated ion transfer
ΔG	Free Energy change associated with a reaction
GC	Guoy Chapman Model of interface
HET	simple heterogeneous electron transfer
i	Current

I_L	Limiting current
I	Intensity of light
i_p	Peak current
i^s	Maximum current of stripping peak
ITIES	Interface between two immiscible electrolyte solutions
j	Current density
k	Boltzmann constant
k^0	Standard rate constant
L	Refers to ligands used in Chapter 4
I_{re}/I_{im}	Real/Imaginary components of current
M	Molecular weight
MCP	Monolayer protected clusters
m_o	Mass transfer coefficient
m_p	Mass of one particle
MVN	Modified Verwey and Niessen model of interface
N	Nuclear number density
n	the number of electrons transferred
O	Oxidised form of redox species
org	Organic phase
PET	Photoinduced electron transfer
PMR	Potential modulated reflectance
PTC	Phase transfer catalysis
Q_p	Charge of one particle
R	Gas Constant
r	Radius
RE	Reference electrode
rh	Effective hydrodynamic radius of the diffusing species
RLS	Resonant Light Scattering
SECM	Scanning electrochemical microscopy
SHE	Standard hydrogen electrode
T	Absolute temperature
t	Time from commencement of experiment
TBA	Tetrabutyl ammonium cation

TCNQ	Tetracyanoquinodiomethane
TDTFMPB	Tetrakis[di-3,5-triflouro-methylphenyl]borate
TIR	Total internal reflection
TPA	Tetraphenyl ammonium cation
TPAs	Tetraphenylarsonium cation
TPB	Tetraphenylborate anion
TPBCl	Tetraphenylborate pentachloride anion
$TPBF_5$	Tetraphenylborate pentafluoride anion
UV-VIS	Ultra violet and visible Absorption spectroscopy
V	Volume
VN	Verwey and Niessen model of interface
WE	Working electrode
x	Distance perpendicular to electrode surface
z	Charge on ion

α	Transfer coefficient/Polarisability
β	Electron tunnelling parameter
ϕ	Galvani potential
γ	Surface tension
η	Overpotential applied to electrode
λ	Dimensionless rate constant/Wavelength
μ	Microelectrode
ν	Potential scan rate
ρ	Density
σ	Polarisable interface between two electrolyte solutions
ω	Frequency

CHAPTER ONE

INTRODUCTION

1.1. Aims of the Project

The main area of interest for this thesis is the electrochemistry of metal nanoclusters at the interface between two immiscible electrolyte solutions (ITIES). The initial stages of nucleation and growth of transition metal clusters at the ITIES, and charge transfer phenomena involving nanoclusters in two-phase systems were investigated. Since the cohesive energy of a metal is much greater than that of a liquid, the ITIES provides an ideal substrate for the study of the electrochemical generation and behaviour of metal particles. Before investigating the electron transfer (ET) reaction leading to the formation of a new phase, the well-established theory and experimental approaches currently applied to simple ET in the two-phase system were considered in order to gain an insight into these interfacial processes.

Cyclic voltammetry was chosen as the main experimental method for the majority of this work due to its versatility. Potential step transients were also employed in the study of interfacial phase formation. In situ spectroscopic techniques coupled to cyclic voltammetry and potential step transients were used to investigate interfacial nucleation and growth reactions and properties of transition metal nanoclusters at the ITIES.

1.2. A Review of the Electrochemical Properties of the ITIES

The "interface between two immiscible electrolyte solutions" (ITIES) refers to the liquid | liquid interface formed when an aqueous and an organic solution, each containing an electrolyte, are contacted. The polarisability of the interface is dependent on the electrolyte in each phase. The "potential window" refers to the potential range for which there is no transfer of supporting electrolyte ions; its size is extended by use of hydrophilic and hydrophobic aqueous and organic supporting electrolytes, respectively. Within the potential window, it is possible to study charge transfer processes. Heterogeneous ET and simple ion transfer (IT) are the most widely studied charge transfer reactions occurring at the ITIES. However, since IT is not a redox reaction, its standard potential is not related to the standard hydrogen potential scale for redox reactions at solid electrodes.[1] In order to facilitate the comparison of experimental results and existing thermodynamic data, a common scale is required. This involves an extra-thermodynamic assumption such as the "TPATPB assumption", which assumes that the standard Gibbs energies of transfer of the tetraphenylarsonium and tetraphenylborate ions are equal for any pair of solvents.[2] Tables of standard transfer potentials of ions have been calculated based on this assumption

The study of charge transfer phenomena at the ITIES have recently attracted interest due to the fundamentally important nature of these processes in many areas of science, including photochemical energy conversion,[3,4] membrane science,[5-9] solvent extraction,[10-14] phase transfer catalysis (PTC)[15,16] and drug delivery.[17] When a barrier to the charge transfer is introduced between the electrolyte solutions,

the ITIES provides a relatively simple bio-mimetic model for the study of biological charge transfer reactions.[18] Finally, since the ITIES allows the study of heterogeneous charge transfers without the complication of surface defects,[19-21] that are typical of solid interfaces, the ITIES provides an ideal surface for the study of phase formation reactions in the absence of interactions with the substrate. This is one reason for the current interest in this system for the study of nanoparticle formation[22-24] and polymer growth.[25-27] Before the kinetics of these charge transfer processes can be considered, an understanding of the microscopic structure of the double layer region at the ITIES is required.

1.2.1. Structure of the double layer at the ITIES

The original model of electrochemical interfaces proposed by Guoy and Chapman (GC) was derived for the metal electrode | dilute electrolyte solution interface; ions were considered to behave as simple point charges and the solvent as a dielectric continuum medium. Based on these assumptions, the Poisson-Boltzmann equation was solved to give the relationship between potential and surface charge density. A modified model of electrochemical interfaces was introduced later on. This considered the interface to include an inner, ion-free layer, composed of highly orientated solvent dipoles, the Stern model.[28] In this model, ions from the base electrolyte could approach the electrode surface to within a certain distance (equal to their hydrated radius) without being specifically adsorbed or desolvated, but the possibility of specific interaction between ions and electrode giving rise to their specific adsorption it also considered.

At the ITIES, there exists an interfacial potential difference due to the partitioning of the ions of a salt between the phases. The first model proposed for the structure of the ITIES (the Verwey and Niessen (VN) model) involved the direct transposition of the GC model derived for the metal electrode | dilute electrolytic solution interface.[29] The electrical double layer was described as consisting of two non-interacting, back-to-back diffuse layers located at either side of the interface. Analysis of the potential dependence of IT kinetics led to a formalism similar to the Butler-Volmer equation for ET at the metal electrode | electrolyte interface.

The modifications proposed by Stern for the model of the metal electrode | electrolyte solution interface were also adopted for the model of the ITIES to give the modified Verwey and Niessen (MVN) model.[30,31] This model considered the interface to include an inner, ion-free layer, composed of highly orientated solvent dipoles, present between two diffuse layers. The potential drop across this ion-free layer is an important parameter in the analysis of the rate of charge transfer across the interface.

The structure of the interfacial layer is a matter of much debate, but the existence of an inner mixed solvent layer whether with[32,33] or without,[34-39] interfacial ion pairing between ions from each adjoining phase is most reasonable. The existence of a mixed solvent layer where ions can penetrate, separating the diffuse layers has also been proposed.[40] The molecular behaviour of the liquid | liquid interface has recently been described using Monte Carlo simulations, suggesting that the interface, although molecularly sharp, possesses thermally fluctuating capillary wave-like distortions.[41] Long-time averaging (several picoseconds) results in a relatively

smooth interface.[42] The "mixed solvent region" theory for describing of the ITIES seems reasonable when the fact that the two solvents forming the interface have a certain, albeit limited, solubility in the other is considered.

The structural model of the interface is simplified when a high ionic strength is present in the aqueous phase, since the aqueous diffuse double layer can be neglected[34] and the interface can be considered to consist of a boundary on the aqueous side formed by the termination of the concentrated aqueous electrolyte.

1.2.2. Charge Transfer

While the first electrochemical study of the ITIES was made in 1902,[43] it was not until ca. 1970 that it was established that this type of interface could be polarised and that the Galvani potential difference between the two phases could be used as a driving force for charge transfer reactions.[44,45] The development of a four electrode potentiostat[46] and the concept of a polarisable interface based upon the standard free energy of IT[47] allowed charge transfer reactions to be studied at the ITIES using modern electrochemical techniques.

As already mentioned, two general categories of heterogeneous charge transfer processes occur at the ITIES, IT and ET. (It should be noted that these two processes can affect each other.) Conventional electrochemical techniques such as cyclic voltammetry,[16,48-53] convolution potential sweep voltammetry,[51] current scan polarography,[48,54,55] and ac impedance spectroscopy,[48,51,56-60] which are based

on the measurement of net charge transfer across the liquid | liquid interface, have been applied to the study of charge transfer phenomena. Since all these methods exhibit an inherent difficulty in discriminating between ET and IT and the accuracy of measurements are greatly affected by uncompensated iR-drop from the organic phase, there is some debate about the accuracy of kinetic parameters obtained using these techniques. In this respect, the advantages of using modern techniques such as scanning electrochemical microscopy (SECM)[61-65] and in situ spectroscopic,[66-72] have been discussed.

1.2.2.1. Ion Transfer (IT)

The transfer of an ion (i) from one phase to the other is accompanied by a faradaic current and can be described by:

$$i(aq) \mid i(org) \qquad (1.1)$$

where aq and org refer to the aqueous and organic phases respectively. The reaction is fast, ($k>10^{-2}$ cms^{-1} at macroscopic interfaces) diffusionally controlled and follows an heterogeneous first order rate law. Facilitated IT (FIT) occurs when the transfer of the ion is facilitated by the presence of an ionophore in the adjacent phase. The presence of the ionophore commonly shifts the ions' transfer potential to within the potential window by decreasing its Gibbs energy of transfer.[73-75]

1.2.2.2. Heterogeneous ET

Heterogeneous ET occurs when a redox couple located in one phase exchanges an electron with a redox couple located in the other phase. For a one-ET process the reaction can be written as:

$$R\,(aq) + O\,(org) \rightleftharpoons O\,(aq) + R\,(org) \qquad (1.2)$$

where O and R refer to the oxidised and reduced forms of the redox species. Reaction (1.2) is second order but analysis is simplified to pseudo-first order by the use of a concentrated solution of a fast redox couple in the aqueous phase.[16] This also means that ET theories, which regard the polar medium as a continuum,[76-79] can be applied, since the aqueous diffuse double layer can be neglected.[34] ET reactions are slower than IT reactions.[16] The reasons for this are the large separation between the redox species and the high reorganisation energies involved. Photoinduced ET (PET) occurs when a photo-excited species (sensitiser) in one phase exchanges an electron with a redox couple (quencher) in the other phase.

Much published work on charge transfer processes at the ITIES has concentrated on IT.[1] In order that ET reactions at the ITIES can be considered simple, the reactants and products of the redox reaction should not partition across the interface or transfer within the potential window, nor should they adsorb at the interface or react with the supporting electrolyte or solvent.[80] Finding an experimental system that meets all of the above criteria is difficult. The lack of an ideal system has meant that few ET systems have been systematically studied and this has led to a limited understanding of ET kinetics at the ITIES.

In one of the earliest examples of ET at the ITIES involving the reduction of a metal ion, it was reported that the application of a current across the liquid | liquid interface to an stable redox system, consisting of aqueous Cu(II) and hexacarbonylvanadate, led to the formation of a metallic film at the interface. Partitioning was not a problem, since the solubility of the redox couples in the adjoining phase was extremely low.[81]

Samec et al.[49,51,52,54,82] and Kihara et al.[55] studied the ET between the hexacyanoferrate couple in water and ferrocene in the organic phase using four electrode cyclic voltammetry (CV). It was concluded that while HET does occur between the two redox centres; the reaction is not ideal, since the ET response is complicated by factors including interfacial ion pairing and decomposition of ferricenium (the oxidation product of ferrocene) in the organic phase. While hexacyanoferrate is unlikely to partition to the organic phase due to its large Gibbs energy of hydration, transfer of the organic couple, or its oxidation product, may occur and affect the ET process. All of these factors made the accurate analysis of results difficult. In some cases, it was not even possible to distinguish between the two processes.[54] Later studies[48] of the same reaction, suggested that the ET reaction is complicated by the transfer of ferricenium to the water phase at negative potentials (IT-ET coupling). AC voltammetry studies of this system have been employed to study the kinetics of the HET process.[60,83]

It was recognised that the use of a more hydrophobic redox couple in the organic phase could solve the problem of coupled IT-ET. HET reactions were reported for

the hexacyanoferrate couple in contact with lutetium[16,60] and tin biphthalocyanines,[15] tetracyanoquinodiomethane (TCNQ),[8,55,60] metalloporphyrins[53] and tetrathiafulvate.[55] ET-IT coupling has been investigated.[48,84] The lutetium biphthalocyanine-hexacyanoferrate system gave the first evidence of true (un-coupled) ET across inhomogeneous media.[16] The extremely hydrophobic nature of this high molecular mass compound makes coupling of IT and ET highly unlikely. The effect of increasing the hydrophobicity of the organic redox couple was studied systematically using substituted ferrocences.[48] However, in this case, experimental complications involving the supporting electrolyte, meant that use of a more hydrophobic redox couple did not have the desired effect on the ET-IT coupling problem.

As already suggested, the choice of supporting electrolyte can have a major effect on the ET process. Alternative anions including tetrakis[di-3,5-triflouromethylphenyl]borate (TDTFMPB) and tetrakis[pentafluorophenyl]borate ($TPBF_5$) were considered by Stewart et al.[85,86] Tetraphenylborate (TPB) and tetrakis[4-chlorophenyl]borate (TPBCl) are most commonly used, since they give a reasonably large potential window. However, much evidence now exists to suggest that the tetraphenylborate (TPB) anion is problematic including. For instance, it can be oxidised by permanganate,[55] or by ferrocene derivatives;[48] it has also been reported that TPAsTPBCl is prone to photodecomposition.[23,87] More recently, similar complications have been avoided by use of the fully fluorinated tetraphenylborate, which is much more difficult to oxidise.[24,88]

The hexacyanoferrate couple has been used widely as aqueous redox species for several reasons,; it is soluble at high concentrations, it undergoes outer sphere ET, both components of the couple are commercially available, it is relatively stable and it has a large Gibbs energy of hydration. The fact that this couple has been so widely used in ET studies facilitates comparison between systems but other aqueous redox couples have also been considered.[55]

The interfacial potential, at a liquid/liquid interface can be controlled electrochemically by applying an external potential,[15,79] or chemically, by use of partitioning ions or of a "phase transfer catalysis" (PTC). PTC is extensively used in organic synthesis and for the preparation of metallic nanoparticles.[89] The influence of the phase transfer catalysis has been comprehensively studied by Cunnane et al.[15] These authors demonstrated that the role of the PTC is to fix the interfacial Galvani potential difference and hence, establish the conditions necessary for ET reactions to take place. An heterogeneous system consisting of hexacyanoferrate and tin diphthalocyanine was employed to demonstrate this principle and spectroscopic techniques were used to monitor the reaction.

1.3. Phase Formation at the ITIES

The two-phase reduction of Au ions by sodium borohydride in the presence of a thiol and a PTC, first introduced by Brust et al.[89] is now commonly employed for the preparation of transition metal particles. Recently, surface modified Ag particles have been formed at the ITIES by use of a PTC and a subsequent homogenous EC process in the organic phase.[90]

Interfacial phase formation at a liquid | liquid interface as a consequence of a HET reaction at the ITIES was demonstrated for Cu deposition in 1975.[81] More recently, Au[23] and Pd[24,91] particles have been deposited at the ITIES by the application of a suitable interfacial Galvani potential difference (or current)[91] to the system consisting of a redox couple in one phase and a metal ion in the other phase. The advantage of using electrochemical techniques to prepare metal colloids is that the supersaturation can be controlled by the applied interfacial potential, whereas in conventional chemical synthesis control of the reaction rate is difficult. The basic theory for nucleation and growth of a metal at the ITIES have been shown to be essentially the same[24] as that for the same process at a metal electrode | electrolyte interface, i.e. any nucleus exceeding the critical size will grow under diffusion control.[92,93] However, due to the nature of the electrode surface (i.e. the ITIES) the system offers some advantages over the metal electrode | electrolyte interface for the study of the nucleation phenomena. For example, the cohesive energy between the newly formed substrate and the interface is much less that that with a metal and the

ITIES is free from defects, which act as preferential nucleation centres. In these respects, the ITIES is considered to be a "soft interface".[94]

Analysis of the nucleation and growth reaction at the ITIES is complicated by the fact that diffusion of both species to the interface must be considered, since neither couple is present in excess. Theoretical aspects of the reaction have been addressed and a nucleation and growth model for the ITIES based on the models derived for the reaction at the metal electrode | electrolyte interface has been derived.[24,91] Interestingly, Johans et. al. concluded, from a consideration of thermodynamic theory, that small particles do not remain at the interface after formation but migrate into solution.[94] The use of growing particles at the interface as a catalyst has been considered.[95]

Another example of a HET reaction leading to phase formation at the ITIES is the production of polymers.[26,27]This reaction involved a HET coupled to an EC mechanism and these authors noted also that the mechanism for the growth of the polymer differed from that observed at a metal electrode.

1.4. In situ Spectroelectrochemistry at the ITIES

The incorporation of in-situ spectroscopic techniques with traditional electrochemical experiments[96-98] and at the ITIES[99] has proven both a popular and effective means of monitoring solution phase reactions. Typically, electrochemical perturbations are introduced and the system responses are monitored

spectroscopically. The speed at which optical responses can be recorded enables more detailed examination of fast processes and the high resolution of these techniques allows the observation of the early stages of the formation of a species.

Unlike electrochemical techniques, the spectroscopic response is specific to the faradaic processes and as a result is less sensitive to iR-drop and double layer effects. Thus, potential modulated spectroscopic techniques can be used to help differentiate between interfacial processes e.g. IT and adsorption or ion-pair formation. Since charge transfer reactions across the ITIES depend highly on these features, this type of information can be used to obtain a more complete understanding of the mechanisms of interfacial reactions.

Chronoabsorptometry and differential cyclic voltoabsorptometry (DCV), carried out in the absorption mode,[72,100,101] and potential modulated reflectance (PMR) spectroscopy,[102-104] which is carried out in the total internal reflectance (TIR) mode, have successfully been applied to the study of charge transfer processes at the ITIES.

For measurements made on the TIR mode, an incident beam is reflected by the interface and the reflected signal is collected. DCV involves the superimposition of a sinusoidal potential signal to a constant dc signal, while chronoabsorptometry involves the application of a potential step to the system and the absorption transient for each is recorded as a function of time. The change in the light intensity reflected from the ITIES due to the absorption of transferring species for IT, or the formation of products for ET, is the fundamental basis for these techniques. PMR involves the

superimposition of a sinusoidal potential signal to a constant dc bias and the reflectance signal is measured at the frequency of ac perturbation. The use of spectroelectrochemistry as a technique to probe charge transfer phenomena at ITIES has been reported for differential cyclic voltfluorometry (DCV),[105] fluorescence[106,107] and in situ electron paramagnetic resonance (EPR) spectroscopy.[69,99]

In situ spectroelectrochemistry techniques have been generally applied to the study of adsorption and IT processes. It was demonstrated that, despite a reversible electrochemical response for fluorescence dyes at the ITIES, dynamic spectroscopic measurements revealed that adsorption processes also take place.[104] The adsorption properties of at the interface were studied by PMR spectroscopy and a potential dependent adsorption process was revealed. From the combined electrochemical-spectroscopic data, these authors suggested that specific adsorption of ions does not necessarily involve interfacial ion pairing as was previously suggested.[40,60]

A similar approach based on the identification of the reaction products generated by a HET process is possible. Ding et al. studied the ET between hexacyanoferrate in the aqueous phase and TCNQ and dimethylferrocene (DMFc) in the organic phase, whereby the generation of products was monitored using in situ UV-VIS spectroscopy. This approach allowed thermodynamic and kinetic information to be obtained.[72,108]

It was previously demonstrated that the growth of a metal film at the liquid | liquid interface could conveniently be followed by non-invasive spectroscopic techniques using transmission UV-VIS spectroscopy[23] and ellipsometry for Au.[109] This approach is possible since colloidal solutions of many transition metal particles absorb strongly in the visible region,[110] due to the excitation of surface plasmon resonances. The optical properties of particles vary with size, symmetry and how close the particles are to each other. An understanding of the kinetics and mechanism of in situ particle formation would undoubtedly provide useful mechanistic information.

1.5. Properties of Nanoparticles

Metal colloids (d >10 nm) have been known since the time of Faraday, but have recently become the focus of intense interest due to their "unusual" properties. The properties of these particles are unlike those of either bulk metal or of the atomic state. The reason for this is that a large percentage of a nanoclusters' atoms lie on the surface and these surface atoms do not necessarily order themselves in the same way as those in the bulk state. As a result, their electrons are confined to a small space, giving rise to quantum size effects.[111]

Since the particles properties are dependent on their size, composition and shape, one of the most immediate goals in this area is the development of methods to achieve a reproducible synthesis of clusters of a predetermined size, composition and shape. Traditionally, chemical methods are used for the synthesis of particles. These methods provide reasonably monodisperse particle syntheses. However, as these are purely chemical reactions, the reduction rate is difficult to control.

1.6. References

(1) Girault, H., Schiffrin, D.J. *Electroanalytical Chemistry*; Marcel Dekker: New York, 1989.

(2) Parker, A. J. *Electrochim. Acta.* **1976**, *21*, 671.

(3) Lahtinen, R. M.; Fermin, D. J.; Jensen, H.; Kontturi, K.; Girault, H. H. *Electrochem. Commun.* **2000**, *2*, 230-234.

(4) Lahtinen, R.; Fermin, D. J.; Kontturi, K.; Girault, H. H. *J. Electroanal. Chem.* **2000**, *483*, 81-87.

(5) Cheng, Y. F.; Cunnane, V. J.; Kontturi, A. K.; Kontturi, K.; Schiffrin, D. J. *J. Phys. Chem.* **1996**, *100*, 15470-15477.

(6) Kontturi, A. K.; Kontturi, K.; Murtomaki, L.; Quinn, B.; Cunnane, V. J. *J. Electroanal. Chem.* **1997**, *424*, 69-74.

(7) Walker, R. A.; Gruetzmacher, J. A.; Richmond, G. L. *J. Am. Chem. Soc.* **1998**, *120*, 6991-7003.

(8) Cheng, Y. F.; Schiffrin, D. J. *J. Chem. Soc.-Faraday Trans.* **1994**, *90*, 2517-2523.

(9) Cunnane, V. J.; Schiffrin, D. J.; Fleischmann, M.; Geblewicz, G.; Williams, D. *J. Electroanal. Chem.* **1988**, *243*, 455-464.

(10) Wisniewski, M.; Szymanowski, J. *Anal. Sci.* **1998**, *14*, 241-245.

(11) Tomaszewski, L.; Lagger, G.; Girault, H. H. *Anal. Chem.* **1999**, *71*, 837-841.

(12) Barker, M. H. Ph.D., The University of Liverpool, U.K. 1999.

(13) Cheng, Y. F.; Schiffrin, D. J.; Guerriero, P.; Vigato, P. A. *Inorg. Chem.* **1994**, *33*, 765-769.

(14) Bustero, I.; Cheng, Y. F.; Mugica, J. C.; Fernandez-Otero, T.; Silva, A. F.; Schiffrin, D. J. *Electrochim. Acta* **1998**, *44*, 29-38.

(15) Cunnane, V. J.; Schiffrin, D. J.; Beltran, C.; Geblewicz, G.; Solomon, T. *J. Electroanal. Chem.* **1988**, *247*, 203-214.

(16) Geblewicz, G.; Schiffrin, D. J. *J. Electroanal. Chem.* **1988**, *244*, 27-37.

(17) Lemoult, S. C.; Cheng, Y.; Kontturi, K.; Schiffrin, D. J. *Electrochem. Commun.* **2000**, *2*, 244-247.

(18) Koryta, P.; Vanysec, M.; Bernzina, J. *J. Electroanal. Chem.* **1976**, *67*, 263.

(19) Girault, H. H. *Charge transfer across liquid liquid interfaces*; Plenum Press,: New York, 1993.

(20) Benjamin, I. *Chem. Rev.* **1996**, *96*, 1449.

(21) Eisenthal, K. B. *Chem. Rev.* **1996**, *96*, 1343.

(22) Bethell, D.; Brust, M.; Schiffrin, D. J.; Kiely, C. *J. Electroanal. Chem.* **1996**, *409*, 137-143.

(23) Cheng, Y. F.; Schiffrin, D. J. *J. Chem. Soc.-Faraday Trans.* **1996**, *92*, 3865-3871.

(24) Johans, C.; Lahtinen, R.; Kontturi, K.; Schiffrin, D. J. *J. Electroanal. Chem.* **2000**, *488*, 99-109.

(25) Evans, N. J.; Gonsalves, M.; Gray, N. J.; Barker, A. L.; Macpherson, J. V.; Unwin, P. R. *Electrochem. Commun.* **2000**, *2*, 201-206.

(26) Gorgy, K.; Fusalba, F.; Evans, U.; Kontturi, K.; Cunnane, V. J. *Synth. Met.* **2001**, *125*, 365-373.

(27) Cunnane, V. J.; Evans, U. *Chem. Commun.* **1998**, 2163-2164.

(28) Stern, O. *Z. Elektrochem* **1924**, *30*, 508.

(29) Verwey, E. J. W.; Niessen, K. F. *Phil. Mag.* **1939**, *28*, 435.

(30) Gavach, C.; Seta, P.; D'Epenoux, B. *J. Electroanal. Chem.* **1977**, *83*, 225-235.

(31) Gavach, C.; Seta, P.; D'Epenoux, B. *J. Electroanal. Chem.* **1977**, *83*, 25.

(32) Girault, H. H.; Schiffrin, D. J. *J. Electroanal. Chem.* **1983**, *150*, 43-49.

(33) Girault, H. H.; Schiffrin, D. J. *J. Electroanal. Chem.* **1983**, *150*, 43-49.

(34) Samec, Z.; Marecek, V.; Homolka, D. *J. Electroanal. Chem.* **1985**, *187*, 31-51.

(35) Samec, Z.; Marecek, V.; Homolka, D. *J. Electroanal. Chem.* **1981**, *126*, 121-129.

(36) Samec, Z.; Marecek, V.; Holub, K.; Racinsky, S.; Hajkova, P. *J. Electroanal. Chem.* **1987**, *225*, 65-78.

(37) Kakiuchi, T.; Senda, M. *Bull. Chem. Soc. Jpn.* **1983**, *56*, 1322-1326.

(38) Kakiuchi, T.; Senda, M. *Bull. Chem. Soc. Jpn.* **1983**, *56*, 1753-1760.

(39) Kakiuchi, T.; Senda, M. *Bull. Chem. Soc. Jpn.* **1983**, *56*, 2912-2918.

(40) Cheng, Y.; Cunnane, V. J.; Schiffrin, D. J.; Mutomaki, L.; Kontturi, K. *J. Chem. Soc.-Faraday Trans.* **1991**, *87*, 107-114.

(41) Benjamin, I. *Annu. Rev. Phys. Chem.* **1997**, *48*, 407-451.

(42) Strutwolf, J.; Barker, A. L.; Gonsalves, M.; Caruana, D. J.; Unwin, P. R.; Williams, D. E.; Webster, J. R. P. *J. Electroanal. Chem.* **2000**, *483*, 163-173.

(43) *Ann. Phys.* **1902**, *8*, 600.

(44) Gavach, C.; Mlodnicka, T.; Gustalla, J. C. R. *Acad. Sci.* **1968**, *266*, 196.

(45) Gavach, C.; Henry, F. *C. R. Acad. Sci.* **1972**, *C274,*, 1545.

(46) Samec, Z.; Mareek, V.; Koryta J.; Khalil, M. W. *J. Electroanal. Chem.* **1977**, *83*, 393.

(47) Koryta, J.; Vanjsec, P.; Khalil, M. *J. Electroanal. Chem* **1977**, *75*, 211.

(48) Cunnane, V. J.; Geblewicz, G.; Schiffrin, D. J. **1995**, *40*, 3005-3014.

(49) Samec, Z.; Marecek, V.; Weber, J. *J. Electroanal. Chem.* **1979**, *103*, 11.

(50) Samec, Z.; Maracek, J.; Weber, J. *J. Electroanal. Chem.* **1977**, *96*, 245.

(51) Samec, Z.; Marecek, V.; Weber, J.; Homolka, D. *J. Electroanal. Chem.* **1981**, *126*, 105-119.

(52) Hanzlik, J.; Samec, Z.; Hovorka, J. *J. Electroanal. Chem.* **1987**, *216*, 303-308.

(53) Cheng, Y. F.; Schiffrin, D. J. *J. Electroanal. Chem.* **1991**, *314*, 153-163.

(54) Hanzlik, J.; Hovorka, J.; Samec, Z.; Toma, S. *Collect. Czech. Chem. Commun.* **1988**, *53*, 903-911.

(55) Kihara, S.; Suzuki, M.; Maeda, K.; Ogura, K.; Matsui, M.; Yoshida, Z. *J. Electroanal. Chem.* **1989**, *271*, 107-125.

(56) Samec, Z.; Marecek, V.; Weber, J. *J. Electroanal. Chem.* **1979**, *100*, 841.

(57) Wandlowski, T.; Marecek, V.; Samec, Z. *J. Electroanal. Chem.* **1988**, *242*, 291-302.

(58) Osakai, T.; Kakutani, T.; Senda, M. *Bull. Chem. Soc. Jpn.* **1984**, *57*, 370.

(59) Osakai, T.; Kakutani, T.; Senda, M. *Bull. Chem. Soc. Jpn.* **1985**, *58*, 2626.

(60) Cheng, Y. F.; Schiffrin, D. J. *J. Chem. Soc.-Faraday Trans.* **1993**, *89*, 199-205.

(61) Tsionsky, M.; Bard, A. J.; Mirkin, M. V. *J. Phys. Chem.* **1996**, *100*, 17881-17888.

(62) Wei, C.; Bard, A. J.; Mirkin, M. V. *J. Phys. Chem.* **1995**, *99*, 16033-16042.

(63) Bard, A. J.; Cliffel, D. E.; Fan, F.-R. F.; Tsionsky, M. *Ann. Chim.* **1997**, *87*, 15.

(64) Solomon, T.; Bard, A. J. *Anal. Chem.* **1995**, *67*, 2787-2790.

(65) Shao, Y. H.; Mirkin, M. V. *J. Phys. Chem. B* **1998**, *102*, 9915-9921.

(66) Kakiuchi, T.; Takasu, Y. *Anal. Chem.* **1994**, *66*, 1853-1859.

(67) Kakiuchi, T.; Takasu, Y. *J. Electroanal. Chem.* **1995**, *381*, 5-9.

(68) Brevet, P. F.; Girault, H. H. In *Liquid-Liquid Interfaces: Theory and Methods*; Volkov, A. G., Deamer, D. W., Eds.; CRC Press: Boca Raton, 1996.

(69) Dryfe, R. A. W.; Webster, R. D.; Coles, B. A.; Compton, R. G. *Chem. Commun.* **1997**, 779-780.

(70) Kakiuchi, T.; Takasu, Y. *J. Phys. Chem. B* **1997**, *101*, 5963-5968.

(71) Ding, Z. F.; Wellington, R. G.; Brevet, P. F.; Girault, H. H. *J. Electroanal. Chem.* **1997**, *420*, 35.

(72) Ding, Z. F.; Reymond, F.; Baumgartner, P.; Fermin, D. J.; Brevet, P. F.; Carrupt, P. A.; Girault, H. H. *Electrochim. Acta* **1998**, *44*, 3-13.

(73) Lauterbach, M.; Engler, E.; Muzet, N.; Troxler, L.; Wipff, G. *J. Phys. Chem. B* **1998**, *102*, 245-256.

(74) Petrukhin, O. M.; Dunaeva, A. A.; Wilke, S.; Muller, H.; Kolycheva, N. V.; Shipulo, E. V.; Genkina, G. K.; Mastryukova, T. A. *J. Anal. Chem.* **2002**, *57*, 240-247.

(75) Rahman, M. A.; Doe, H.; Okamoto, M.; Arakawa, R. *Electrochim. Acta* **1998**, *44*, 39-46.

(76) Marcus, R. A. *J. Phys. Chem.* **1991**, *95*, 2010-2013.

(77) Marcus, R. A. *J. Phys. Chem.* **1990**, *94*, 4152-4155.

(78) Kharkats, Y. I.; Volkov, A. G. *J. Electroanal. Chem.* **1985**, *184*, 435-442.

(79) Girault, H. H. J.; Schiffrin, D. J. *J. Electroanal. Chem.* **1988**, *244*, 15-26.

(80) Quinn, B.; Kontturi, K. *J. Electroanal. Chem.* **2000**, *483*, 124-134.

(81) Guainazzi, M., Silvestri, G. *J. Chem. Soc., Chem. Commun.* **1975**, 201.

(82) Samec, Z.; Marecek, V.; Homolka, D. *J. Electroanal. Chem.* **1983**, *158*, 25.

(83) Chen, Q. Z.; Iwamoto, K.; Seno, M. *Electrochim. Acta* **1991**, *36*, 291-296.

(84) Maeda, K.; Kihara, S.; Suzuki, M.; Matsui, M. *J. Electroanal. Chem.* **1991**, *303*, 171-184.

(85) Stewart, A. A.; Shao, Y.; Pereira, C. M.; Girault, H. H. *J. Electroanal. Chem.* **1991**, *305*, 135-139.

(86) Samec, Z.; Marecek, V.; Colombini, M. P. *J. Electroanal. Chem.* **1988**, *257*, 147-154.

(87) Samec, Z.; Brown, A. R.; Yellowlees, L. J.; Girault, H. H. *J. Electroanal. Chem.* **1990**, *288*, 245-261.

(88) Fermin, D. J.; Duong, H. D.; Ding, Z. F.; Brevet, P. F.; Girault, H. H. *PCCP Phys. Chem. Chem. Phys.* **1999**, *1*, 1461-1467.

(89) Brust, M.; Walker, M.; Bethell, D.; Schiffrin, D. J.; Whyman, R. *J. Chem. Soc.-Chem. Commun.* **1994**, 801-802.

(90) Johans, C.; Clohessy, J.; Fantini, S.; Kontturi, K.; Cunnane, V. J. *Electrochem. Commun.* **2002**, *4*, 227-230.

(91) Johans, C.; Kontturi, K.; Schiffrin, D. J. *J. Electroanal. Chem.* **2002**, *526*, 29-35.

(92) Scharifker, B.; Hills, G. *Electrochim. Acta* **1983**, *28*, 879-889.

(93) Gunawardena, G.; Hills, G.; Montenegro, I.; Scharifker, B. *J. Electroanal. Chem.* **1982**, *138*, 225-239.

(94) Johans, C.; Liljeroth, P.; Kontturi, K. S. *Phys. Chem. Chem. Phys.* **2002**, *4*, 1067-1071.

(95) Schiffrin, D. J.; Cheng, Y. *The Electrochemical Society and The International Society of Electrochemistry* **1997**, *97-2*, Abstract No. 961.

(96) Kuwana, T.; Heineman, W. R. *Acc. Chem. Res.* **1976**, *9*, 241.

(97) Bancroft, E. E. *Anal. Chem.* **1981**, *53*, 1862.

(98) Sailausa, N. *J. Am. Chem. Soc.* **1979**, *101*, 455.

(99) Webster, R. D.; Dryfe, R. A. W.; Coles, B. A.; Compton, R. G. *Anal. Chem.* **1998**, *70*, 792-800.

(100) Ding, Z. F.; Brevet, P. F.; Girault, H. H. *Chem. Commun.* **1997**, 2059-2060.

(101) Ding, Z. F.; Wellington, R. G.; Brevet, P. F.; Girault, H. H. *J. Electroanal. Chem.* **1997**, *420*, 35-41.

(102) Fermin, D. J.; Ding, Z.; Brevet, P. F.; Girault, H. H. *J. Electroanal. Chem.* **1998**, *447*, 125-133.

(103) Osakai, T.; Jensen, H.; Nagatani, H.; Fermin, D. J.; Girault, H. H. *J. Electroanal. Chem.* **2001**, *510*, 43-49.

(104) Nagatani, H.; Iglesias, R. A.; Fermin, D. J.; Brevet, P. F.; Girault, H. H. *J. Phys. Chem. B* **2000**, *104*, 6869-6876.

(105) Kakiuchi, T.; Takasu, Y.; Senda, M. *Anal. Chem.* **1992**, *64*, 3096-3100.

(106) Ding, Z. F.; Wellington, R. G.; Brevet, P. F.; Girault, H. H. *J. Phys. Chem.* **1996**, *100*, 10658-10663.

(107) Dryfe, R. A. W.; Ding, Z. F.; Wellington, R. G.; Brevet, P. F.; Kuznetzov, A. M.; Girault, H. H. *J. Phys. Chem. A* **1997**, *101*, 2519-2524.

(108) Ding, Z. Ph.D. Thesis, EPFL, Switzerland, 1999.

(109) Gomis-Bas, C.; Schiffrin, D. J. *unpublished results* .

(110) Creighton, J. A.; Eadon, D. G. *J. Chem. Soc.-Faraday Trans.* **1991**, *87*, 3881.

(111) Pool, R. *Science* **1990**, *248*, 1186.

CHAPTER TWO

THEORY

2.1. Charge Transfer processes at the ITIES

2.1.1. Thermodynamics of Charge Transfer processes at the ITIES

2.1.1.1. Simple Ion Transfer (IT)

The transfer of an ion (i) from one phase (α) to another (β) is accompanied by a faradaic current and can be described as follows:

$$i(\alpha) \mid i(\beta) \qquad (2.1)$$

When two phases are contacted, a Galvani potential difference ($\Delta_\alpha^\beta\phi = \phi^\beta - \phi^\alpha$) between the two phases results. At equilibrium, the Galvani potential difference ($\Delta_\alpha^\beta\phi_i$) is given by:

$$\Delta_\alpha^\beta\phi_i = \Delta_\alpha^\beta\phi_i^o + \frac{RT}{z_iF}\ln\left(\frac{a_i^\alpha}{a_i^\beta}\right) \qquad (2.2)$$

where $\Delta_\alpha^\beta\phi_i^o$ is the standard potential for IT of the ion i from the phase α to β and a is the activity of the ion.

If two phases containing the same electrolyte (AB) are contacted, the equilibrium is

$$AB(\alpha) \rightleftarrows AB(\beta) \qquad (2.3)$$

where AB can dissociate into a cation A and an anion B. When these concentrations are equal, the Galvani potential difference ($\Delta_\alpha^\beta\phi$) is given by:

$$\Delta_\alpha^\beta\phi = \frac{\Delta_\alpha^\beta\phi_A^o + \Delta_\alpha^\beta\phi_B^o}{2} + \frac{RT}{2F}\ln\left(\frac{\gamma_A^\alpha\gamma_B^\beta}{\gamma_A^\beta\gamma_B^\alpha}\right) \qquad (2.4)$$

where γ is the activity coefficient of the ion, T is the absolute temperature, R is the gas constant and F the Faraday constant. In this case $\Delta_{\alpha}^{\beta}\phi$ is independent of the electrolyte concentration and the interface formed is electrochemically nonpolarizable. Phase Transfer Catalysis (PTC) represents a specific example of a nonpolarizable interface. The equilibrium is described as:

$$C\,D\,(\alpha) \rightleftarrows C\,E\,(\beta) \qquad (2.5)$$

This represents is a special case of Equation 2.3 where only one common ion (C) is present in the two phases and only C can transfer across the interface. The potential difference between the two phases is determined by the activities of the common ion in each phase, according to the Nernst equation at ITIES given by:

$$\Delta_{\alpha}^{\beta}\phi = \Delta_{\alpha}^{\beta}\phi_{C}^{o} + \frac{RT}{F}\ln\left(\frac{a_{C}^{\alpha}}{a_{C}^{\beta}}\right) \qquad (2.6)$$

where $\Delta_{\alpha}^{\beta}\phi_{C}^{o}$ is the standard potential for the transfer of C. C is called a potential determining ion and can be used as a chemical method of fixing the interfacial potential.

Charge transfer phenomena at a liquid | liquid interface are studied using a polarisable interface. In this case the two phases contain dissimilar electrolytes A general example of a polarisable ITIES is given below:

$$A\,B\,(\alpha) \rightleftarrows C\,D\,(\beta) \qquad (2.7)$$

The electrical field in the interfacial region controls the Galvani potential difference and this can be altered using an external source. As the electrical field is altered, ions cross the interface to re-establish electrochemical equilibrium. In the potential region where this current is small, the interface is considered polarisable, and this region is

called the potential window or the polarisation window. In practice, an ITIES can be polarised if the aqueous and the organic electrolytes are respectively very hydrophilic and very hydrophobic.

2.1.1.2. Heterogenous electron transfer (HET)

Heterogenous electron transfer (HET) occurs when a redox couple located in one phase (α) exchanges an electron with a redox couple located in the other phase (β), for a one ET process the reaction can be written as follows:

$$R_1(\alpha) + O_2(\beta) \not\subset O_1(\alpha) + R_2(\beta) \qquad (2.8)$$

Where O and R refer to the oxidised and reduce forms of the redox species respectively. Reaction 2.8 can be considered to be pseudo-first order when the concentration of one redox couple is greatly in excess of the other. At equilibrium, the Galvani potential difference for ET ($\Delta_\beta^\alpha\phi_{ET}$) is given by:

$$\Delta_\beta^\alpha\phi_{ET} = \Delta_\beta^\alpha\phi^o + \frac{RT}{F}\ln\left(\frac{a_{R_1}^\alpha a_{O_2}^\beta}{a_{O_1}^\alpha a_{R_2}^\beta}\right) \qquad (2.9)$$

where $\Delta_\beta^\alpha\phi^o$ is the standard potential electron transfer potential:

$$\Delta_\beta^\alpha\phi^o = E_{O_2/R_2}^{o,\beta} - E_{O_1/R_1}^{o,\alpha} \qquad (2.10)$$

Equation (2.9) is the general relationship between the thermodynamic properties of the redox components and the position of equilibrium in a two phase redox system, and it shows that the position of equilibrium is determined by the standard potentials of the redox couples and by the interfacial Galvani potential difference. In this manner the redox phenomena in a two phase system differs from those in a single phase system, since for the latter the position of equilibrium is determined only by

the standard potentials of the redox couples. For a given two phase system the position of the equilibrium can be determined electrochemically, by applying an external Galvani potential difference, or chemically, by the use of a partitioning ion which is not a part of the redox system. From Equation 2.9, it is clear that it is necessary to match the standard potentials of two redox couples as closely as possible, in order to observe interfacial ET within the limited potential window available for ITIES studies. In theory it should be possible to observe ET between two redox couples provided that this condition is fulfilled, irrespective of the magnitude of their standard redox potentials.

2.2. Electrochemically controlled Nucleation

As already discussed, the advantage of using electrochemical techniques to prepare metal particles is that the supersaturation can be controlled by the applied interfacial potential, whereas in conventional chemical synthesis control of the reaction rate is difficult.

Experimentally, electrochemical nucleation can be studied in one of two ways, at controlled potential or at controlled current. The transients obtained relate to the current flowing through the cell and the potential developed between the working and the reference electrodes respectively. Cyclic voltammetry indicates the presence of nucleation by an enhanced peak separation of an otherwise normal mass transport-controlled voltammogram, and by the presence of a characteristic crossover of the current in the cathodic branch (nucleation loop). Potential step (I-t) transients can be used to determine the induction time, nucleation rate constant and nuclear number

density[1] for nucleation and growth process.[2] Since the growth of nuclei of electrodepositing metals can only take place by a faradaic process the observed current provides an exact measure of the combined rate of nucleation and growth of nuclei. The characteristic appearance of the transient is a rising section, corresponding to the growth of the electroactive area as established nuclei grow and as new nuclei are formed, followed by a slow decrease due to diffusionally controlled growth. The maximum current (I_m) at time (t_m) of the transients can be used to identify the nucleation behaviour of the system in two extreme conditions.

In the galvanostatic experiment, on the other hand, current is controlled and hence nucleation occurs at a pre-determined rate, the degree of supersaturation is monitored as an overpotential throughout the process. The current step is also a useful means of detecting the presence of nucleation and potential maxima occur at the beginning of the transition time. The height of the maxima is related to the formation of the new phase.

Since the basic theory for the nucleation and growth of a metal at the ITIES is essentially the same[3] as those for the same process at a metal electrode | electrolyte interface, it is necessary to first consider the theory derived for this process.

The deposition of a monolayer of a metal onto an inert substrate is a two-step process. The first step involves the formation of a nucleus (3-dimensional growth centre) of the new phase by nucleation and this requires a large overpotential. Until nuclei are formed, this is a relatively slow process. At this stage, nuclei grow independently of each other by hemi-spherical diffusion. The second step involves

the subsequent overlap of growth centres, until eventually growth is controlled by linear diffusion and follows the Cottrell equation (2-dimensional growth). Several models have been proposed for the intermediate time interval.[4-7]

The geometry of the growth centre is highly sensitive to the interaction between the deposit and the substrate. The situation is complex since growth at several centres (and the overlap of their diffusional zones) is involved.

The parameters (nucleating rate constant, nucleus density and growth rate) for the hemi-spherical diffusion controlled growth can be controlled by applied potential and information on these parameters can be obtained from analysis of the current-time transient.

2.2.1. Thermodynamics of Nucleation

Nucleation at the metal electrode | electrolyte solution interface is a homogenous process except in the ET step. The reaction can be described as follows:

$$M^{z+} + ze^{-} \rightarrow M^{0} \qquad (2.11)$$

where M is the metal of charge z+. The Nernst Equation gives the equilibrium potential of this reaction:

$$E_e = E^{o} + \frac{RT}{F} \ln\left(\frac{a_{M^{z+}}}{a_{M^{o}}}\right) \qquad (2.12)$$

where E^{o} and E_e are the standard and the equilibrium electrode potentials respectively. The surface activity of ad-atoms at equilibrium is $a^{*}_{M_{ads}}$. If the electrode

potential is changed to a value ($E_e+\eta$) where η is the overpotential, the surface activity of ad-atoms is determined by the relationship:

$$\frac{a_{M_{ads}}}{a^{*}_{M_{ads}}} = \exp\left(\frac{-nF\eta}{RT}\right) \qquad (2.13)$$

In classical nucleation theory (i.e. homogenous nucleation, which is based on the nucleation of a liquid drop in the absence of a substrate), the free energy of formation of a spherical nucleus (ΔG) is the driving force for phase formation. It represents the thermodynamic stability of the new phase with respect to the initial bulk phase and can be described by:

$$\Delta G = \delta G_{bulk} + \delta G_{surface} \qquad (2.14)$$

$$\delta G_{bulk} = \frac{4}{3}\pi r^3 \Delta G_V \qquad (2.15)$$

where r is the radius of the particle formed, ΔG_V is the Gibbs free energy of formation of the bulk phase per unit volume (V). This is always a negative quantity when an overpotential is applied and is given by:

$$\Delta G_v = \frac{nF\rho\eta}{V} \qquad (2.16)$$

where ρ is the density of the deposit. The surface contribution to the Gibbs energy of formation is given by:

$$\delta G_{surface} = 4\pi r^2 \gamma \qquad (2.17)$$

where γ is the surface tension. $\delta G_{surface}$ is associated with the formation of the new phase and is a positive quantity. For small values of r, the δG_{bulk} term is negligible and $\Delta G \approx \delta G_{surface}$. Thus ΔG is a positive quantity. Conversely for large values of r, the second term ($\delta G_{surface}$) is negligible, so $\Delta G \approx \delta G_{bulk}$ which is a negative

quantity. Differentiation of equation (2.14) with respect to r yields the following expression for the maximum free energy.

$$\Delta G_{max} = \frac{16M^2\gamma^3}{3(\rho nF\eta)^2} \qquad (2.18)$$

where M is the molecular weight. The particular value of the radius (r_c) where the Gibbs free energy has this maximum value is known as the critical radius (a nucleus having a radius equal to the critical radius is called a critical nucleus.) where:

$$r_c = -\frac{2\gamma}{\Delta G_V} \qquad (2.19)$$

This relationship is called the Gibbs-Kelvin equation and it relates the Gibbs free energy of an interface to its radius of curvature. According to equation (2.19) above, a nucleus with a radius in excess of the critical radius will tend to be stable and grow spontaneously while a nucleus with a radius smaller than the critical radius will be unstable and will decay. The critical radius is related to the overpotential as follows:

$$r_c = -\frac{2\gamma M}{zF\eta} \qquad (2.20)$$

2.2.2. Kinetics of Nucleation

The rate constant for nucleation of a critical nucleus is related to the energy barrier (ΔG_c) as follows:

$$\text{rate} = A\exp\left(\frac{-\Delta G_c}{kT}\right) \qquad (2.21)$$

where A is the pre-exponential factor.

For nuclei growing under conditions of mass transfer control, the current density at a time t, for fixed numbers of crystallites, N, growing by hemispherical diffusion flux is given as:[1]

$$I(t) = \frac{zFN\pi(2Dc)^{3/2}\sqrt{Mt}}{\sqrt{\rho}} \qquad (2.22)$$

where c is concentration and D is the diffusion coefficient and N is the nuclear number density. This nucleation regime, where fresh nuclei are formed instantaneously, is referred to instantaneous nucleation. The hemispherical shape relates to the depletion zones around the growing crystallites more so than the crystallites themselves, as the former advance much more rapidly radially that the perimeters of the crystallites do.

It is observed in many experiments that the nuclear number density, N, rapidly reaches a limiting, constant value. This condition of arrested nucleation is referred to as progressive nucleation.

$$I(t) = \frac{2zFAN_{\infty}\pi(2Dc)^{3/2}M^{1/2}t^{3/2}}{3\rho^{1/2}} \qquad (2.23)$$

where N_{∞} is the nuclear number density at long times. The ratio of the slopes of plots of the current time dependence of the progressive to instantaneous nucleation regimes can be used to evaluate $\frac{AN_{\infty}}{N}$, which gives a good indication of the magnitude of the rate constant.[1] The direct determination of A along with N is possible using the current maximum from a single transient.[6,8]

In each case (progressive and instantaneous nucleation) the current passes through a maximum and then approaches the limiting diffusion current predicted for mass

transfer to a planar electrode. The current (I_m) and time (t_m) corresponding to the maximum can be evaluated.[2] The product $I_m^2 t_m$ is a convenient diagnostic criterion of the type of nucleation occurring since it is independent of the nucleation and growth rates. Thus, at a given bulk concentration of electrodepositing species $I_m^2 t_m$ should not vary with overpotential (where the overpotential is high enough to ensure that the surface concentration of the diffusing species is zero). The diffusion coefficient of the diffusing species can be obtained using this product and the following equation:[1]

$$I_m^2 t_m = 0.1629(zFc)^2 D \qquad (2.24)$$

Alternatively, the transients can be presented in non-dimensional form[4] by plotting I^2/I_m^2 versus t/t_m and compared with the theoretical expressions:

$$\left(\frac{j}{j_m}\right)^2 = 1.9542\left(\frac{t}{t_m}\right)\left(1-\exp\left[-1.2564\left(\frac{t}{t_m}\right)\right]\right)^2 \qquad (2.25)$$

$$\left(\frac{j}{j_m}\right)^2 = 1.2254\left(\frac{t}{t_m}\right)\left(1-\exp\left[-2.3367\left(\frac{t}{t_m}\right)^2\right]\right)^2 \qquad (2.26)$$

for instantaneous and progressive nucleation respectively. In both cases the current density approaches nFk_3' at long times, since the remaining growth is restricted to the perpendicular direction.

The nuclear number density (N), at a given overpotential, can be calculated from the current maxima from:[4]

$$I_m = 0.682zFDc\sqrt{kN} \qquad (2.27)$$

where k is a constant depending on the reaction conditions, given by: $k = \sqrt{8\pi cV}$, and V is the volume of the deposited phase.

2.3. Electrochemical Nucleation at the ITIES

The generation of low valent transition metal complexes can be carried out electrochemically at the liquid/liquid interface if a metal salt is dissolved in either the organic or in the aqueous phase with a suitable reductant in the opposite phase. For the general reaction:

$$R\,(o) + M^{z+}\,(aq) \rightleftharpoons O\,(o) + M\,(\sigma) \qquad (2.28)$$

The Galvani potential difference is given by:

$$\Delta_{\beta}^{\alpha}\phi_{ET} = \Delta_{\beta}^{\alpha}\phi^{o} + \frac{RT}{F}\ln\left(\frac{a^{O(o)}a^{M(\sigma)}}{a^{R(o)}a^{M^{+l}(aq)}}\right) \qquad (2.29)$$

a_M is the activity of the newly formed metal phase formed at the interface, which is a constant and equal to unity when M covers the interface with more than a monolayer. According to equation 2.29 it should be possible to deposit metallic particles electrochemically at the interface using an appropriate aqueous redox couple and applying an interfacial potential difference to shift the position of equilibrium or by the use of a PTC. As already discussed, the standard potentials of the two couple must be as close as possible to one another so as to ensure that ET is observed within the polarisation window of the two-phase system.[9,10]

A model has been developed for nucleation processes at the ITIES, taking the diffusion fields on both side of the interface into account. The process was observed to be different to that at solid electrodes, due to the absence of surface defects. It was also determined that nucleation rate depends exponentially on the applied Galvani potential difference.[3]

2.4. References

(1) Hills, G. J.; Schiffrin, D. J.; Thompson, J. **1974**, *19*, 657.

(2) Gunawardena, G.; Hills, G.; Montenegro, I.; Scharifker, B. *J. Electroanal. Chem.* **1982**, *138*, 225-271.

(3) Johans, C.; Lahtinen, R.; Kontturi, K.; Schiffrin, D. J. *J. Electroanal. Chem.* **2000**, *488*, 99-109.

(4) Scharifker, B.; Hills, G. *Electrochim. Acta* **1983**, *28*, 879-889.

(5) Gunawardena, G.; Hills, G.; Montenegro, I.; Scharifker, B. *J. Electroanal. Chem.* **1982**, *138*, 225-239.

(6) Scharifker, B. R.; Mostany, J. *J. Electroanal. Chem.* **1984**, *177*, 13-23.

(7) Mirkin, M. V.; Nilov, A. P. *J. Electroanal. Chem.* **1990**, *283*, 35-51.

(8) Mostany, J.; Mozota, J.; Scharifker, B. R. *J. Electroanal. Chem.* **1984**, *177*, 25-37.

(9) Geblewicz, G.; Schiffrin, D. J. *J. Electroanal. Chem.* **1988**, *244*, 27-37.

(10) Girault, H. H. J.; Schiffrin, D. J. *J. Electroanal. Chem.* **1988**, *244*, 15-26.

CHAPTER THREE

EXPERIMENTAL

3. 1. Chemicals

3. 1. 1. Solvents

In order to form a stable interface between two solvents, they should have an extremely low mutual solubility, low vapour pressures and have appreciably different densities. Spectrophotometric grade 1,2-Dichloroethane (1,2-DCE, 99%+ Aldrich) and ultra pure water (MilliQ, resistivity is 18.2 MΩ cm) were used as solvents for all liquid | liquid experiments. The former was used as received.

3. 1. 2. Supporting electrolytes

The size of the available potential window is extended by use of hydrophilic and hydrophobic aqueous and organic supporting electrolytes respectively.

Organic phase: The following supporting electrolytes were prepared by the general procedure described below: tetraphenylarsonium tetrakis(4-chlorotetraphenyl)borate (TPAsTPBCl), bis(triphenylphosphoranylidene) ammonium tetrakis(pentafluoro-phenyl)borate (BTPPATPBF$_5$) and tetraphenylarsonium tetrakis(pentafluoro-phenyl)borate (TPAsTPBF$_5$).

The following reagents were used for the synthesis of the organic supporting electrolyte without further purification: (bis[triphenylphosphoranylidene] ammonium chloride (BTPPACl, Purum, 98.0%, Aldrich), potassium tetrakis(4-chlorophenyl)-

borate (KTPBCl, Selectophore ≥98%, Fluka), tetraphenylarsonium chloride (TPAsCl, Fluka), lithium tetrakis(pentafluoro-phenyl)borate etherate, diethyl ether solvate ($LiTPBF_5$, Boulder Scientific, USA.). The organic supporting electrolytes used had the general formula XY and were prepared by metathesis of the corresponding salts (XCl and Li/Na/KY) in a 2:1 mixtures of methanol (AnalaR, BDH) and water (MilliQ). The resulting precipitate was washed with water (MilliQ), recrystallised twice from acetone (AnalaR, Fisons) and dried under vacuum for 3 days before use. CHN microanalyses were performed on the organic supporting electrolytes to confirm purity.

The following organic supporting electrolytes were used as received: tetrabutyl-ammonium tetraphenylborate (TBATPB, Puriss, Fluka), tetrahexyl-ammonium hexafluorophosphate ($THAPF_6$, Aldrich) and tetrahexylammonium tetrakis-4-chlorotetraphenylborate (THATPBCl, Fluka).

Aqueous phase: Lithium chloride (LiCl, Ultrapure, 99.99%, Johnson Matthey), lithium sulfate monohydrate ($Li_2SO_4.H_2O$, MicroSelect, Fluka), hydrochloric acid (HCl, AnalR, BDH), sodium thiosulphate pentahydrate ($Na_2S_2O_3.5H_2O$, 99.5%, Sigma) and citric acid trisodium dihydrate ($C_6H_5Na_3O_7$ $2H_2O$, 99+%, Aldrich) were used without further purification.

The aqueous phase commonly featured a high ionic strength in order to decrease the partitioning of the organic species between both phases by salting out.[1,2]

3. 1. 3. Redox species

Organic phase: The ruthenium complexes used for electron transfer studies (trans-Ru(1,2-bis(diphenylphosphino)ethane)$_2$Cl$_2$ **(1)** , trans-Ru(bis(diphenylphosphino)-methane)$_2$Cl$_2$ **(2)** and trans-Ru(1,1-bis(diphenylphosphino)ethene)$_2$Cl **(3)**, were obtained from Dr. Simon Higgins, The University Of Liverpool, U.K.

Dimethylferrocene (DMFc, 97%, Aldrich) and decamethylferrocene (DCMFc, ≥95%, Aldrich) were used as received.

Aqueous phase: The aqueous redox species used for electron transfer studies were potassium ferrocyanide and potassium ferricyanide ($K_4Fe(CN)_6$ and $K_3Fe(CN)_6$, microselect, 99%, Fluka) and were used without further purification. The metal salts mercurous nitrate dihydrate ($Hg_2(NO_3)_2.2H_20$, 97+%, Aldrich), hydrogen tetrachloroaurate ($HAuCl_4$, Aldrich), silver sulphate (Ag_2SO_4, 99.9%, Aldrich), ammonium tetrachloropalladate ($(NH_4)_2PdCl_4$, Puratronic, 99.999%, Aldrich), sodium tetrachloroplatinate ($(NH_4)_2PtCl_4$, 99.99%, Aldrich) were used as supplied.

3. 2. Instrumentation

All electrochemical measurements were carried out in a Faraday cage at room temperature.

3. 2. 1. Four electrode potentiostat

The electrochemical experiments on heterogeneous electron transfer (Chapter 4), nucleation (Chapter 5) and colloid charging (Chapter 7) were carried out using a commercially available four-electrode potentiostat (Autolab, PGSTAT 20, Eco Chemie, Netherlands) with iR drop compensation. For spectroscopic measurements (Chapter 6) and ac voltammetry (Chapter 7), the water | DCE interface was polarised using a custom-made four-electrode potentiostat with a waveform generator (Hi-Tek Instruments PPR1). The iR drop is considered fully compensated when the feedback potential is set at a value slightly less than that generating oscillation of the electronics.

3. 2. 2. Reference electrodes (RE)

The RE's used for voltammetric experiments were either a Saturated Calomel Electrode (SCE, Radiometer Copenhagen, Denmark) or home made Ag/AgX wire electrodes. When the anion of the aqueous supporting electrolyte is a halide, a silver/silver halide reference electrode can be used, e.g. when the reference phase supporting electrolyte is LiCl, Ag/AgCl is used as the RE. In the spectroscopic experiments on silver nucleation, experiments Ag/Ag_2SO_4 was used as the reference

electrode. (The presence of any trace of halide would cause the immediate precipitation of AgX.) These electrodes give a stable potential.

The Ag/AgX electrodes were prepared by electrolysis of a clean Ag wire (Goodfellow, 99.9%) in a saturated solution of the anion. Passing a low anodic current through the Ag wire for prolonged time (20 minutes) caused the Ag wire to be coated with a dense layer of chloride.

All glassware used for electrochemical measurements was cleaned by immersion overnight in a bath of concentrated acid (50:50 HNO_3 : H_2SO_4, BDH, AnalaR), followed by multiple rinsing with water purified by a MilliQ purification system.

3. 3. Techniques

3. 3. 1. Cyclic voltammetry

Cyclic voltammetry is a highly versatile technique used for preliminary studies of electroactive species. In the traditional three-electrode configuration, a triangular potential profile is applied between the working (WE) and counter electrodes (CE) with reference to an electrode of known potential provided by a high impedance reference electrode (RE). The RE is positioned close to the surface of the WE[3,4] and the current response is recorded as a function of the applied potential. The cyclic voltammogram can be used to determine the potentials at which electrochemical processes occur at an electrode surface. For a faradaic reaction at a metal-electrolyte interface, the relationship between the concentration of the redox species at the electrode surface and electrode potential is given by the Nernst equation:[3,4]

$$E=E^{\circ}+\frac{RT}{nF}\ln\left(\frac{a_O}{a_R}\right) \qquad (3.1)$$

where E and E° are the potentials applied to the electrode and the standard potentials of the couple, a_o and a_R are the activities of the oxidised and the reduced species at the electrode surface, F is the Faraday constant, R is the gas constant and T is the absolute temperature. For diffusion limited mass transfer to a macroscopic planar electrode surface, the voltammetric peak current (i_p) is related to the sweep rate ν, and diffusion coefficient D, according to the Randles-Sevcik equation:[5]

$$i_p=2.69\times10^5 n^{3/2} A D^{1/2} \nu^{1/2} c \qquad (3.2)$$

where n is the number of electrons exchanged per mole of reacting species, A is the interfacial area and c is the concentration of the transferring species. Cyclic voltammetry can provide information about the reversibility of an electrode process. The diagnostic test for a reversible transfer process is based on the separation of forward and reverse peak maxima (E_p^a and E_p^c respectively). For a reversible process (linear diffusion to a planar electrode):

$$\Delta E_p = E_p^a - E_p^c = 59/n \text{ mV} \qquad (3.3)$$

Under quasi-reversible to irreversible conditions, kinetic information can be obtained from this technique.

3.3.1.1 Cyclic Voltammetry at a Microelectrode

An electrode with a diameter in the range of 10^{-6} m is termed a microelectrode. This type of electrode possesses some significant advantages over the traditionally sized macroelectrodes, in a size range of 10^{-3} m.

Since the current measured at the electrode is a function of the electrode area, the current measured at a microelectrode is significantly lower than that from a conventional electrode, nA for microelectrodes as opposed to mA for macroelectrodes. As a result, microelectrodes induce much less electrolysis in the solution studied and consequently the diffusion layer is narrower. Thus, the concentration gradients induced across a microelectrodes will be correspondingly high and the rate of mass transport to microelectrodes is much greater than that for macroelectrodes. Mass transfer is governed by approximately spherical diffusion at a

planar microelectrode surface, in contrast to linear diffusion at a macroscopic planar electrode. This becomes especially important when investigating fast electrode process and generally the use of microelectrodes enables the electrochemical investigation of much faster reactions. For microelectrode measurements, a two-electrode experimental arrangement is used rather than a three-electrode one, since the iR drop is greatly reduced.

A current is required to change the potential applied to the working electrode (the charging current) and since the potential in a CV experiment is constantly changing, there is an (approximately) constant charging current throughout the experiment that contributes to the background current. In addition, the charging current is directly proportional to the scan rate, whereas the peak current is proportional to the square root of the scan rate, therefore, the charging current also limits the maximum scan rate that can be used. The much reduced electrode area of a microelectrode means that microelectrodes suffer much less distortion from this charging current, thus improving the analytical capabilities of the technique and allowing much faster sweep rates to be used.

Finally, the use of microelectrodes allows voltammetry to be carried out in a much smaller volumes than those traditionally used, so electrochemical measurements can be carried out in-vivo.[6-9]

For microelectrode experiments involving a planar microdisc electrode, the diffusion limiting current (i_L) is proportional to the concentration, the diffusion coefficient and the size of the electrode according to:[10]

$$|I_L| = 4nFcDA \qquad (3.4)$$

where I_L is the limiting current and r is the radius of the microelectrode. (Note: at a microelectrode, the limiting current is at steady state and thus I_L does not vary with scan rate.)

The current-potential response at a microdisc electrode in the case of one-electron transfer reversible electrochemical reaction is an S-shaped wave with the half wave potential lying at the mid-point of the curve. The half-wave potential is the potential at half wave height. An irreversible redox reaction at a microelectrode also yields an S-shaped wave, but its position is shifted on the potential scale to more negative or more positive potentials for reduction and oxidation respectively.

Semi-logarithmic analysis of the steady state polarisation curves is carried out in order to determine the reversibility of the redox reactions and to obtain the half wave potential for the redox couples. For a reversible process:[3]

$$E = E_{\frac{1}{2}} + \frac{RT}{nF}\log\left(\frac{I_L}{I} - 1\right) \qquad (3.5)$$

I is the current measured a potential E, $E_{1/2}$ is the half wave potential. In this case, a semi-logarithmic plot of E vs log $[(I_L\text{-}I)/I]$ is linear with a slope of 59/n mV/decade and the y-intercept corresponds to the formal potential for the redox couple ($E_{1/2}$).

The microelectrode experiments were carried out with a 10 μm diameter Pt microelectrode[11]. The electrode was cleaned by consecutive cleaning with alumina powder grades 1.0, 0.3 and 0.05μm (Beuhler, U.K.), in a suspension of MilliQ water

on a microcloth (Beuhler, U.K.). The electrode was placed in an ultrasonic bath for several minutes between polishing with each grade of alumina powder and allowed to dry before being placed in the electrochemical cell. A SCE (Radiometer, Copenhagen) was used as a combined counter-reference electrode.

3. 3. 2. Chronoamperometry

In the chronoamperometry or potential step technique, the potential of the WE is changed instantaneously and the current response is measured as a function of time. The resulting transient (current-time response) follows the Cottrel equation. For a macroscopic planar electrode, the current (I) at a time t is given by:

$$i(t) = \frac{nFc\sqrt{D}}{\sqrt{\pi t}} \qquad (3.6)$$

In section 2.2.2, it was described how the mechanism of nucleation and growth of a new phase can be followed using chronoamperometry data measured at short times.

3. 3. 3. AC voltammetry

AC voltammetry is a high-precision technique, which involves the superimposition of a sinusoidal varying (AC) potential signal of small amplitude onto a DC potential scan profile. In the absence of charge transfer processes; the differential capacitance can be calculated from the admittance response using an equivalent circuit composed of a resistance (uncompensated iR drop, R) and a capacitance (interfacial capacitance, C) in series. The capacitance can be calculated from the modulated

potential $\Delta_o^w\varphi_1$, frequency, ω, and real and imaginary currents measured, I_{re}, I_{im} as follows:[12]

$$C = \frac{I_{re}^2 + I_{im}^2}{I_{im}\omega\Delta_o^w\varphi_1} \qquad (3.7)$$

Additional information is given in Section 7.2.3.

3. 3. 4. In Situ UV-visible Spectroelectrochemistry at the ITIES

In situ spectroelectrochemistry involves the combination of electrochemical and spectroscopic techniques so that the two measurements may be performed simultaneously in an electrochemical cell. Traditional electrochemical methods may be complemented by spectroscopic techniques to yield information on the faradaic process. Typically, an electrochemical perturbation is introduced and the system spectroscopic response is monitored. The spectroscopic response was measured in transmission, reflection and scattering modes.

One of the main advantages of such techniques at the ITIES is their versatility; a wide range of charge transfer processes can be investigated. Also, spectroscopic approaches are less sensitive to uncompensated resistance and double layer effects than electrochemical techniques. The spectroelectrochemical methods used in this thesis are further discussed in Chapter 6.

3. 4. Electrochemical Cells

The cell shown in Figure 3.1 was used for all microelectrode studies. The specifications of the electrochemical cell used for liquid | liquid experiments vary depending on requirements. For example, cyclic voltammetry and potential transient experiments were carried out in the basic four-electrode cell shown in Figure 3.2. A modified form of this cell was used for spectroscopic work (Figure 3.3) while another cell which allowed for de-aeration, was used for de-oxygenation experiments (Chapter 7).

3. 4. 1. Microelectrode cell design and experimental set-up

The two-compartment microelectrode cell depicted in Figure 3.1 was used for the study of the redox behaviour of the organic and aqueous couples used. The WE was a 10 μm diameter Pt disc.

3. 4. 2. Four electrode (ITIES) cell design and experimental set-up

The cell used for electron transfer studies at the ITIES had three-compartments and was similar to the one developed by Samec.[13] The interfacial area was 0.125 cm^2 and the volumes of the aqueous and organic compartments were 2 and 1.7 ml respectively. The CE's were large surface area Pt gauze electrodes positioned perpendicular to the interface (to facilitate the filling of the cell) in each phase. The interfacial potential difference is altered by means of a two RE's immersed in

separate side compartments but connected to the central compartment by means of Luggin capillaries. The interface is situated between the two Luggin capillaries. By placing the Luggin as close as possible to the interface, the effective iR drop is minimised. This factor is high for organic solutions, introducing a large iR drop across the organic solution. Since the Luggin capillary cannot be placed in direct contact with the interface it is important to correct for this factor using a positive feedback loop.[14-16] The current across the interface is measured via the two CE's. The WE surface area is smaller than the CE so that, comparatively, no polarisation of the latter occurs. In this way reactions that may occur at the CE do not significantly contribute to the overall cell response.

This cell design allows for quick filling and a reproducible interfacial area and is suitable for the study of electron (ET) and ion transfer (IT) reactions.

3. 4. 3. Spectroelectrochemical cell

A schematic representation of the three-compartment spectroelectrochemical cell is shown in Figure 3.3. The glass tube was filled with the aqueous phase and dipped into an organic phase. The interfacial area is 0.22 cm^2. A flat water | DCE liquid junction was formed by means of a piston burette (E274, Metrohm). It was important that the interface was both small and supported for these measurements since a large, unsupported interface is prone to oscillations as a potential is applied, leading to an unstable baseline.

As shown in Figure 3.3, the interface was illuminated from the organic phase by a 150W Xenon arc lamp (Applied Photophysics) fitted with a 150 or 500 micron diameter pin-hole and then focused onto the interface. For experiments made in the reflection mode the light was focused at an incident angle of approximately 75° (the critical angle for the water | DCE interface is 67°). The full spectrum light beam was collected using a 400 μm optical fibre and recorded using a spectrograph (TRIAX 190, Jobin Yvon) equipped with a CCD camera (model 3500, Jobin Yvon). The spectrograph, CCD camera and data acquisition were controlled using a home-made program (LabView, National instruments). Potential modulation and phase sensitive detection were performed by a Lock-in amplifier (SR830, Stanford Research).

3. 5. Data Analysis

3. 5. 1. Correction for microelectrode organic soluble redox species

The cell potential was referred to the aqueous phase by introducing a well-defined organic/aqueous phase reference junction, having the common ion TBA^+ in both phases. The applied potential is the sum of several contacting potential differences across each interface and is thus, arbitrary, relating only to the system being studied. The following (Cell 3.1) is the general cell used for microelectrode experiments:

$$\text{SCE} \;\Big|\; \underset{(aq)}{x\ \text{TBACl}} \;\Big|\; \underset{(DCE)}{x\ \text{TBATPBCl}} \;\Big\|\; \text{Pt } 10\,\mu\text{m}$$

Cell 3.1

where x is the concentration of salt used. The measured cell potential for cell 3.1 can be converted to the absolute scale using an extra-thermodynamic assumption.[17] The following relation can be used to convert cell scale to that vs. SHE:

$$E^{0'} = E_{1/2} + E_{SCE} + \Delta_o^w\phi_{TBA^+} \qquad (3.8)$$

where $E_{1/2}$ is the measured half-wave potential on the cell potential scale, E_{SCE} is the potential of the saturated calomel electrode vs. SHE and $\Delta_o^w\phi_{TBA^+}$ refers to the potential drop across the 1,2-DCE | water reference interface on the absolute Galvani scale. This latter term can be estimated using the Nernst equation:

$$\Delta_o^w\phi_{TBA^+} = \Delta_o^w\phi^{\theta}_{TBA^+} + \frac{RT}{zF}\ln\left(\frac{\alpha\gamma_{org}c_{org}}{\gamma_{aq}c_{aq}}\right)_{TBA^+} \qquad (3.9)$$

where $\Delta_o^w\phi^\theta_{TBA^+}$ is the standard Galvani potential of transfer of the TBA^+ ion from the aqueous to the organic phase, ($\Delta_o^w\phi^\theta_{TBA^+}$ = -0.225 V),[18] c is the concentration of TBA^+ in the appropriate phase, α is the degree of dissociation in the low permittivity 1,2-DCE phase and γ the activity coefficient of the ion. All other symbols have their usual meaning. Partial dissociation of the electrolytes was considered for the non-aqueous phase only. The activity coefficient of the ion (γ) in each phase was calculated from the extended form of the Debye-Huckel equation:[19]

$$-\log\gamma_i = \frac{A\sqrt{\alpha_i c_i}}{\left(1+Ba\sqrt{\alpha_i c_i}\right)} \qquad (3.10)$$

where A and B are constants and a is the ion size parameter.[19] The degree of dissociation of TBA in the non-aqueous phase (α_{org}) was calculated from the association constant (K_a) for the electrolyte in that solvent:

$$K_a = \frac{(1-\alpha_i)}{c_i\alpha_i^2\gamma_i} \qquad (3.11)$$

It is assumed that the activities of the anion and the cation are equal. The association constants and the ion size parameters were taken from the literature.[20] The activity coefficient, γ_i, was calculated from equations (3.10) and (3.11) above by an iterative procedure using an Excel spreadsheet.

3. 5. 2. Galvani Correction for liquid | liquid results

For the general cell used for the study of charge transfer processes at the liquid | liquid interface (3.2), σ represents the interface under investigation (the ITIES).

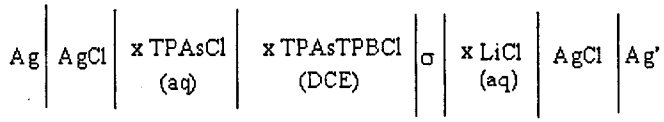

Cell 3.2

Again, the measured cell potential E is the sum of all the potential drops across each interface. The potential applied to the cell (E) is:

$$E=E_{SCE_{(R)}}-E_{SCE_{(L)}}+\Delta_o^w\phi-\Delta_o^w\phi_{TPAs^+} \qquad (3.12)$$

where E_{SCE} is the potential of the saturated calomel electrode with respect to the standard hydrogen electrode, $\Delta_o^w\phi$ is the potential drop across the polarisable interface. $\Delta_o^w\phi_{TPAs^+}$ can be estimated from the Nernst equation analogous to that given in the previous section for the tetrabutylammonium cation. The standard Galvani potential of transfer of the TPAs ion from DCE to water is $\Delta_o^w\phi^\theta_{TBA^+}$ = -0.364 V.[18]

For reporting the results obtained with four-electrode cyclic voltammetry, the standard convention was used when presenting potentials, i.e. an increase in cell potential is associated with the potential of the aqueous phase becoming more positive with respect to the organic phase. thus a positive current corresponds to electron transfer from 1,2-DCE to the water phase.

Table 3. 1 Table of association constants for typical organic supporting cations, where A is the association constant values for the corresponding $TPhB^-$ or $TPhBCl^-$ salts and d is the distance of closest approach.

C^+	d /Å	A_{20}
TMA^+	6.2	12,400
TEA^+	6.4	2,500
$TPrA^+$	6.6	2,100
TBA^+	6.8	1,715
$TPAs^+$	6.6	600

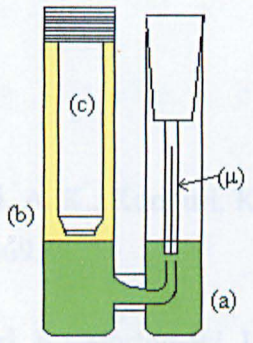

Figure 3.1 Schematic drawing of the cell used for microelectrode measurements. (a) organic phase (green), (b) organic reference phase (yellow), (c) SCE, (μ) Pt electrode (d=10 μm).

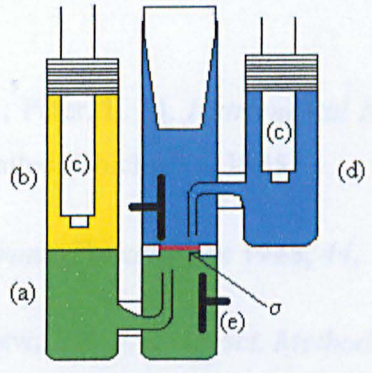

Figure 3.2 Schematic drawing of the electrochemical cell used for liquid | liquid charge transfer measurements where the organic solvent is more dense than water. (a) organic phase (green), (b) organic reference phase (yellow), (c) SCE, (d) aqueous phase (blue), (e) Pt CE and σ is the interface under investigation (red).

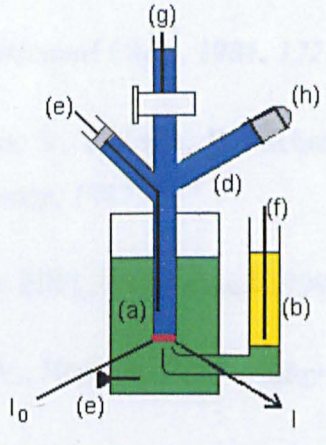

Figure 3.3 Schematic representation of the electrochemical cell used for PM spectroscopy[21] (in TIR mode). (a) organic phase (green), (b) organic reference phase (yellow), (d) aqueous phase (blue), (e) Pt counter electrode, (f) Ag/AgCl RE, (g) Ag/Ag_2SO_4 RE, (h) piston burette, I_0 and I are the incident and reflected light intensities respectively and δ is the interface under investigation (red).

3. 6. References

(1) Geblewicz, G.; Kontturi, A. K.; Kontturi, K.; Schiffrin, D. J. *J. Electroanal. Chem.* **1987**, *217*, 261-269.

(2) Kontturi, A. K.; Kontturi, K.; Murtomaki, L.; Schiffrin, D. J. *J. Chem. Soc.-Faraday Trans.* **1990**, *86*, 931-936.

(3) Bard, A. J., Faulkner, L. R., *Electrochemical Methods*; John Wiley: New York, 1980.

(4) Greef, R.; Peat, R.; Peter, L. M. *Instrumental Methods in Electrochemistry*; Ellis Horwood Limited: Chichester, 1985.

(5) Randles, J. E. B. *Trans. Faraday Soc* **1948**, *44*, 327.

(6) Marinesco, S.; Carew, T. J. *J. Neurosci. Methods* **2002**, *117*, 87-97.

(7) Meulemans, A. *Neurosci. Lett.* **2000**, *294*, 125-129.

(8) Ye, B. X.; Xia, P.; Lin, L. *Microchem J.* **2000**, *64*, 125-130.

(9) Meulemans, A. *Neurosci. Lett.* **1993**, *157*, 7-12.

(10) Oldham, K. B. *J. Electroanal Chem.* **1981**, *122*, 1.

(11) Fleishmann, M., Pons, S., Rolison, D., Schmidt, P *Ultramicroelectrodes*, Datatech Systems London, 1987.

(12) Ding, Z. Ph.D. Thesis, EPFL, Switzerland 1999.

(13) Samec, Z.; Marecek, V.; Homolka, D. *Faraday Discuss.* **1984**, 197-208.

(14) Kihara, S.; Suzuki, M.; Maeda, K.; Ogura, K.; Umetani, S.; Matsui, M.; Yoshida, Z. *Anal. Chem.* **1986**, *58*, 2954-2961.

(15) Kihara, S.; Yoshida, Z.; Fujinaga, T. *Bunseki Kagaku* **1982**, *31*, E297-E300.

(16) Wilke, S. *J. Electroanal. Chem* **1991**, *301*, 67-75.

(17) Parker, A. J. *Electrochim. Acta.* **1976**, *21*, 671.

(18) Czapkiewicz, J., Czapkiewicz-Tutaj, B. *J. Chem. Soc. Faraday Trans. I* **1980**, *76*, 1663.

(19) Robinson, R. A. Stokes, R. H. *Electrolyte Solution, 2nd Ed,*: Butterworths Scientific Publications, London, 1959.

(20) Abraham, M. H., Danil de Amor, A. F. *J. Chem. Soc. Faraday Trans. I* **1976**, *72*, 955.

(21) Nagatani, H.; Iglesias, R. A.; Fermin, D. J.; Brevet, P. F.; Girault, H. H. *J. Phys. Chem. B* **2000**, *104*, 6869-6876.

CHAPTER FOUR

ELECTRON TRANSFER

4.1. Introduction

The purpose of the work described in this chapter was to study simple heterogeneous electron transfer (HET) reactions across the water | 1,2-DCE interface. The reactions considered are:

$$O_1^w + R_2^o \rightleftharpoons R_1^w + O_2^o \qquad (4.1)$$

where O and R are the oxidised and reduced components of the redox couples present in the aqueous (w) and organic (o) phases respectively.

HET reactions are important processes in several areas of chemistry, physics and biology and these have been studied both theoretically[1,2] and experimentally.[3,4] Progress in reaching a complete understanding of this ubiquitous reaction is slow and has been hampered by a lack of experimental data. This is due to the small number of systems available which are not complicated by additional reactions such as partitioning of neutral species, coupled ion transfer or competing chemical reactions. The experimental requirements to study electron transfer (ET) without side reactions include, stability of both the oxidised and reduced forms of the redox species in the chosen solvents, absence of partitioning and inert base electrolytes.

Finding an experimental system that meets all of the above criteria is difficult. Choice of a suitable organic redox couple is often the main stumbling block. The hexacyanoferrate - ferrocene system in nitrobenzene[4-6] and DCE[7] was found to be complicated by interfacial ion pairing and the transfer of the ferricenium ion respectively. The hexacyanoferrate | lutetium bis-phthalocyanine system[8] and the

hexacyanoferrate | TCNQ system[9] at the water | 1,2-DCE interface have also been studied. However, it was the hexacyanoferrate-lutetium biphthalocyanines system that gave the first evidence of true ET across inhomogeneous media.[3] The extremely hydrophobic nature of this high molecular mass compound makes coupling of ion (IT) and ET highly unlikely. Ruthenium based complexes have also been used previously as the organic redox species. For example, Cheng and Schiffrin investigated the redox behaviour of the hydrophobic, DCE soluble, stable complex bis(pyridine)*meso*-tetraphenylporphyrinato ruthenium(II).[10]

In the present study three Ru^{+2} six-coordinate ruthenium complexes with a general structure- trans-$Ru(L\text{-}L)_2Cl_2$, where L is one of three bidentate ligands (a diphosphine), were chosen as the organic redox couples. The three ligands were 1,2-bis(diphenylphosphino)ethane (**1**), bis(diphenylphosphino)methane (**2**), and 1,1-bis(diphenylphosphino)ethene (**3**) (see Figure 4.1). There has been a great deal of recent interest in this type of complex due to its importance in homogenous catalysis.[11-14] From an electrochemical viewpoint coordinatively saturated complexes of Ru^{+2} have the twin advantages of chemical stability and accessible Ru^{+2}/Ru^{+3} redox states. Importantly for measurements at the interface between two immiscible liquids (ITIES), the complexes are soluble in 1,2-DCE yet sufficiently hydrophobic to ensure they do not transfer to the aqueous phase in the potential region of interest. In addition, their synthesis is relatively straightforward.[15-16] It was expected that conclusions regarding values of the measured rate constants could be drawn by considering the structures of the complexes.

To ensure that HET occurs within the available potential window, the equilibrium potential of the aqueous redox couple and the formal potential of the organic redox

species should not differ significantly.[3] For this reason the redox properties of the aqueous and organic redox species were first studied separately in order to determine the equilibrium and formal potentials respectively. The redox properties of the ruthenium complexes were characterised at the Pt microelectrode | electrolyte interface in 1,2-DCE using cyclic voltammetry. This allowed the assessment of electrochemical reversibility as well as measurement of their formal half wave potentials.

The ferro/ferricyanide couple (a fast redox couple) was chosen as the aqueous redox species for the following reasons. The couple is soluble at high concentrations and it undergoes outer sphere ET. Both components are commercially available and are stable under the experimental conditions chosen, and the equilibrium potential of the hexacyanoferrate couple can be easily changed by varying the Fe^{2+} : Fe^{3+} concentration ratio and the value calculated through the Nernst equation. Moreover, this couple has been widely used in similar studies and comparison of the results with published data[3,6,7,10,17,18] is facilitated.

Techniques for the determination of reversible[19] and quasi-reversible[20-21] kinetics are used to study the electron transfer involving these redox species at both the metal | electrolyte and electrified liquid | liquid interfaces.

4.2. Experimental

4.2.1. Oxidation of Ru(II) complexes at a Pt microelectrode

The supporting electrolytes used were $TBAPF_6$ in the organic phase and TBACl in the aqueous reference phase. Fresh solutions were prepared prior to each measurement. The electrochemical experiments were carried out using the set-up described in Chapter 3. Measurements were preformed using a three-electrode potentiostat (PGSTAT 20, Eco Chemie, Netherlands) in a two-electrode configuration. A Pt microelectrode was used as the working electrode and a SCE reference electrode, dipped in the aqueous reference phase, served as the reference electrode. Cell 4.1 was used for all the microelectrode experiments.

SCE	10mm TBACl (aq)	2mM $TBAPF_6$ +0.5mM RuL_2Cl_2 (DCE)	Pt (10 μm)

Cell 4.1

Typically, a 350 μl aliquot of a 2 mM stock solution of the analyte in 1,2-DCE was added to the organic phase (1.4 ml) using an Eppendorf micropipette. The organic phase was allowed to equilibrate for 5 minutes prior to recording the cyclic voltammograms. The steady state polarisation curve was then recorded at a sweep rate of 5 mVs^{-1} to avoid hysteresis associated with higher sweep rates. The cell potential was converted to the formal potential referred to an aqueous reference electrode (SHE) as described in Chapter 3.

4.2.2. Equilibrium potential of the hexacyanoferrate redox couple

The equilibrium potentials of solutions with various ratios of ferrocyanide : ferricyanide in 1M Li_2SO_4, were measured versus SCE using a high impedance voltmeter. A large area Pt coil electrode was used. The measured potentials correspond to Cell 4.2.

$$\text{SCE} \left| \begin{array}{c} 1\text{M } Li_2SO_4 \\ +\,y Fe^{+2}/z Fe^{+3} \\ (aq) \end{array} \right| \text{Pt}$$

Cell 4.2

The ratio y/z was varied between 0.01 and 100.

4.2.3. Oxidation of Ru(II) complexes at the ITIES

Having characterised separately the aqueous and organic redox couples and successively matched the potentials, heterogeneous electron transfer at the ITIES could be studied. Four-electrode cyclic voltammetry measurements at the liquid | liquid interface were carried out as described in Chapter 3 and iR compensation was employed in all cases.

The electrochemical cell 4.3 was used for all liquid | liquid voltammetric experiments. The supporting electrolytes were LiCl and Li_2SO_4 in the aqueous phase and TPAsTPBCl in the organic phase. Fresh solutions were prepared prior to each measurement. Electrochemical experiments were carried out using an Autolab potentiostat (PGSTAT 20, Eco Chemie) in the four-electrode mode. A SCE and Pt coil served as aqueous reference and counter electrodes respectively while a Pt coil and SCE dipped in a 10 mM TPAsCl aqueous solution served as the organic counter and reference electrodes respectively. σ represents the polarisable water | 1,2-DCE interface under investigation. A schematic representation of the cell used for these experiments is given in Chapter 3.

SCE | 10mm TPAsCl (aq) | 10mM TPAsTPBCl + r mM RuL_2Cl_2 (DCE) | σ | x M $[Li^+]$ 0.001M/0.1M Fe^{+2}/Fe^{+3} (aq) | SCE

Cell 4.3

The applied potential is the sum of the several contacting potential differences as described in Chapter 2. An increase in cell potential is associated with the potential of the aqueous phase becoming more positive with respect to the organic phase.

4.3. Results and Discussion

4.3.1. Oxidation of Ruthenium complexes on a Pt microelectrode

The cyclic voltammetry for the oxidation of the three Ru(II) complexes studied on a Pt microelectrode is shown in Figure 4.2. As expected, only one oxidation wave is observed corresponding to the oxidation of Ru^{+2} to Ru^{+3}. Cell potentials were converted to the SHE scale as described in Section 3.3.1.1 and the potential scale in all graphs is referred to this electrode.

Due to the small size of the microelectrode (d = 10 μm), mass transfer is controlled by approximately spherical diffusion (inlaid microdisc) and the current-voltage response is at steady state. The diffusion coefficients were calculated from the limiting current, i_L, using Equation 3.4 and the values obtained are shown in Table 4.1.

4.3.1.1. Evaluation of the reversibility of the reaction

Semi-logarithmic analysis of the steady state polarisation curves was carried out in order to determine the reversibility of the redox reactions and to obtain the half wave potential for the redox couples. For a reversible process a plot of E vs. log $[(I_L-I)/I]$ is linear with a slope of 59/n mV $decade^{-1}$ and the y-intercept corresponds to the half wave potential ($E_{1/2}$) for the Ru^{+2}/Ru^{+3} couple according to equation 3.5, n is the number of electrons transferred. Typical results are shown in Figure 4.3. and a linear

(in all cases R^2>0.995) dependence was observed. The slopes of these plots and values $E^{1/2}$ are given in Table 4.1.

The polarisation curve for **2** was typical of a diffusionally controlled, one electron transfer process with a slope of 60 mV/decade. Previously, it had been reported that the Ru^{+2}/Ru^{+3} redox reaction for complex **2** is reversible.[15,16] Here the redox chemistry of this complex is found to be reversible. However the slope of the semi-logarithmic plots for **1** and **3** are 85 and 76 mV/decade respectively, implying that these processes are quasi-reversible.

Voltammograms were also analysed for reversibility according to the Tomes criteria,[22] which predicts $|E_{3/4}-E_{1/4}|=56.4/n$ mV at 25 °C for reversible charge transfer. $E^{3/4}$ and $E^{1/4}$ refer to the three and one-quarter wave potentials respectively.

From the experimentally determined $n\Delta E^{1/4}$ and $n\Delta E^{3/4}$ ($\Delta E^{1/4}=E^{1/4}-E^{1/2}$ and $\Delta E^{3/4}=E^{3/4}-E^{1/2}$), values for the transfer coefficient (α), $n\Delta E^{0'}$ and λ were obtained from Reference[20] where $E^{0'}$ is the formal potential and λ is the dimensionless rate constant given by:[20]

$$\lambda = k^{0,\mu} / m_o \qquad (4.2)$$

where $k^{0,\mu}$ is the standard rate constant and m_o is the mass transfer coefficient. Boundary values of $15 \geq \lambda \leq 10^{-2(1+\alpha)}$ have been suggested for quasi-reversible species.[22]

4.3.1.2. Evaluation of the rate constant

The standard rate constants for the quasi-reversible processes at the microelectrode | electrolyte solution interface ($k^{0,\mu}$) were calculated to be 0.65 x $10^{-2}$and 0.13 x 10^{-2} cm s^{-1} for complexes **1** and **3** respectively using the following equation:[20]

$$k^{o,\mu} = D\frac{\lambda}{r}. \qquad (4.3)$$

D is the diffusion coefficient of the redox species. The boundary values $0.3v^{1/2} \geq k^0 \leq 2 \times 10^{-5}\ v^{1/2}$cm s^{-1} for the rate constant of a quasi-reversible species has been suggested.[22]

It is interesting to compare the values of the rate constant for the complexes. Complex **2** retains its trans geometry upon electrochemical oxidation,[23] thus the reaction under investigation is:

$$trans\text{-}Ru^{II}(L\text{-}L)_2Cl_2 \rightleftarrows trans\text{-}Ru^{III}(L\text{-}L)_2Cl_2 + e^- \qquad (4.4)$$

Since there is no change in conformation upon reaction, it would be expected to be fast i.e. the inner reorganisation should be small. Furthermore molecular modelling (Hyperchem Version 7) of this complex shows that its redox centre is the most open of the three. Both of these reasons explain why the ET reaction for this complex can occur with relative ease.

3 is also known to retain its trans geometry upon electrochemical oxidation[15] and it is likely that **1** behaves in an analogous fashion, however molecular modelling shows that the Ru centres for both of these complexes are more shielded by the ligands than is the case for complex **2** which may account for the differences in the rates of the ET

step. Molecular models show that the redox centre in **3** is the most shielded of the three and as a result the rate constant for **3** is lower than the other complexes.

4.3.1.3 Evaluation of diffusion coefficients

Diffusion coefficients (D) of 4.2, 4.0 and 3.6x 10^{-6} cm^2s^{-1} were calculated for complexes **1, 2** and **3** respectively, using values of the limiting current (I_L) obtained from Figure 4.2 and Equation 3.4.

4.3.1.4. Evaluation of the effective hydrodynamic radii

The effective hydrodynamic radius of the diffusing species (r_h) can be calculated using the Stokes Einstein Equation.[24,25]

$$r_p = \frac{kT}{6\pi\eta D} \qquad (4.5)$$

where k is the Boltzmann constant, T is the absolute temperature and η is the viscosity of the solvent. The value of r_h is related to the movement of the species through the solution. Values of r_h and the molecular radius are in reasonably close agreement for all of the complexes (Table 4.3), however the Stokes Einstein equation predicts that complex **3** has the largest diameter of the three, while its molecular radius is slightly smaller than the others. As the diffusion coefficients differ only slightly (Table 4.3) it is expected that the hydrodynamic radii for all three species would be similar.

4.3.1.5. Evaluation of the formal reduction potential

For a reversible couple, formal reduction potential, ($E^{0'}$) is given approximately by $E^{1/2}$,[22] while for quasi-reversible processes E^0 is calculated from the following relationship:[20]

$$n\Delta E^{o} = E^{o'} - E_{1/2} \qquad (4.6)$$

The values of $E^{o'}$ obtained here are within approx. 150mV of those in literature (Table 4.8). This is reasonable when the fact that the literature values are not corrected for the liquid junction is considered. Complex **2** has the lowest $E^{o'}$ (557 mV), it the least difficult of the three to oxidise. The ligand has a shorter carbon backbone than **1**, hence the metal centre in this complex is the least sterically crowded of the three. **3** has an $E^{o'}$ (748 mV) that is mid-way between that of the other two complexes, resulting form the relative shape and size of this ligand being intermediate between the other two. As can be seen from Table 4.8 altering the donor atom for these compounds affects the Ru^{+2}/Ru^{+3} potentials.

4.3.2. Equilibrium measurements of the ferrocyanide/ferricyanide couple

Close matching of the potentials of the two redox couples was necessary to ensure that ET was observed within the potential window. To do this the equilibrium potentials for various concentration ratios of the Fe^{+2}: Fe^{+3} couple were measured. The supporting electrolyte was 1 M Li_2SO_4. The results are shown in Table 4.4. (all potentials are quoted versus the SHE).

The theoretical equilibrium electrode potential (E^{eq}) was calculated for each of the different ratios according to the following approximation of Nernst equation:

$$E^{eq} = E^{o} + \frac{RT}{F} \ln \frac{[Fe^{+3}]}{[Fe^{+2}]} \qquad (4.7)$$

The values calculated for the equilibrium electrode potential were compared with the experimentally determined values. E^{o} is the standard potential of the reaction, $[Fe^{+2}]$ and $[Fe^{+3}]$, the experimental concentrations of the ferricyanide and ferrocyanide solutions were used in place of activities. The number of electrons involved in the reaction is one and E^{0} for the $[Fe(CN)_6]^{3-}/[Fe(CN)_6]^{4-}$ redox couple is 358mV vs SHE.[26]

It was found that the equilibrium potential of the $[Fe(CN)_6]^{3-}$: $[Fe(CN)_6]^{4-}$ couple provides the correct range of potentials to match those of the organic couples. For this reason the hexacyanoferrate system was deemed suitable to study the electron transfer at the liquid-liquid interface for the Ru couples.

4.3.3. Heterogenous electron transfer involving Ru complexes

Information obtained from the studies of the redox behaviour of the ruthenium based electron donors and the electron acceptor Fe^{2+}/Fe^{3+} in their respective phases, allows the matching of the potentials of the two couples. This makes it possible to study the heterogeneous electron transfer process in a liquid | liquid system.

It is important that the concentration of the aqueous redox couple should be much greater than that of the organic redox couple. Since in a liquid | liquid system peak separation in excess of 60 mV may be observed under reversible conditions as a result of diffusion unless the concentration of one species is greatly in excess of the other.[27] For the conditions under which these experiments were carried out, reaction 4.1 can be considered to be pseudo-first order reaction. The reversible half-wave potential for the HET reaction studied ($\Delta_o^w\phi^{0,ET}$) is considered to be dependent on the difference between the standard redox potential of the organic redox couple and the equilibrium potential of the aqueous redox couple measured with respect to the same reference electrode, $E^{o,org}_{Ox_2/Red_2}$ and $E^{o,aq}_{Ox_1/Red_1}$ [20,21,28-30] i.e.

$$\Delta_o^w\phi^{o,ET} = E^{o,org}_{Ox_2/Red_2} - E^{o,aq}_{Ox_1/Red_1} \qquad (4.8)$$

Typically the concentrations used were 100 and 2 mM respectively for all experiments so that the current response could be considered to be limited only by the diffusion of the organic redox couple to the interface.

Figure 4.4 shows the cyclic voltammogram for the base electrolyte of the ITIES system studied. The limits of the polarisation window result from the transfer of the ionic components of the supporting electrolyte. The numerical value of the limits are determined by the activity and Gibbs energies of transfer of the ions in question, in accordance with the criteria described in Chapter 2 for an ideally polarised ITIES. In the case of the system described in Cell 4.2, the negative limit is due to the transfer of $TPAs^+$ from the organic to the aqueous phase and the positive limit to the transfer of $TPBCl^-$ (or Li^+) in the opposite direction. As outlined in the previous section, it is

possible to match the equilibrium redox potential of the aqueous redox couple with the formal redox potential of the organic redox species to obtain heterogeneous electron transfer within this available potential window.

In the two-phase system with a concentrated aqueous redox system, the analysis of results can be carried out using the classical theory for metal electrodes,[22] since diffusion of the dilute reactant is the limiting process.

The addition of the aqueous redox couple to Cell 4.3 in the absence of the organic couple had no effect on the voltammetric response. Similarly, adding only the organic redox couple to the system, it was observed that for all three redox species the resulting voltammograms follow the baseline, as shown for compound **1** in Figure 4.4. Due to the hydrophobic nature of the organic redox couples considered, it can be assumed that they do not partition between the organic to the aqueous phases.

When both redox active species are present there is a clear change in the voltammetric response. Figure 4.5 shows the sweep rate dependence for Cell 4.3 where the aqueous base electrolyte is 10mM LiCl. The interfacial reaction was:

$$Fe(CN)_6^{-3}(w) + [Ru^{+2}Cl_2L_2]\,(o) \rightleftarrows Fe(CN)_6^{-2}(w) + [Ru^{+3}Cl_2L_2]^{+}\,(o) \qquad (4.9)$$

The response is peak shaped as expected for linear diffusion of a redox species to a planar macroelectrode surface. The oxidation occurs quite close to the positive edge of the available potential window making it difficult to accurately determine peak potentials and currents. However, a higher concentration of the aqueous base electrolyte (Li_2SO_4), has a salting-out effect on the transfer of the base electrolyte ions which enlarges the available potential window[31,32] and makes it possible to

observe electron transfer without the complication of simultaneous base electrolyte transfer. The effect of increasing the aqueous base electrolyte concentration on the available potential window can be seen by comparing Figures 4.5 and 4.6. The peak potential ($\Delta^{w}_{o}\phi$) for the oxidation was 78 mV and the peak separation was 157 mV at a sweep rate of 1 mVs^{-1}.

Even at the slowest scan rate considered (1 mVs^{-1}), the peak separation is considerably larger than predicted for a one electron reversible transfer process (157, 206 and 105 mV for **1**, **2** and **3** respectively). If it is assumed that the electron transfer reaction is simple and that the apparent quasi-reversible to irreversible response is a reflection of the electron transfer step, the standard rate constant is very small. For sweep rates greater than 90 mVs^{-1} the peak separation increased to such an extent that the peak maxima could not be measured as it occurred outside the potential window. In order to ascertain that this effect was not an artefact due to poor iR compensation the transfer of TMA^{+} was investigated under similar experimental conditions. The cyclic voltammetry obtained in this case were as expected for reversible charge transfer i.e. a peak separation of 59 mV invariant with increasing sweep rate.

For two of the redox couples considered, (**1** and **3**) this result is not unexpected as the response at a metal electrode | electrolyte interface was also characteristic of slow electron transfer kinetics. However, for the oxidation of **2**, the semi-logarithmic analysis of the microelectrode results showed reversible electron transfer. Thus, the irreversibility observed for **2** at the ITIES is not due to the reorganisation energy of the complexes, neither can this effect be due its chemical instability in contact with

aqueous solution.[15] Previously, Cunnane et al.[7] reported similar behaviour, i.e. irreversible electron transfer between two redox couples at the ITIES couples, although each couple behaved reversibly when in contact with a metallic electrode. It was proposed that the lower value of the rate constant at the ITIES resulted from the larger separation between the redox centres in the organic and aqueous phases. It is likely that this distance effect is also responsible for the increased irreversibility observed for all three couples at the ITIES in the present study and this effect is discussed in more detail in the following section. Adsorption and/or competing (coupled) reactions may also play a part in the observed differences.

The most striking feature that is apparent from the cyclic voltammetry experiments is the dependence of the peak separation, $\Delta(\Delta^{w}_{o}\phi)$, on scan rate, showing that the complexes behave irreversibly at the ITIES (Figures 4.6, 4.7 and 4.8 refer to complexes **1**, **2** and **3** respectively). This was anticipated from the microelectrode results for **1** and **3**. Peak separation of 72 and 121 mVs^{-1} was predicted for **3** at sweep rates of 1 and 40 mVs^{-1}respectively based upon its behaviour at the microelectrode for example. The observed behaviour, however, was indicative of slower than predicted kinetics and the actual peak separations for **3** at these sweep rates were 105 and approximately 350 mV. For complex **2,** it was necessary to extend the negative limit of the voltammogram by 200 mV, in order that both peak maxima occurred within the potential window, on increasing the scan rate from 10 to 40 mVs^{-1}.

Further evidence for the irreversibility of the redox reactions at the ITIES came from the dependence of the peak potential (E_p) on sweep rate. A representative plot is shown in Figure 4.9. As predicted from the theory of irreversible electron transfer

reactions, the peak potential was linearly dependent on the log υ. The peak current was linearly dependent on the square root of the sweep rate but no conclusions could be made from this about the reversibility of the reaction since at low sweep rates quasi-reversible and irreversible reactions show this dependence.[19]

Comparison of the reduction potentials obtained from the microelectrode and liquid | liquid systems shows that the complex that had the most positive redox potential at the microelectrode has the least positive potential at the liquid-liquid interface and vice versa. This strengthens the suggestion that factors other than those seen at the metal electrode | electrolyte interface, are observed in the liquid | liquid system e.g. a greater separation between the redox centres. Of the three complexes, **2** has the highest value of $\Delta^{w}_{o}\phi^{1/2}$ at the liquid-liquid interface (149 mV) i.e., it is most difficult to oxidise. Again **3** has a reduction potential that is intermediate between the other two complexes (52 mV).

The value for the dimensionless rate constant parameter (Ψ) was determined from the peak separation (measured at the slowest sweep rate 1 mVs^{-1}) with tables published in literature.[22,33] The standard rate constant for the HET reaction of the quasi-reversible species at the ITIES ($k^{o,\,ITIES}$) was obtained from:[19,34]

$$\psi = k^{0,ITIES} / \sqrt{D_O \pi \nu (nF/RT)} \qquad (4.10)$$

In what follows the diffusion coefficients of the oxidised and reduced forms are assumed to be equal. The values obtained for the rate constant for the electron transfer reaction at the ITIES ($k^{0,\,ITIES}$) is extremely low for all three Ru complexes

(Table 4.6), much lower than those measured at the microelectrode | electrolyte interface (Table 4.2).

Experimentally the degree of reversibility of a system is determined by the sweep rate, at small sweep rates (long times) irreversible systems may yield reversible waves while at larger sweep rates (shorter times) the reaction appears irreversible. For a quasi-reversible system the wave shape and the peak separation are functions of scan rate, k^0, α and E^{λ} (switching potential of cyclic voltammogram), ie i_p E^p and $E^{p/2}$ depend on the parameters lambda (Λ) and alpha (α).

The most interesting result obtained here is the greater decrease in the value of the rate constant when replacing a metal electrode by a redox couple present in high concentrations in the aqueous phase. This result is discussed in the following section.

4.3.4. Estimation of the distance of closest approach at the ITIES

ET is usually considered to occur via tunnelling of the electron between states in the electrode and those in the reactant. The rate of electron tunnelling decreases exponentially with increasing distance and is controlled by the tunnelling parameter β, which depends on the height of the energy barrier and the nature of the intervening medium. The standard rate constant, k^0, relates to the tunnelling decay constant according to:[35-39]

$$k^0(x) = k^0(0)\exp[-\beta(x - x_0)] \qquad (4.11)$$

where $k^0(0)$ and $k^0(x)$ are the standard heterogeneous rate constants for the HET reaction at the distance of closest approach (x_0) and at a distance of x from the electrode surface respectively.

Knowing the standard rate constants in each system and assuming that β is constant. it is possible to calculate the difference between the distances of closest approach at the ITIES and at the Pt microelectrode (Δx) as follows:

$$\Delta x = x^{ITIES} - x^{\mu} = \frac{1}{\beta}\ln\left[k^0(x)^{\mu} / k^0(x)^{ITIES}\right] \qquad (4.12)$$

The increased distance between the two redox species at the ITIES over the distance between the Pt microelectrode and the redox couple explains why the values of the rate constant for the HET at the ITIES ($k^{0,\ ITIES}$) is significantly lower than those measured at the microelectrode | electrolyte interface ($k^{0,\mu}$).

As previously mentioned, the value of β is dependent on the nature of the medium through which electron tunnelling takes place. The value of β for a saturated hydrocarbon spacer (CH_2) is well established (≈1 $Å^{-1}$).[37,39-42] For all complexes the Ru redox centre is strongly chelated by hydrocarbon ligands, and electron tunnelling must occur through the ligand layer as well as through the intervening medium. The intervening medium for the electrochemical measurements at the Pt microelectrode is a chlorinated hydrocarbon while in the ITIES system the aqueous and organic couples are separated by a solvent layer at each side of the ITIES due to their extremely hydrophilic and hydrophobic natures respectively. For the purpose of the calculations it is assumed that the value of the tunneling decay constant for the two systems are not appreciably different.

4.4. Conclusions

The oxidation of ruthenium complexes was investigated using a Pt microelectrode. Tomes criteria and semi-logarithmic analysis, both indicated that the oxidation of complex **2** is reversible, while the other two compounds studied are quasi-reversible. This difference can be rationalised by considering differences in geometry of the complexes particularly the shielding of the redox centre in the couple.

The reduction potentials obtained at the microelectrode are in line with data obtained in literature. This is expected as the systems used are similar (i.e. the metal electrode electrolyte solution interface).

At the ITIES, potential match between the ruthenium complexes and the fast redox couple Fe^{+2}/Fe^{+3} was possible and the system showed faradaic current, i.e. HET was observed.

Comparison of the experimental results obtained from microelectrode and ITIES measurements show some differences (Table 4.8). The systems are similar in that in both cases an electron acceptor is present in the phase adjacent to the oxidisible ruthenium complex and when a suitable potential is applied, HET takes place. It is possible that adsorption of the redox active complex occurs at the metal electrode, facilitating ET. At the liquid | liquid interface, the adsorption of redox active species is negligible. The increased distance between the two couples explains why the rate of electron transfer at the ITIES is lower that that at the metal electrode | electrolyte solution interface.

Complex **2** at the liquid | liquid interface showed deviations from the behaviour expected from the microelectrode results, the other two redox couples were quasi-reversible at the metal electrode and also show quasi-reversible kinetics at the liquid | liquid interface. However, all three complexes were quasi-reversible at the ITIES.

As can be seen from Table 4.8 altering the donor atom for these compounds effects the Ru^{+2}/Ru^{+3} potentials for this family of complexes, this is clearly seen from the values for the half wave potentials for the three complexes at the platinum microelectrode and at the ITIES. However this difference is more marked at the liquid-liquid interface than at the metal | electrolyte interface.

The present system meets many of the criteria set down for an ideal heterogeneous liquid-liquid electron transfer system. Due to their highly hydrophobic nature it is unlikely that the oxidised forms partition to any extent, the reduced forms do not partition, thus the coupling of ion and electron transfer is unlikely.

Table 4.1 Experimental results obtained from the analysis of the cyclic voltammetry for 0.5 mM $RuCl_2L_2$ at a sweep rate of 5 mVs^{-1} on a 10 μm Pt microelectrode ($E_{½}$ versus SHE).

Complex	Colour	$E_{1/2}$ /mV	Slope /mVdecade^{-1}	I_L /nA	10^6D /cm^{2}s^{-1}	$E_{3/4}$-$E_{1/4}$ /mV
1	Orange	796	85	0.406	4.21	86
2	Yellow	557	60	0.381	3.95	59
3	Brown	678	76	0.344	3.56	76

Slope refers to the slope of the semi-logarithmic current function analysis and D is the diffusion coefficient of the complex.

Table 4.2 Kinetic parameters obtained from the experimental data obtained from Figure 4.2 using Reference[20].

Complex	$\Delta E_{1/4}$ /mV	$\Delta E_{3/4}$ /mV	α	λ	$n\Delta E^{o'}$ /mV	$10^{-2}k^{0,\mu}$ /cm s^{-1}	$E^{o'}$ /mV
1	42	44	0.6	0.77	37.4	0.65	833
2	29	30	-	>10	0	<2.1	557
3	37	39	0.77	0.18	69.6	0.13	748

Where $\Delta E_{1/4}$ and $\Delta E_{3/4}$, are the experimentally determined, one and three quarter potentials respectively, n is the number of electrons transferred per mole of reactant. Values for k^0 and $E^{o'}$ are and calculated using parameters obtained in Table II of Mirkin et al.[20]. α is the transfer coefficient, λ the dimensionless rate constant and $E^{o'}$ the formal potential.

Table 4.3 Hydrodynamic radii (r_h) calculated from Equation 4.5 and average radii of the complexes estimated from molecular models (r_{av}).

Complex	r_h /Å	r_{av} /Å
1	13.0	13.5
2	13.8	13.5
3	15.3	13

Table 4.4 Theoretical and measured equilibrium potentials for various concentration ratios of Fe^{+2}: Fe^{+3} vs SHE. The supporting electrolyte was 1M Li_2SO_4.

$[Fe^{+2}]$ /M	$[Fe^{+3}]$ /M	E_{meas} /mV	E_{calc} /mV
0.1	0	315	-
0.1	0.001	398	240
0.1	0.01	456	299
0.1	0.1	521	358
0	0.1	701	-
0.001	0.1	628	476
0.01	0.1	572	417

Table 4.5 Data obtained from analysis of two-phase experiments for r mM $RuCl_2L_2$ at a sweep rate of 1 mVs^{-1}, the aqueous supporting electrolyte is 0.5M Li_2SO_4.

L	r /mM	$\Delta^w_o\phi^{1/2}$ /mV	$\Delta(\Delta^w_o\phi)$ /mV
1	2.00	005	157
2	1.75	149	206
3	1.75	052	105

Table 4.6 Calculated Ψ and $k^{0,\ ITIES}$ values for the complexes at the ITIES based on peak separation at 1mV s^{-1}, (D was calculated using data obtained from microelectrode measurements). Δx is the the difference between the distances of closest approach at the ITIES and at the Pt microelectrode.

Complex	*E_{pa}-E_{pc} /mV	Ψ	$10^{-4}k^{0,\ ITIES}$ /cm s^{-1}	Δx/Å
1	157	0.25	1.79	3.6
2	206	0.1	0.70	5.7
3	105	0.5	3.30	3.7

* Determined from experiment at a sweep rate of 1 mVs^{-1}.

Table 4.7 Parameters *Ψ and Ψ relate to actual and predicted behaviour of the complexes at the ITIES respectively. (Similarly $\Delta(\Delta^{w}_{o}\phi)$and $^{*}E_{pa}$-E_{pc} correspond to actual and predicted peak separation at the ITIES.) Predicted behaviour was based on observed behaviour at the Pt electrode | electrolyte solution interface (at a scan rate 1 and (40) mVs^{-1}). Obtained from References[22,33].

L	$\Delta(\Delta^{w}_{o}\phi)$ /mV	ψ /mV	*Ψ /mV	$^{*}E_{pa}$-E_{pc} /mV
1	157	0.25	9.03 (1.42)	63 (84)
2	206	0.1	-	<61
3	105	0.50	1.94 (0.31)	72 (121)

Table 4.8 Comparison of experimentally determined electron transfer potentials ($E^{0,calc}$) at a metal microelectrode, literature values ($E^{0,ref}$) and in the two-phase liquid | liquid system ($\Delta^{w}_{o}\phi^{1/2}$).

Complex	$E^{0,\mu}$ /mV	$^{*}E^{0,ref}$ /mV	$\Delta^{w}_{o}\phi^{ET}$ /mV	$^{**}\Delta^{w}_{o}\phi^{1/2}$ /mV
1	833	710[a]	5	205
2	557	420[b]	149	-71
3	748	590[c]	52	120

Where a=reference[16] b=reference [23] and c=reference[15]

*not corrected for the liquid junction

**calculated using Equation 4.8.

(a)

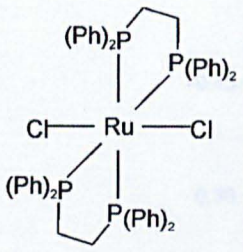

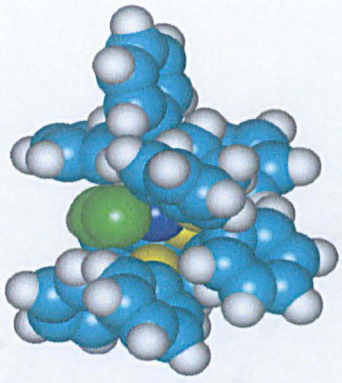

(b)

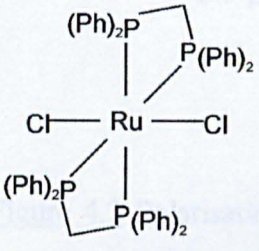

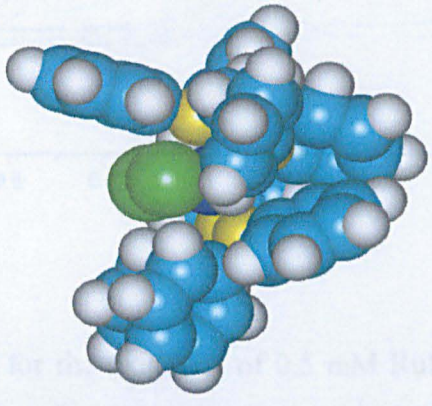

(c)

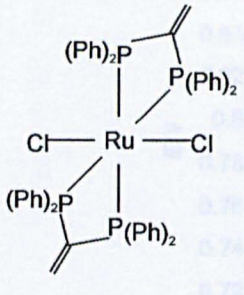

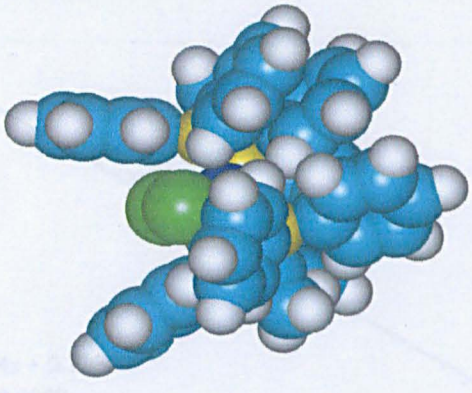

Figure 4.1 Molecular model images of the RuL_2Cl_2 complexes investigated (a) **1**, (b) **2** and (c) **3**. Ru=dark blue, Cl=green, P=yellow, C=pale green and H=white/grey.

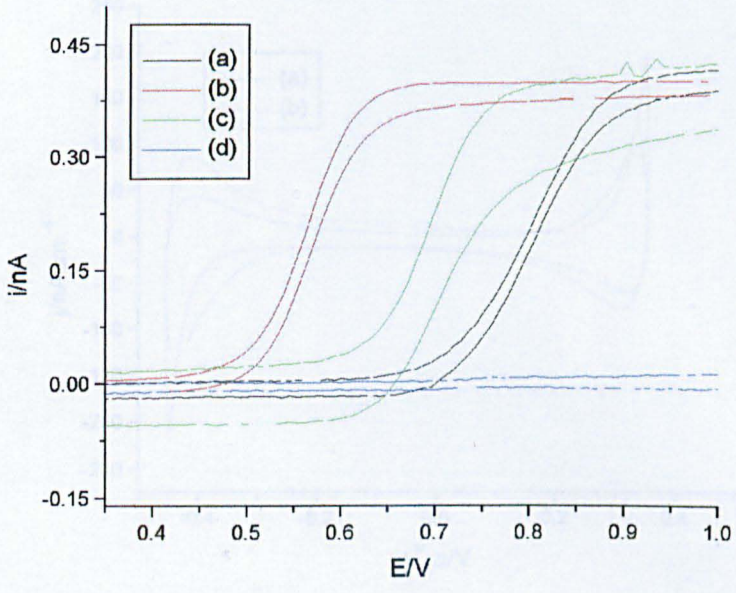

Figure 4.2 Polarisation curves for the oxidation of 0.5 mM RuL_2Cl_2 on a 10 μm Pt microelectrode in 1,2-DCE. The potential scale has been referred to the SHE scale. (a) **1**, (b) **2**, (c) **3** and (d) baseline.

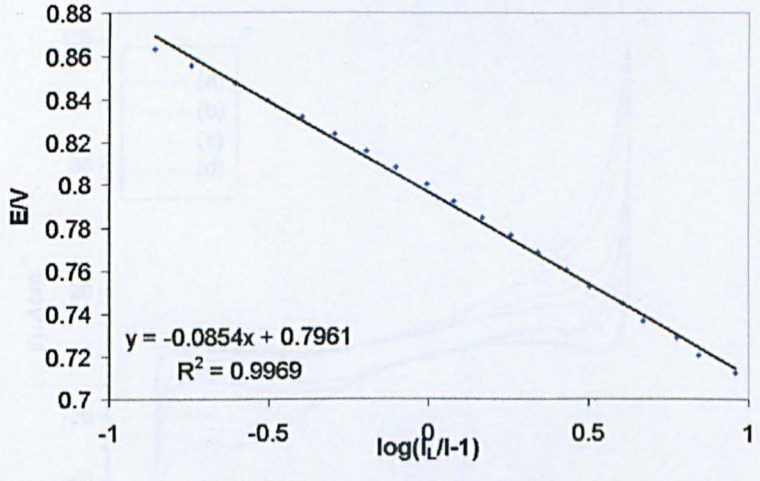

Figure 4.3 Semi-logarithmic plot of the steady state polarisation curve for the data in Figure 4.2 for the oxidation of 0.5 mM of compound **1** on a 10 μm Pt microelectrode in 1,2-DCE, showing a slope of 85 mV/decade.

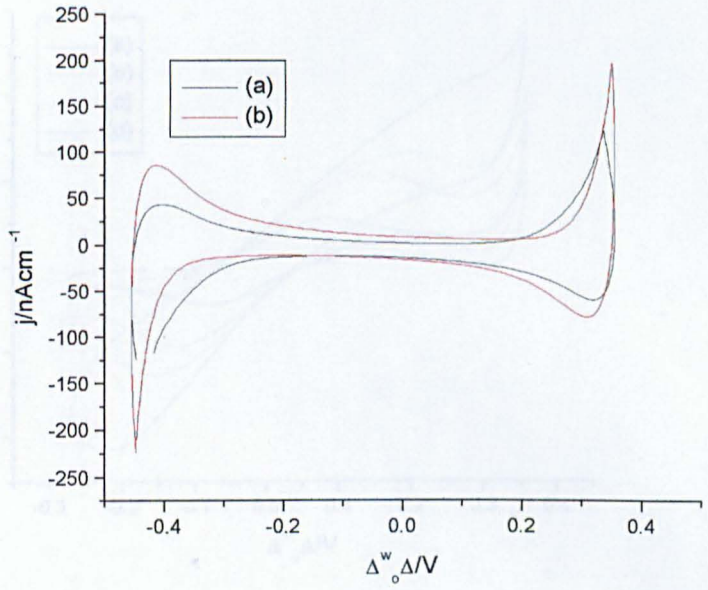

Figure 4.4 Cyclic voltammetry for the system described in Cell 4.3 at a sweep rate of 5 mVs^{-1}. The aqueous base electrolyte was 10mM LiCl. (a) in the absence of either electroactive species and (b) as (a), but with 2 mM of **1** present in the organic phase. No aqueous redox species was present.

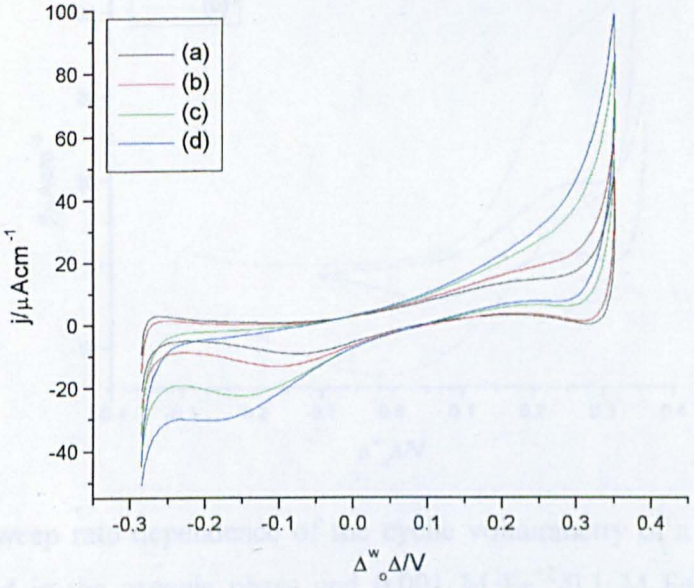

Figure 4.5 Sweep rate dependence for Cell 4.2 with 2mM **1** dissolved in the organic phase and 0.001 M Fe^{+2}/0.1 M Fe^{+3} present in the aqueous phase. The aqueous electrolyte was 10 mM LiCl. The sweep rates were: (a) 5, (b) 10, (c) 40 and (d) 90 mVs^{-1}.

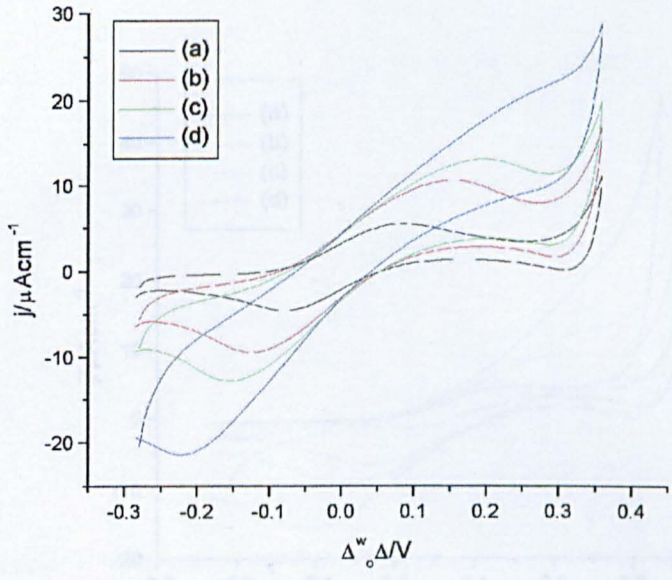

Figure 4.6 Sweep rate dependence of the cyclic voltammetry of a 2 mM solution of **1** dissolved in the organic phase and 0.001 M Fe^{+2}/0.1 M Fe^{+3} in the aqueous phase. The aqueous electrolyte was 1 M Li_2SO_4. The sweep rates were: (a) 1, (b) 5, (c) 10 and (d) 40 mVs^{-1}.

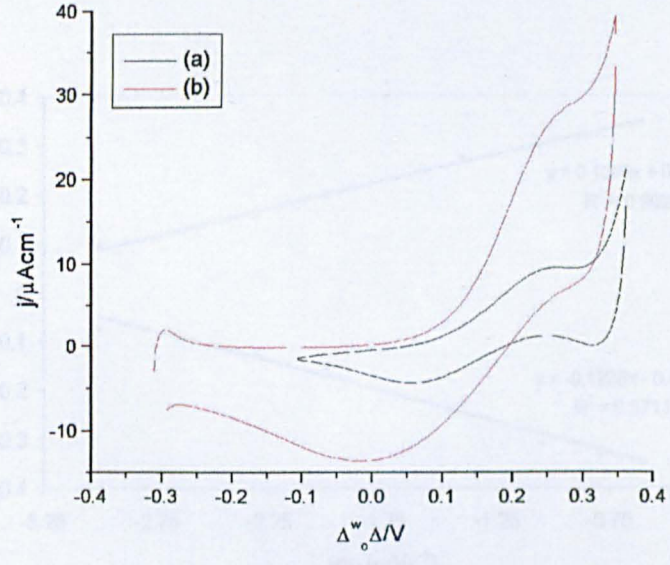

Figure 4.7 Sweep rate dependence of the cyclic voltammetry of a 1.75mM solution of **2** dissolved in the organic phase and 0.001 M Fe^{+2}/0.1 M Fe^{+3} in the aqueous phase. The aqueous electrolyte was 0.5 M Li_2SO_4. The sweep rates were: (a) 1 and (b) 40 mVs^{-1}.

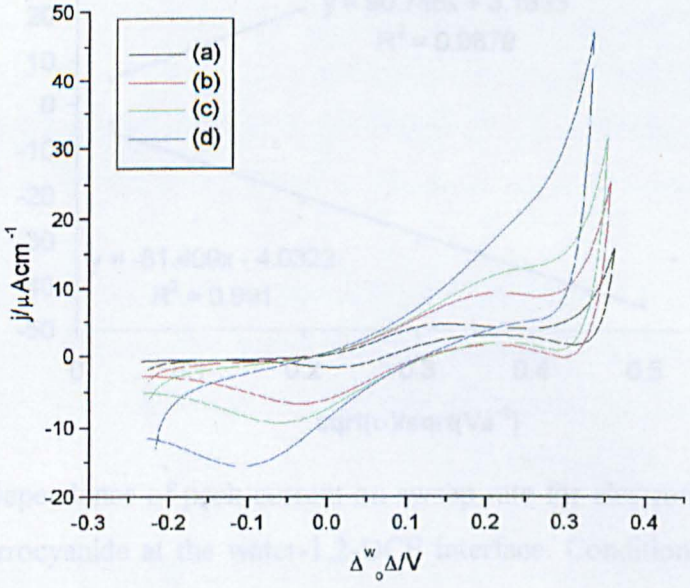

Figure 4.8 Sweep rate dependence of the cyclic voltammetry of a 1.75 mM solution of **3** dissolved in the organic phase and 0.001 M Fe^{+2}/0.1 M Fe^{+3} in the aqueous phase. The aqueous electrolyte was 0.5 M Li_2SO_4. The sweep rates were: (a) 1, (b) 5, (c) 10 and (d) 40 mVs^{-1}.

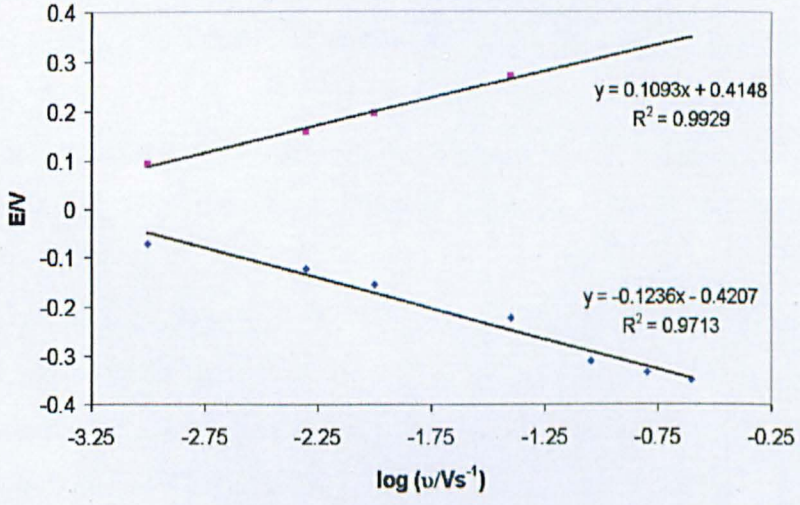

Figure 4.9 Dependence of peak potential on sweep rate for electron transfer between **1** and the hexacyanoferrate couple at the water-1,2-DCE interface. Conditions are the same as in Figure 4.6.

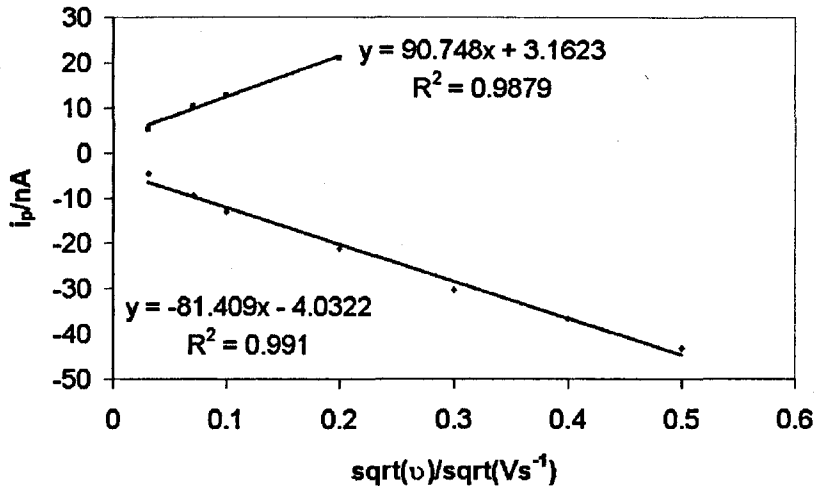

Figure 4.10 Dependence of peak current on sweep rate for electron transfer between 1 and ferri-ferrocyanide at the water-1,2-DCE interface. Conditions are the same as in Figure 4.6.

4. 5. References

(1) Girault, H. H. J.; Schiffrin, D. J. *J. Electroanal. Chem.* **1988**, *244*, 15-26.

(2) Kharkats, Y. I.; Volkov, A. G. *J. Electroanal. Chem.* **1985**, *184*, 435-442.

(3) Geblewicz, G.; Schiffrin, D. J. *J. Electroanal. Chem.* **1988**, *244*, 27-37.

(4) Samec, Z.; Marecek, V.; Weber, J.; Homolka, D. *J. Electroanal. Chem.* **1981**, *126*, 105-119.

(5) Samec, Z., Marecek, V., Homolka, D., *J. Electroanal. Chem.* **1983**, *158*, 25.

(6) Samec, Z.; Marecek, V.; Weber, J. *J. Electroanal. Chem.* **1979**, *103*, 11.

(7) Cunnane, V. J.; Geblewicz, G.; Schiffrin, D. J. **1995**, *40*, 3005-3014.

(8) Cheng, Y. F.; Schiffrin, D. J. *J. Chem. Soc.-Faraday Trans.* **1993**, *89*, 199-205.

(9) Cheng, Y. F.; Schiffrin, D. J. *J. Chem. Soc.-Faraday Trans.* **1994**, *90*, 2517-2523.

(10) Cheng, Y. F.; Schiffrin, D. J. *J. Electroanal. Chem.* **1991**, *314*, 153-163.

(11) Kundig, E. P.; Saudan, C. M.; Bernardinelli, G. *Angew. Chem.-Int. Edit.* **1999**, *38*, 1220-1223.

(12) Cucullu, M. E.; Nolan, S. P.; Belderrain, T. R.; Grubbs, R. H. *Organometallics* **1999**, *18*, 1299-1304.

(13) Nishibayashi, Y.; Takei, I.; Uemura, S.; Hidai, M. *Organometallics* **1998**, *17*, 3420-3422.

(14) Doucet, H.; Ohkuma, T.; Murata, K.; Yokozawa, T.; Kozawa, M.; Katayama, E.; England, A. F.; Ikariya, T.; Noyori, R. *Angew. Chem.-Int. Edit.* **1998**, *37*, 1703-1707.

(15) Barkley, J. V.; Higgins, S. J.; McCart, M. K.; Pounds, T. J. *Inorg. Chem.* **1997**, *36*, 6188-6196.

(16) Champness, N. R.; Levason, W.; Pletcher, D.; Webster, M. *J. Chem. Soc.-Dalton Trans.* **1992**, 3243-3247.

(17) Hanzlik, J.; Hovorka, J.; Samec, Z.; Toma, S. *Collect. Czech. Chem. Commun.* **1988**, *53*, 903-911.

(18) Quinn, B.; Lahtinen, R.; Murtomaki, L.; Kontturi, K. *Electrochim. Acta* **1998**, *44*, 47-57.

(19) Greef, R.; Peat, R.; Peter, L. M. *Instrumental Methods in Electrochemistry*; Ellis Horwood Limited: Chichester, 1985.

(20) Mirkin, M. V.; Bard, A. J. *Anal. Chem.* **1992**, *64*, 2293-2302.

(21) Galus, Z., Golas, G., Osteryoung, J. *J. Phys. Chem.* **1988**, *92*, 1103.

(22) Bard, A. J., Faulkner, L. R., *Electrochemical Methods*; John Wiley: New York, 1980.

(23) Sullivan, B. P.; Meyer, T. J. *Inorg. Chem.* **1982**, *21*, 1037-1040.

(24) Atkins, P. W. *Physical Chemistry*; 4th ed.; Oxford University Press: Suffolk, 1990.

(25) Robinson, R. A.; Stokes, R. H. *Electrolytic Solutions*: London, 1959.

(26) *CRC Handbook of Chemistry and Physics*; 76th ed., 1995.

(27) Stewart, A. A.; Campbell, J. A.; Girault, H. H.; Edddowes, M. *Ber. Bunsen-Ges. Phys. Chem. Chem. Phys.* **1990**, *94*, 83-87.

(28) Dryfe, R. A. W.; Webster, R. D.; Coles, B. A.; Compton, R. G. *Chem. Commun.* **1997**, 779-780.

(29) Beattie, P. D.; Delay, A.; Girault, H. H. *J. Electroanal. Chem.* **1995**, *380*, 167-175.

(30) Oldham, K., Zoski, C., Bond, A. M. *J. Electroanal. Chem.* **1988**, *248*, 467.

(31) Geblewicz, G.; Kontturi, A. K.; Kontturi, K.; Schiffrin, D. J. *J. Electroanal. Chem.* **1987**, *217*, 261-269.

(32) Kontturi, A. K.; Kontturi, K.; Murtomaki, L.; Schiffrin, D. J. *J. Chem. Soc.-Faraday Trans.* **1990**, *86*, 931-936.

(33) Nicholson, R. S.; Shain, I. *Anal. Chem.* **1965**, *37*, 1351-1355.

(34) Nicholson, R. S. *Anal. Chem.* **1965**, *37*, 1351.

(35) Miller, C.; Cuendet, P.; Gratzel, M. *J. Phys. Chem.* **1991**, *95*, 877-886.

(36) Miller, C.; Gratzel, M. *J. Phys. Chem.* **1991**, *95*, 5225-5233.

(37) Becka, A. M.; Miller, C. J. *J. Phys. Chem.* **1992**, *96*, 2657-2668.

(38) Li, T. T. T.; Weaver, M. J. *J. Am. Chem. Soc.* **1984**, *106*, 6107-6108.

(39) Finklea, H. O.; Hanshew, D. D. *J. Am. Chem. Soc.* **1992**, *114*, 3173-3181.

(40) Khoshtariya, D. E.; Dolidze, T. D.; Zusman, L. D.; Waldeck, D. H. *J. Phys. Chem. A* **2001**, *105*, 1818-1829.

(41) Slowinski, K.; Majda, M. *J. Electroanal. Chem.* **2000**, *491*, 139-147.

(42) Slowinski, K.; Fong, H. K. Y.; Majda, M. *J. Am. Chem. Soc.* **1999**, *121*, 7257-7261.

CHAPTER 5

NUCLEATION AT THE ITIES

5.1. Introduction

The purpose of the work described in this chapter was to find two-phase nucleation systems that could be used to probe the initial stages of nucleation and growth of transition metals at the liquid-liquid interface. Preliminary investigations were carried out using cyclic voltammetry and once a system had been deemed suitable for further investigation, potential step transients were used to study the initial stages of nucleation and growth. In the next chapter, studies on the initial stages of nucleation, using a combination of spectroscopic and electrochemical techniques, are described.

Metal colloids (d >10 nm) have been known since the time of Faraday, but have recently become the focus of intense interest. There are two main reasons for this interest in the study of nanosized metallic particles. Firstly, the particles exhibit unusual properties compared to the bulk metal. It has been well documented, for example, that particles in the nanometer size-range have electronic and optical properties that differ from those of either the atomic or bulk states.[1] The reason for these differences is that a large percentage of a nanoclusters' atoms lie on the surface and these surface atoms do not necessarily order themselves in the same way as those in the bulk state. In addition, the fact that their electrons are confined to a small space gives rise to quantum size effects.[2] Having a much higher surface area-to-volume ratio than larger particles, the particles' properties are highly sensitive to the state of their surface. Secondly, nanometer sized particles are of potential use in a variety of fields including; semiconductors and catalysis. The use of nanoparticles as highly selective catalysts is discussed in a later Chapter.

Since the properties of nanoparticles e.g. catalytic activity and optical properties, vary as a function of size, one of the most immediate goals in this area is the development of methods to achieve a reproducible synthesis of clusters of a predetermined size, composition and shape. An understanding of the mechanism of particle formation would undoubtedly facilitate the design of a reliable synthesis. Few investigations into the mechanism of nanocluster formation have been reported for two reasons. Firstly, the lack of suitable synthetic methods, and secondly, the lack of methods to monitor the formation of nanoclusters in real time.

Traditionally, four general methods for transition metal nanocluster synthesis have been used; chemical reduction of the metal salt, thermal or photochemical decomposition, ligand reduction and displacement from organometallic compounds, and metal vapour synthesis.[3] These methods provide reasonably monodisperse particle syntheses. For example, gold colloids of various sizes, depending on the reaction conditions, have been prepared by the reduction of $AuCl_4$ in water[4] or in organic solvents.[5,6] However, these are purely chemical reactions and the reduction rate is difficult to control. A fifth and more recently proposed method for particle preparation is by electrochemical means. This has been proven to be convenient for growing isolable transition metal nanoclusters that can be re-dissolved in non-aqueous solution. Electrochemical methods allow control over the degree of supersaturation during particle formation. Hence the reaction rate and ultimately the particle size can be controlled by changing the overpotential of the substrate undergoing nucleation. In this respect, the use of electrochemical techniques for the

preparation of nanoparticles appears to have distinct advantages over chemical methods.

Another important aspect of the study is in the area of nanoparticle stabilisation. Nanoclusters, although kinetically stable are thermodynamically unstable and prone to aggregation. Thermodynamic stabilisation can be accomplished in one of the following ways: electrostatic (charge), steric (uncharged) stabilisation or by a combination of the two. There have also been reports of nanoparticle stabilisation by solvent molecules, in the absence of charge or steric stabilisers.[7,8]

A large-scale, size-selective, electrochemical synthesis of colloidal palladium has been previously described by Reetz.[9] A simple electrochemical cell was used; an anode of the desired metal was immersed in a solution containing a tetra-alkyl ammonium and a metal salt. The tetra-alkyl ammonium salt functions both as the supporting electrolyte and as the stabilising agent for the particles produced. It was observed that greater stability is provided by longer-chain R_4N^+ cations. The technique allows for control of the size of the particle (higher current densities producing smaller particles) and the particles can be easily isolated by precipitation and re-dissolved. This synthetic method allows the preparation of a variety of metal particles at a high yield (>95%). One drawback is that nanocluster formation and growth cannot be followed directly, thus limiting the amount of mechanistic information that can be obtained.

It was first demonstrated that metal films could be deposited at the interface between two immiscible electrolyte solutions (ITIES) in 1975.[10] Since then gold[11] and

palladium nanoparticles[12-14] have been deposited at the ITIES by electron transfer (ET) reactions. The reaction is markedly irreversible. The basic theory and concepts of nucleation and growth at the liquid-liquid interface are essentially the same as those described for the process at a solid electrode, i.e. any nucleus exceeding the critical size will grow under diffusion control.[15,16] The system that is being considered here consists of an organic solvent, immiscible with water, containing an organic redox couple, in contact with an aqueous solution of metal ions. Application of a suitable interfacial Galvani potential difference induces heterogeneous ET (HET), leading to the electrodeposition of a metal phase at the interface.

The interface between two immiscible electrolyte solutions offers an ideal substrate for the study of nucleation phenomena for two reasons. Nucleation on any electrode surface is affected by the interaction between the newly formed phase and the electrode substrate. Since the cohesive energy between the newly formed substrate and a metal is much greater than that with a liquid, the ITIES provides an ideal substrate for the study of the electrochemical generation of metal nanoparticles. Also, heterogeneous nucleation is highly sensitive to the presence of irregularities on the electrode surface since these sites act as nucleation centres. For an ITIES the electrode surface is free from defects. Despite these fundamental advantages, there is a lack of studies in this area. The majority of research on HET at the ITIES has centred on simple reversible systems.[17-21] There is clearly a need for further studies of the deposition of metallic particles at the liquid | liquid interface.

As previously mentioned, there is a lack of preferential nucleation sites on the liquid/liquid interface and although this is advantageous from a theoretical

viewpoint, experimentally it may prove problematic. Defects act by lowering the activation energy for the nucleation process to take place. The nucleation process occurring at the liquid | liquid interface has been shown to be significantly slower than at solid electrodes.[12] This is most likely related to the aforementioned lack of defects on the electrode surface.

Nucleation at the liquid | liquid interface occurs via a HET that resemble the simple systems used in the last chapter, in that interfacial transfer reactions occur. However, some important differences exist between the two systems. As already mentioned, ideal ET requires a system that is not complicated by additional reactions such as partitioning of neutral species, coupling of ion and ET, or the presence of competing chemical reactions. The experimental requirements to study ET without side reactions include stability of both the oxidised and reduced forms of the redox species, absence of partitioning and inert base electrolytes. However, the HETs discussed in this Chapter differ from those in Chapter 4 in that in the present examples, the aqueous redox couple is a metal salt, the reduction of which is an irreversible reaction. Also, in this case, HETs across the ITIES leads to the nucleation of a new phase at the interface. In this case the concentrations of the two species were similar in both phases. Therefore, any analysis of the results of nucleation and growth phenomena at ITIES requires that diffusion in both phases must be considered, since the current is limited by the diffusion of each of the redox couples to the interface. In consequence, the analysis cannot be carried out using the classical theory developed for metal electrodes. The nucleation systems investigated here resemble those described by Stewart,[22] with zero initial concentration of products and therefore, the criteria used previously to characterise voltammetric

results[18] i.e. one redox couple is present in excess therefore it is assumed to have the same properties as a metal electrode, cannot be used and diffusion in both phases must be considered.

5.2. Experimental

5.2.1. Nucleation at a metal electrode | electrolyte interface

Prior to potential scanning, in all the metal nucleation experiments described, the electrode was held at a potential positive of where reduction takes place and the potential was then scanned to negative potentials to electrodeposit the metal. The standard potentials for the metal salts studied are given in Table 5.1. All potentials are quoted versus the standard hydrogen electrode (SHE).

5.2.2. Nucleation at the water | 1,2-DCE interface

All the systems were initially studied using cyclic voltammetry. The cell was cleaned after each measurement to ensure a clean interface. Prior to potential scanning, the interface was held at a potential negative (i.e. the potential of the aqueous phase is negative with respect to the organic phase) to the value required to observe reduction. The interfacial Galvani potential difference $\Delta_o^w\phi$ was scanned in the positive direction causing ET from the organic to the aqueous phase, thereby reducing the metal ion at the interface. A positive current is defined as transfer of a positive charge from the aqueous to the organic phase. All potentials are quoted on the standard Galvani scale. The applied potentials were transformed to the Galvani scale as described in Chapter 3, using $\Delta_o^w\phi_{TPAs^+} = -364\,mV$.[23] Potential step experiments were carried out on an identical system to that used for cyclic voltammetry. Fresh solutions were always used to ensure a clean interface, without preferential nucleation sites.

5.2.3. Non-electrochemical measurements

Equilibrium studies (i.e. in the absence of an externally applied potential) were carried out by contacting the aqueous and organic phases to check for any sign of spontaneous reactions or interfacial film formation.

5.3. Results

Tetrachloroaurate, tetrachloroplatinate, tetrachloropalladate and silver ion are easily reduced to the zero valent state by mild aqueous reductants, such as citrate.[24-26] The standard potential for the reduction of the metal ions used here are given in Table 5.1.

Preliminary voltammetric experiments were carried out on the nucleation of a series of transition metal complexes at the liquid | liquid interface with an electron donor in the organic phase, in order to determine their suitability for further investigation of the kinetics of the nucleation and growth processes. The choice of metals for these studies must be made based on several factors; the complex chosen must be sufficiently soluble in the aqueous phase and it must not partition between the phases. It is also important that neither the metal ion nor its counter-ion transfer within the potential window. The substituted ferrocenes dimethylferrocene (DMFc) and decamethylferrocene (DCMFc) were chosen as the organic-phase electron donor.

Table 5.1:Standard Reduction Potentials of the metal ions used. (E^0 vs SHE)

Reaction	E^0/mV
$Hg(NO_3)_2/Hg$	610*
Au^{+3}/Au^{+}	1,401
Au^{+}/Au	1,692
$AuCl_4^{-}/Au$	1,002
Pd^{2+}/Pd	951
$PdCl_4^{2-}/Pd$	591
$PtCl_4^{2-}/Pd$	755
$Ag(S_2O_3)_2^{3-}/Ag^0$	-350*

All values were taken from reference [27] except * which was measured at a Pt electrode.

5.3.1. Mercury

The electrochemical nucleation of Hg onto a foreign substrate has frequently been studied due to the high rate of the reaction:

$$Hg_2^{2+} + 2e^- \rightarrow Hg \qquad (5.1)$$

and the fact that the product is a well-defined liquid.[28]

Before liquid | liquid voltammetry was carried out, the redox behaviour of mercurous nitrate was first probed at a Pt electrode | electrolyte solution interface using Cell 5.1(i). In common with all the metal deposition experiments reported in

this chapter, prior to potential scanning, the electrode was held at a positive potential where no reduction takes place and then scanned negatively.

SCE | 10 mM HNO_3 / 1mM $Hg(NO_3)_2$ (aq) | Pt

Cell 5.1(i)

The voltammetry (Figure 5.1.1) shows classical deposition-stripping behaviour - a reduction peak on the forward scan (630 mV) and a sharp stripping peak on the reverse scan (720 mV). Secondary stripping peaks are sometimes observed at more positive potentials (850 mV in Figure 5.1.1). This is most likely due to an inhomogeneous accessibility of the deposit on the electrode surface.

Two-phase liquid | liquid voltammetry was carried out in the system described in Cell 5.1(ii).

SCE | 10mM TPAsCl (aq) | 10mM TPAsTPBF$_5$ / 5mM DCMFc (DCE) || 10 mM HNO_3 / 1mM $Hg(NO_3)_2$ (aq) | SCE

Cell 5.1.(ii)

The supporting electrolyte anion TPBCl was unsuitable for use with Hg_2^{2+} since the formation of a Hg deposit at the interface was observed in the absence of an organic redox couple. $TPBF_5^-$ was considered a suitable alternative to $TPBCl^-$ as it is much more difficult to oxidise (with reduction potentials of 2 V and 0.8 V respectively). When $TPBF_5^-$ was used in place of $TPBCl^-$, chemical reduction of Hg_2^{+2} was not observed in the absence of the organic reductant (Figure 5.1.2). $TPBF_5^-$ was used as the organic supporting electrolyte for all mercury nucleation studies presented here.

The increased current observed at the negative end of the potential window seen in Figure 5.1.2 is due to Hg_2^{2+} transfer. It was therefore necessary to limit the window (from -200 to -125 mV) in order to be able to observe HET. On addition of the redox couple to the organic phase (Figure 5.1.3) an increase in current due to HET leading to nucleation of metallic mercury was observed. It was also observed that the metal electrodeposition current decreases on successive scans. This peak current depression is probably due to the combination of two factors. Firstly, the diffusion limitation i.e., there is a decrease in concentration of reducing agent at the interface, due to the irreversible formation of mercury metal, and secondly, due to the passivation of the particle's surfaces. Mercury is extremely sensitive to contamination and therefore it is likely that the particles adsorb ions from the organic phase base electrolyte after formation of nuclei, thus passivating their surface and preventing further growth. This effect was observed for all the metal electrodeposition experiments described in this chapter.

The ET reaction taking place is:

$$m Hg_2^{+2} + m\ DCMFc\ (o) \rightarrow 2Hg_m^{\sigma} + m\ DCMFc^{+}\ (o) \qquad (5.2)$$

where Hg_m^{σ} is a mercury particle deposited at the interface containing m atoms.

5.3.2. Gold

The electrochemical reduction of the tetrachloroaurate anion was investigated at the Pt microelectrode. The measured potentials refer to Cell 5.2(i) and were referred to the SHE.

SCE | 0.5 M LiCl, 1 mM $HAuCl_4$ (aq) | Pt

Cell 5.2 (i)

Two well-separated reduction steady state polarisation waves were obtained (Figure 5.2.1). The half wave potential of the first process was 780 mV with a limiting current of approximately 2 nA. A diffusion coefficient was estimated for $AuCl_4^-$ in water of 3.9 $\times 10^{-6}$ cm^2s^{-1} from the diffusion coefficient (4.9 $\times 10^{-6}$ cm^2s^{-1})[11] by considering the viscosities of water and 1,2-DCE (0.89 and 0.779 mPas respectively[27]). From Equation 3.4, a value of n of 2.6-2.7 was estimated. This confirmed that this wave corresponds to the three electron reduction of Au^{+3} to Au^0. The second reduction wave, occurring at a potential of 100 mV, corresponds to the reduction of the proton.

The electrochemical reduction of $AuCl_4^-$ was studied at the DCE | water interface.

SCE | 10mM TPAsCl (aq) | 10mM TPAsTPBCl, 2mM DCMFc (DCE) || 30 mM $Na_2S_2O_3$, 2 mM $AuCl_4^-$ (aq) | SCE

Cell 5.2 (ii)

Cheng[11] used a hydrophobic Au salt to facilitate the matching of potential for ET with the aqueous ferro/ferricyanide redox couple. In the present work, the reduction strategy adopted was to have Au in the aqueous phase, thereby taking advantage of

the fact that the standard potential of gold in aqueous media is less negative than that in organic solutions.[11,27] However, since the transfer of $AuCl_4^-$ occurs within the polarisation window,[11] sodium thiosulphate was added to the aqueous phase in order to increase further the hydrophilicity of the gold complex.

SCE	10mM TPAsCl (aq)	10mM TPAsTPBCl xmM DCMFc (DCE)		30 mM $Na_2S_2O_3$ 1 mM $AuCl_4^-$ (aq)	SCE

Cell 5. 2 (iii)

It was found that at S_2O_3 : Au ratios greater than approximately 5:1 IT is not observed in Cell 5.2(ii). The addition of a reducing agent to the organic phase leads to an increase in faradaic current; i.e. HET between tetrachloroaurate and DCMFc is observed (Figure 5.2.2). However, reduction is extremely irreversible, so much so that no peak is observed within the available polarisation range. This is due to the strong stabilisation of Au(III) relative to the zero valent metal and therefore, reduction is energetically less favourable and slow. In addition the electrochemistry of gold is complicated by disproportionation reactions. The interfacial ET reaction is represented by:

$$m\,Au(S_2O_3)_p + mDCMFc\,(o) \rightarrow Au_m^{\sigma} + pm(S_2O_3)^{3-}(w) + mDCMFc^{+}(o) \qquad (5.3)$$

where Au_m^{σ} is a gold particle deposited at the interface containing m atoms, and p is the oxidation state of Au.

The thiosulphate ligand not only increases the hydrophilicity of the gold but also stabilises the ion, making the reduction by DCMFc very unfavourable. For this reason the gold system was considered unsuitable for further investigation.

5.3.3. Palladium

Cell 5.3 was used for all palladium nucleation studies Fc refers to the ferrocene derivative used as the reducing agent in the organic phase (DMFc and DCMFc).

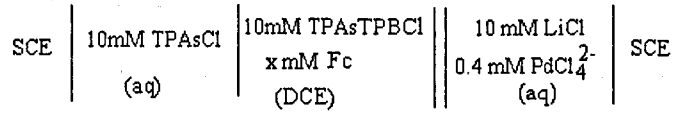

Cell 5.3

Figure 5.3.1 shows the cyclic voltammetry for the system described in Cell 5.3. When both the organic redox species and the aqueous ammonium palladate solutions were present, two processes were observed to occur. Transfer of $DMFc^+$, with a half wave Galvani potential of –100 mV and the irreversible response, with a Galvani peak potential of 125 mV corresponding to the electrochemical reduction of $PdCl_4^{2-}$. When either redox couple is present in Cell 5.3 the voltammetry follows the baseline, indicating that neither couple transfers within the potential window and that $PdCl_4^{2-}$ is not reduced by the organic phase supporting electrolyte. Figure 5.3.1 also shows that when a second scan was run immediately after the first, $PdCl_4^{2-}$ reduction occurs at a slightly less positive potential ($\Delta_o^w\Phi$ = 120 mV). The particles formed during the first scan act as preferential nucleation sites or growth centres at the interface, facilitating further nucleation and growth. The current density maximum for the reduction peak decreased with successive scanning (from 54 to 38 μA). This peak current depression is due to a combination of the effects. Firstly, the newly formed particles are most likely passivated by the tetraalkylammonium ions, and which block further growth, and secondly, due to a decrease in DMFc concentration due to the formation of $DMFc^+$. The Pd-DMFc system is complicated by transfer of the oxidation product of DMFc ($DMFc^+$), and the transfer of $DMFc^+$ becomes less

reversible (the peak separation for the $DMFc^+$ transfer peak increases) on successive scans.

Figure 5.3.2 shows the electrochemical reduction of $PdCl_4^{2-}$ by DCMFc. Choosing a more hydrophobic organic redox couple simplifies the voltammetry since transfer of the ion $DCMFc^+$ does not occur within the potential window. For this reason DCMFc was used in preference to DMFc for the remainder of the nucleation studies.

The presence of either DMFc or DCMFc in the organic phase leads to the appearance of an irreversible reduction with peaks at +125 and –10 mV respectively. The interfacial ET reaction is:

$$mPdCl_4^{2-}(w) + mFc\,(o) \rightarrow Pd_m^{\sigma} + 4mCl^-(w) + mFc^+(o) \qquad (5.4)$$

where Pd_m^{σ} is a palladium particle deposited at the interface containing m atoms, Fc and Fc^+ are the reduced and oxidised forms of the substituted ferrocene used.

In the absence of an applied potential, when contacting the two phases. spontaneous reduction to metallic palladium in the form of a visible interfacial precipitate at the interface is observed. In addition, a colour change was detected in the organic phase (from yellow to green). This behaviour was most apparent for higher concentrations of $PdCl_4^{2-}$. Coupling of ion and ET in the DMFc-$PdCl_4^{2-}$ system may induce the spontaneous reduction of palladate. Figure 5.3.1 shows that an ion transfer reaction takes place in addition to the reduction of Pd. It is supposed that this is due to the transfer of $DMFc^+$ formed during the reduction of Pd according to:

$$DMFc^+(o) \rightarrow DMFc^+(w) \qquad (5.5)$$

$PdCl_4^{2-}$ has a relatively low reduction potential (591 mV). It is difficult to decide whether the spontaneous reaction is a result of the combined effect of ET-IT coupling and the low reduction potential of the $PdCl_4^{2-}$, in the case of DMFc. However, coupling of ET and IT is unlikely when DCMFc is used as the organic redox couple, yet the reduction is still spontaneous. Thus the magnitude of the reduction potential of the metal is considered to be the essential factor in determining whether or not the nucleation reaction at the ITIES will be spontaneous. Altering experimental conditions has been shown to stabilise the palladate and hence decrease the rate of its spontaneous reduction, but the spontaneous reaction cannot be prevented in this manner.[12]

The effect of using a Pd salt that was more difficult to reduce was investigated. Equilibrium studies made by contacting $PdCN^{2-}$ and an organic soluble reducing agent showed no signs of palladium reduction (or any other side reactions) even after prolonged contacting times (up to 24 hours) even at higher concentrations of both species (up to 5 mM). However, voltammetry carried out at the liquid-liquid interface using $Pd(CN)_4^2$ in contact with an organic soluble reducing agent showed no current increase due to the HET reaction. It is concluded that the reduction of the tetracyano salt is energetically too demanding for this system.

Ideally, for the present studies, a system is required in which the nucleation is under potential control (i.e. not involving the spontaneous deposition of particles). However, information obtained from the study of the present system still allows important conclusions to be made about the process of nucleation at the ITIES. The

present work demonstrates clearly that nucleation of metal particles at the liquid | liquid interface via the HET reaction between an aqueous soluble metal salt and a reducing agent in the organic phase is possible. It was concluded that the nature of the reduction reaction (i.e. its spontaneity) was concerned mainly with the nature of the metal and less so with the nature of the organic redox couple. (Interfacial nucleation was detected irrespective of which organic redox couples was used, but was dependent on which palladate was used.) The palladate-ferrocene system was deemed unsuitable for kinetic measurements. In order to study the potential dependence of metal nucleation it is necessary to ensure that no preferential nucleation sites exist at the interface.

5.3.4. Silver

Silver is an ideal candidate for nucleation studies at the ITIES for several reasons. It is frequently studied and relatively inexpensive, it is of practical importance in photography,[29,30] catalysis,[31] surface enhanced Raman spectroscopy,[32] and analysis[33]. Also, Ag has a narrow intense plasmon absorption in the visible region which is very susceptible to surface/interfacial effects [34] making it suitable for spectroscopic studies.

The study of silver nucleation at the ITIES presented two initial problems. Firstly, finding a suitable aqueous supporting electrolyte since the presence of halides would result in the precipitation of the silver halide and the presence of any precipitate would effect the nucleation rate by acting as nucleation sites. Secondly, Ag^+ transfers within the potential window. In order to overcome this problem a similar approach

was taken as with the Au system, i.e. $S_2O_3^{2-}$ was used as a complexing agent in the aqueous phase. $S_2O_3^{2-}$ acted by increasing the hydrophilicity of silver, increasing the Galvani transfer potential, thus preventing its transfer to the organic phase within the potential window. Thiosulphate reacts with silver according to:

$$Ag^+ + 2(S_2O_3)^{2-} \rightarrow Ag(S_2O_3)_2^{3-} \qquad (5.6)$$

The complex formed, $Ag(S_2O_3)_2^{3-}$, is reduced according to:[35]

$$Ag(S_2O_3)_2^{3-} + e^- \rightarrow Ag + 2S_2O_3^{2-} \qquad (5.7)$$

Thus $S_2O_3^{2-}$ behaves as both a complexing ligand and as aqueous supporting electrolyte. Silver thiosulphate was formed in-situ, by slowly adding dilute solutions of silver sulphate to the $S_2O_3^{2-}$ solution. At lower $S_2O_3^{2-}$: Ag^+ ratios (< 5 : 1) the formation of a black precipitate was observed, corresponding to the following reaction:[36]

$$2Ag^+ + S^{2-} \rightarrow Ag_2S \qquad (5.8)$$

This precipitation does not occur when higher concentrations of $S_2O_3^{2-}$ are used, provided that the reaction mixture is vigorously stirred while forming the salt.[37] Microelectrode voltammetric experiments were carried out in order to study the effect of varying the $S_2O_3^{2-}$: Ag^+ ratio on the reduction of Ag using Cell 5.4(i).

SCE | ymM $Na_2S_2O_3.5H_2O$, 0.5 mM Ag_2SO_4 (aq) | Pt

Cell 5.4 (i)

Typical results from the microelectrode study are shown in Figure 5.4.1 and presented in Table 5.2 It can be seen that as the $S_2O_3^{2-}$ concentration is altered, a

change in peak characteristics results. While increasing the $S_2O_3^{2-}$: Ag^+ ratio has little effect on the potential at which nucleation takes place, it has a significant effect on both the peak maximum and the peak position of the stripping peak. For higher ligand concentrations the reduction potential (E_{red}) is slightly decreased.

Table 5.2 Reduction of Ag in $S_2O_3^{2-}$ solutions at a microelectrode using Cell 5.4(i). Where i^s and E_s refer to the current maximum and peak potentials for the stripping peak respectively.

[y] $Na(S_2O_3)$ /mM	E_s /mV	i^s /nA	E_{red} /mV
5	220	2.3	-310
20	260	10.3	-310
80	220	12.7	-330

The half wave reduction potential was approximately -350 mV vs SHE. This value differs significantly from previous determinations of the equilibrium potential of $Ag^+/S_2O_3^{2-}$ solutions of similar concentrations. Gonnissen et al.[38] reported a value of -457 mV vs SHE. A similar discrepancy is observed for the range of reduction potentials measured by Simons et al.[39,40] These authors found that nucleation and growth on a silver electrode occurred in the potential range of –470 to –510 mV. The difference between these experiments and the data obtained in the present work is in the solutions employed. Although in the present work and that in references[39,40] the ratio of $Ag^+/S_2O_3^{2-}$ was similar, an additional high concentration of $NaNO_3$ (0.1M) and a very alkaline condition (pH 12) were employed in Reference[39,40].

Having determined the optimum reaction conditions, the interfacial ET between silver DCMFc and $S_2O_3^{2-}$ was studied using Cell 5.4(ii). When either redox couple alone was present, the voltammetry followed the baseline.

SCE	10mM TPAsCl (aq)	10mM TPAsTPBCl xmM DCMFc (DCE)		30 mM $Na_2S_2O_3$ 0.5 mM Ag_2SO_4 (aq)	SCE

Cell 5.4(ii)

Addition of DCMFc to the organic phase led to the observation of HET between DCMFc and Ag^+. On the second and successive scans, a wave at negative potentials, which increased to a constant current after several scans, is observed. It is proposed that this is a result of transfer of the $DCMFc^+$ formed during silver reduction from the organic to the aqueous phase. The transfer of $DCMFc^+$ is probably assisted by the presence of a doubly charged anion in the aqueous phase. It was also noted that on successive scanning the height of the reduction wave decreased.

An increase in the concentration of the electron donor in the organic phase (DCMFc) results in increased reduction currents (Figure 5.4.3). However, the reaction is not first order with respect to DCMFc, showing that the reduction rate is not limited by its concentration, but most likely by the rate of nucleation and growth.

Potential step experiments were carried out on the same system as used for voltammetry, Cell 5.4(ii). Figure 5.4.4 shows the current transient responses for a series of potential step experiments. All measurements were made by first applying a potential of -150 mV, where no electrochemical deposition takes place, for 25 seconds, and then stepping to the desired potential. Current-transients at higher potentials exhibit nucleation and growth features typically observed for metal

deposition at solid electrodes.[15,16,41-43] The response passes through a peak and decreases towards a steady state current at longer times. The current increase corresponds to growing reaction area, whereas the subsequent decrease is due to the onset of linear diffusion conditions.

The current-time transients for silver nucleation were analysed in reduced coordinate plots.[15] Figures 5.4.5 and 5.4.6 show these results from which it can be concluded that the experimental transients at short times can be analysed using traditional theory. This is not true of the current behaviour at longer times. The transient current decays to a constant current at long times and do not decay to zero as predicted by classical nucleation theory, even after prolonged times (5000 seconds). This is not due to convection effects and it could be due to the occurrence of a chemical reaction[44] with the base electrolyte ($TPBCl^-$ or with $S_2O_3^{2-}$). It is also possible that $S_2O_3^{2-}$ stabilises the silver particles and that they transfer into the aqueous phase. The latter is the proposed origin of the current observed at long times. A comparison of the transients shown in Figures 5.4.5 and 5.4.6 indicates that as the overpotential is increased, the nucleation mechanism (at short times) changes from instantaneous to progressive.

The nucleation and growth transients were used to calculate the nuclear number density (N) and the diffusion coefficient at each of the applied potentials. The former was calculated from the current at the maximum of the transient (I_m) and Equation 2.27 and the latter from $J_m^2 t_m$, where t_m is the time to the maximum in the current and J_m the maximum current density, using Equation 2.24. The results of these calculations are given in Table 5.3. The average value for the diffusion coefficient

($8.1\times10^{-6}cm^2s^{-1}$) was in good agreement with that obtained by previous workers of $6\times10^{-6}cm^2s^{-1}$.[37]

Table 5.3 Table of parameters calculated from Ag nucleation experimental transients at various applied potentials ($\Delta^w{}_o\Phi$). Where J_m and t_m are the current density and time maxima, D is the diffusion coefficient and N is the nuclear number density.

$\Delta^w{}_o\Phi$ /mV	10^5J_m /Acm^{-2}	t_m /s	$10^9I_m{}^2tm$ /$Acm^{-2}s$	10^6D /cm^2s^{-1}	$10^{-4}N$ /cm^{-2}
150	11.2	86	10.8	7.1	3.1
250	16.2	70	18.3	12.1	6.5
300	28.1	10	0.8	5.2	19.6

Knowing the total number of nuclei per cm (N) and the total charge of the particles (Q, given by the area under the peak in the current transients) it was possible to determine the charge per site (Q_p). The mass of a particle (m_p) was then determined using the following relationship (all other parameters have their usual meaning).

$$m_p = \frac{Q_pM}{nF} \qquad (5.9)$$

Using the density of silver (10.5 gcm^{-3})[27] the average radius of one particle (r_p) was determined at each overpotential. As can be seen from Table 5.4, the average particle size decreased as the applied potential increased. The average size of the particles formed within the potential range investigated was in the order of nm, which confirms that nanoparticles were formed at the interface with the application of an interfacial potential.

Table 5.4 Parameters involved in calculation of the size of the Ag particles formed. Q_p and m_p are the charge and size of one particle and r_p is the average radius of the particles.

$\Delta^w_o\Phi$ /mV	$10^9 Q_p$ /C	$10^{-12} m_p$ /g	r_p /nm
150	8.4	9.4	590
250	6.5	7.2	541
300	0.5	0.6	232

Neither voltammetry nor potential step experiments made at the ITIES show any increase in current in the absence of the organic redox couple. Addition of DCMFc to the organic phase, however, leads to an increase in current. This confirms that the peak observed in the potential transients is due to Ag^0 formation and not to the precipitation of Ag^+X^-, (e.g. X=TPBCl). If Ag^+X^- formation occurs in the absence of the organic redox couple, an increase in current would be observed.

The rate of Ag nucleation is low, because the reaction is complicated by the decomposition of the base electrolyte. Thiosulphate increases the hydrophilicity of the silver ion but also stabilises it. It is for this reason that an optimum concentration ratio had to be established, if the concentration were too low there was a risk of the transfer of Ag form the aqueous to the organic phase, while at excessively high concentrations of ligand, the metal ion was difficult to reduce. Decomposition of the thiosulphate ligand is possible within the potential window e.g.

$$S_2O_3^{2-} + 6OH^- \rightarrow 2SO_3^{2-} + 3H_2O + 4e^- \qquad (5.10)$$

$$S_2O_3^{2-} \rightarrow S_4O_6^{2-} + 2e^- \qquad (5.11)$$

It is possible that products of the decomposition reaction passivate the particle surface preventing further growth. For this reason it was assumed that the particles formed remain small. In the next Chapter, in-situ spectroscopic experiments are carried out on the silver system at the externally polarised ITIES in transmission, scattering and reflectance modes.

5.3.5. Platinum

Pt was chosen as a metal ion for nucleation studies for several reasons. Firstly, this metal has practical importance as an electrocatalyst with the long-term aim of its use in fuel cells.[45-48] Secondly, a wide variety of salts in both the (+IV) and (+II) oxidation states are available. Also, Pt complexes tend to be less reactive than their Pd analogues [27] for this reason it was expected that the Pt metal nucleation reaction would be less likely to occur spontaneously at the liquid-liquid interface. Unfortunately, the plasmon absorption band of Pt lies outside the UV-visible region and a quartz cell would be required for any spectroscopic measurements.

Cell 5.5 was used for all platinum nucleation studies.

SCE | 10mM TPAsCl (aq) | 10mM TPAsTPBCl 5mM DCMFc (DCE) || 10 mM LiCl 1mM $PtCl_4^{2-}$ (aq) | SCE

Cell 5.5

Figure 5.5.1 shows the voltammetric response when tetrachloroplatinate was present in the aqueous phase and without the addition of a reducing agent. There was no evidence of spontaneous reactions, or of reduction of the metal ion by the organic base electrolyte. However, the current at the negative potential end was greatly

enhanced due to the transfer of tetrachloroplatinate from the aqueous to the organic phase. Reversible Pt ion transfer was previously observed close to the negative edge of the available potential window.[49] Thus it was necessary to limit the potential window to ensure that the reduction could only occur by a heterogeneous pathway by limiting the potential scan from -250 to 350 mV. Figure 5.5.2 shows that on addition of DCMFc to the organic phase a large increase in current results. Figure 5.5.3 shows the effect of successive scanning on the voltammetric response. In common with the other metals studied, the current maximum of the reduction peak decreases from the first to the second and the third scans respectively.

Potential step experiments were carried out on the same system as used for cyclic voltammetry. For all measurements a potential of -150 mV was applyied for 30 s, where no electrochemical deposition occurs and then the system was stepped to the desired potential. Figure 5.5.4 shows typical I-t transient responses to a single potential step for the system described in Cell 5.5. The transients recorded at higher overpotentials are characteristic of a typical nucleation and growth process. It can be seen that well formed rising transients are obtained and that the response passes through a peak and falls towards a steady state current at longer times. The increase in current corresponds to a growing reaction area and the subsequent decrease is due to the onset of linear diffusion conditions.

Figures 5.5.5 and 5.5.6 compare the transients expressed in reduced coordinates with the theoretical predictions. At short times, the transients show reasonable agreement with those predicted for instantaneous nucleation.

While the experimental transients at short times can be analysed using traditional theory, this is not true for the current behaviour at longer times where the current becomes almost independent of the applied potential and does not decay to zero. As mentioned before for other metals, this is most likely due to the occurrence of a chemical reaction[44] or because the particles once formed migrate from the interface into the solution.

The nuclear number density (N), diffusion coefficient of the diffusing species (D) and average radii of the particles were calculated at each overpotential, as described previously for Ag. Results are shown in Tables 5.5 and 5.6 The average value for the diffusion coefficient of $PtCl_4^{2-}$ ($3.6\times10^{-6}cm^2s^{-1}$) was in close agreement to the obtained by Barker in a similar system ($4.7\times10^{-6}cm^2s^{-1}$).[49]

Table 5.5 Table of parameters calculated from Pt nucleation experimental transients at various applied potentials ($\Delta^{w}_{o}\Phi$). Where J_m and t_m are the current density and time maxima, D is the diffusion coefficient and N is the nuclear number density.

$\Delta^{w}_{o}\Phi$ /mV	$10^{5}J_m$ /Acm^{-2}	t_m /s	$10^{9}J_m t_m$ /Acm^{-2}s	$10^{6}D$ /c^{2}ms^{-1}	$10^{-6}N$ /cm^{-2}
-30	1.7	2.8	0.8	1.5	1.1
5	3.1	1.9	1.8	3.4	3.7
10	5.0	1.2	2.9	5.4	9.7
15	5.7	0.7	2.1	4.0	13.0

Table 5.6 Parameters involved in calculation of the size of the Pt particles formed. Q_p and m_p are the charge and size of one particle and r_p is the radius of the particle. The density of Pt is 21.45 gcm^{-3}.[27]

$\Delta^{w}_{o}\Phi$ /mV	$10^{11}Q_p$ /C	$10^{-14}m_p$ /g	r_p /nm
-30	24.0	27.0	180
5	11.1	13.1	140
10	1.0	1.2	63
15	0.8	0.9	58

The nucleation reaction is much faster than that for Ag. It is proposed that this is a consequence of the absence in this case of a ligand capable of passivating the metal particles formed. This makes the Pt nucleation reaction somewhat easier to analyse than the Ag reaction. In contrast with the Pd system Pt is less reactive and as a result no spontaneous nucleation was detected in equilibrium measurements.

5. 4. Conclusions

The work described in this chapter aimed to find a system suitable for the investigation of heterogeneous nucleation kinetics parameters. The ITIES provides an ideal substrate for the study of the electrochemical generation of metal particles since the interaction energy between the newly formed phase and the substrate (the liquid | liquid interface in this case) is minimal and the interface provides a surface that is free from defects. The first requirement for the system is that the nucleation reaction occurs under potential control. If the reaction can occur spontaneously by chemical reaction then particles form on contacting the two phases and these can act as preferential nucleation sites for further nucleation and growth. Information obtained from observing the system in the absence of an applied potential was used to determine the suitability of the various systems in this respect. A spontaneous reaction leads to a visible colour change in the organic phase (from yellow to green) and the formation of a precipitate at the interface (Section 5.3.3). Any system which led to spontaneous metal deposition, no matter how slow the reaction was taking place, was deemed unsuitable for kinetic investigation.

For simple heterogeneous ET reactions it is essential that the metal salt and the reducing agent both remain in their respective phases. Results obtained from cyclic voltammetry and potential step experiments at the ITIES when only one redox couple was present, were used to confirm that the reacting species do not transfer within the available potential window. The potential window was limited in cases where the metal ion transferred at the edge of the potential window (Sections 5.3.1 and 5.3.5). In cases where the ion transferred in the middle of the potential window a

hydrophilic ligand was added to the system in order to create a more hydrophilic metal complex (Sections 5.3.2 and 5.3.4). It is also important that no side reactions occur between the redox species and the base electrolyte (Section 5.3.1). Thus platinum and silver were considered to be more suitable for kinetic investigations than gold, palladium or mercury. Platinum was not suitable for spectroscopic investigations since the maximum of its plasmon resonance band occurs below 300 nm.

It was demonstrated that metallic particles, with the exception of gold, could be electrochemically deposited at the ITIES by reduction of aqueous metal salt using a substituted ferrocene in the organic phase as electron donor. The electrodeposition reaction was studied using cyclic voltammetry and potential step transients. It was shown that the current responses depend strongly on the applied Galvani potential. It was also demonstrated from the I-t transients that nucleation at the liquid/liquid system occurs at times much longer than for a metal electrode/electrolyte system. This is due to the absence of defects on the former.[12]

Potential step transients and cyclic voltammetry provide a simple procedure for the rapid investigation of nucleation at the ITIES. Information on the choice of metal, reducing agent, and supporting electrolytes can easily be obtained.

Models created for diffusion controlled nucleation at metal electrodes were shown to be in good agreement with experiments at short times.

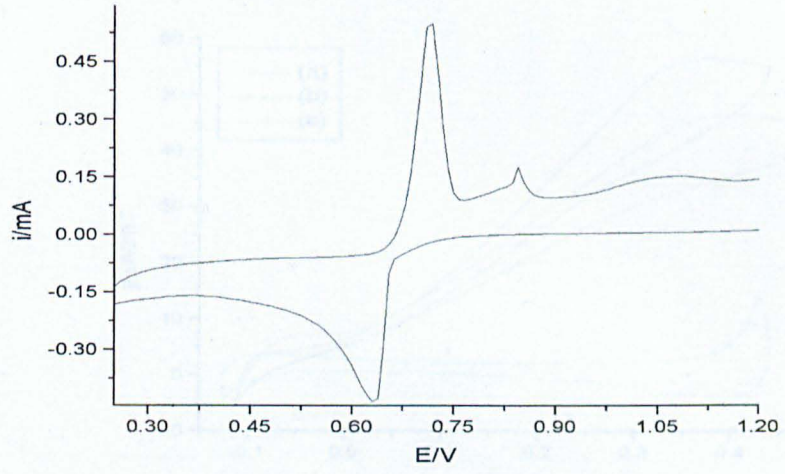

Figure 5.1.1 Cyclic voltammetry for the reduction of 1mM $Hg(NO_3)_2$ at a Pt electrode using Cell 5.1(i) at a scan rate of 500 mVs^{-1}.

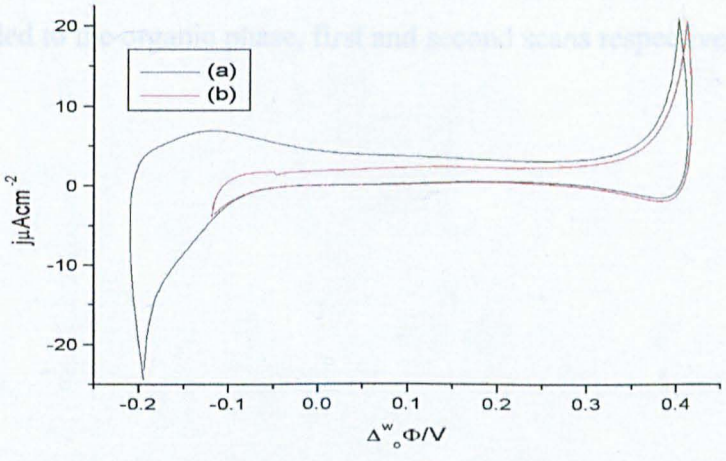

Figure 5.1.2 Transfer of Hg_2^{2+} from the aqueous to the organic phase at a scan rate of 50 mVs^{-1}, conditions as in Cell 5.1(ii). (a) baseline, (b) 1 mM $Hg_2(NO_3)_2$ added to the aqueous phase. No organic redox species was present in either scan.

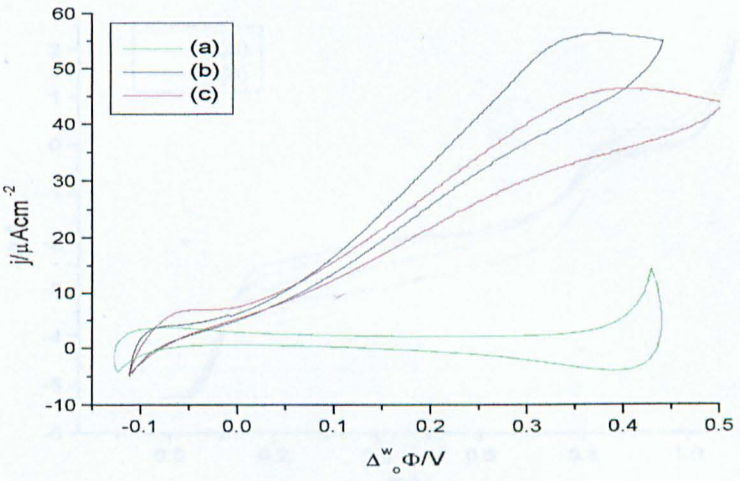

Figure 5.1.3 Cyclic voltammetry showing the interfacial ET between $Hg_2(NO_3)_2$ and DCMFc, conditions as in Cell 5.1(ii), at a scan rate of 50 mVs^{-1}. (a) 1 mM Hg_2^{2+} added to the base electrolyte system, (b) and (c) conditions as in (a) but with 5 mM DCMFc added to the organic phase, first and second scans respectively.

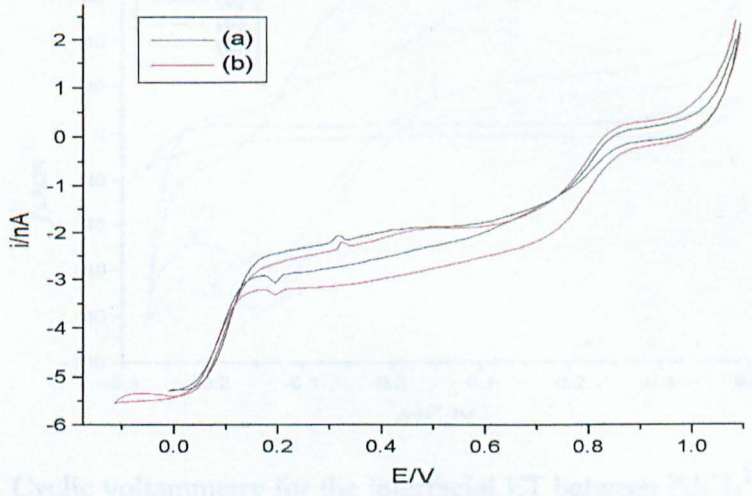

Figure 5.2.1 Cyclic voltammetry showing $AuCl_4^-$ reduction at a Pt microelectrode using Cell 5.2(i), showing two reduction peaks. The scan rates were (a) 25 and (b) 50 mVs^{-1}.

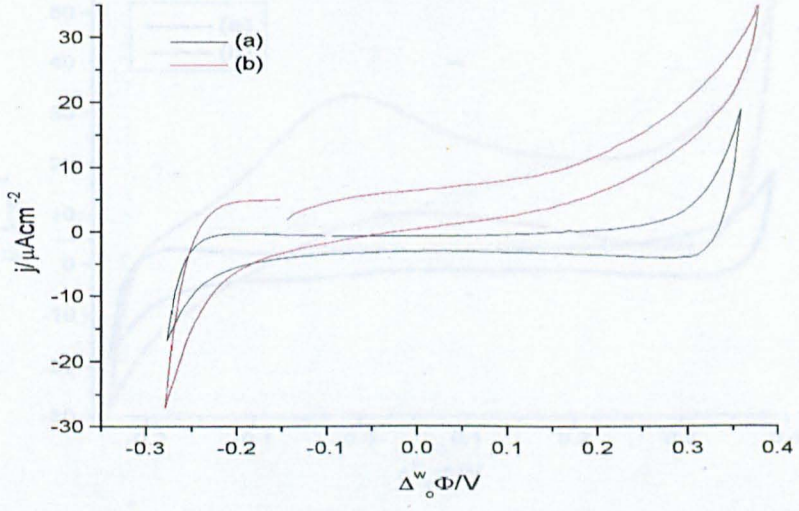

Figure 5.2.2:Cyclic voltammetry for the interfacial ET between 2 mM $AuCl_4^-$ and 2 mM DCMFc at a sweep rate of 50 mVs^{-1}. All conditions as described in Cell 5.2(iii). (a) Baseline and 2 mM $AuCl_4^-$ (b) as (a) but with 2 mM DCMFc added to the organic phase.

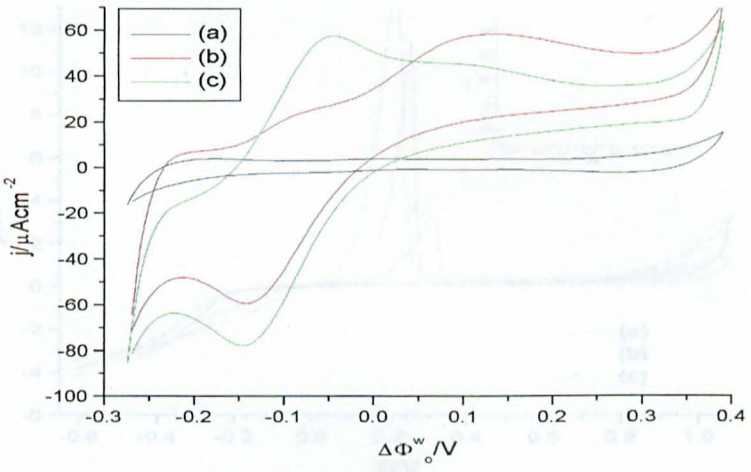

Figure 5.3.1 Cyclic voltammetry for the interfacial ET between $PdCl_4^{2-}$ and DMFc at a sweep rate 50 mVs^{-1}, conditions as described in Cell 5.3. (a) Baseline with 0.4 mM $PdCl_4^{2-}$ added to the aqueous phase, (b) and (c) as (a) but with 0.4 mM DMFc added to the organic phase, the first and second scans respectively.

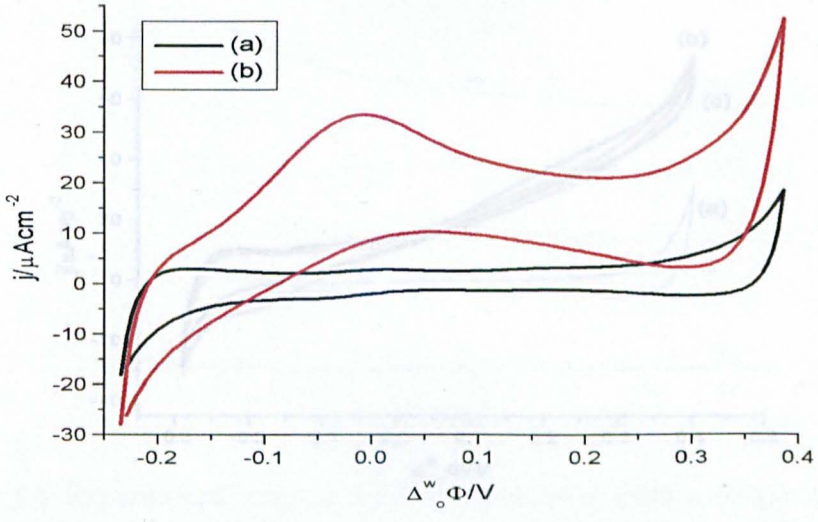

Figure 5.3.2 Cyclic voltammograms for the interfacial ET between $PdCl_4^{2-}$ and DCMFc at a sweep rate of 25 mV s^{-1}, conditions as described in Cell 5.3. (a) Baseline with 0.4 mM $(NH_4)_2PdCl_4$. in the aqueous phase, (b) as (a) but with the addition of 1 mM DCMFc to organic phase.

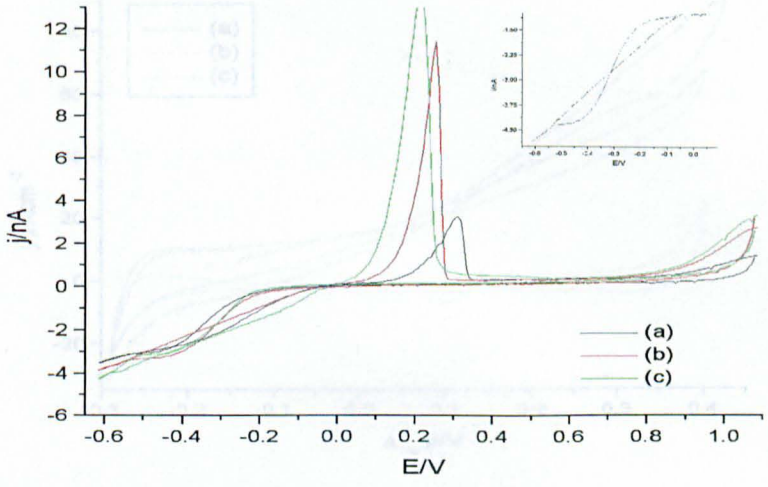

Figure 5.4.1 Microelectrode study of 1mM Ag^+ with varying ratios of sodium thiosulphate at a scan rate of Cell 5.4(i). The concentration of sodium thiosulphate was (a) 5 (b) 20 and (c) 80 mM. The inset shows the typical crossover (nucleation loop) observed on the reverse scan for (c).

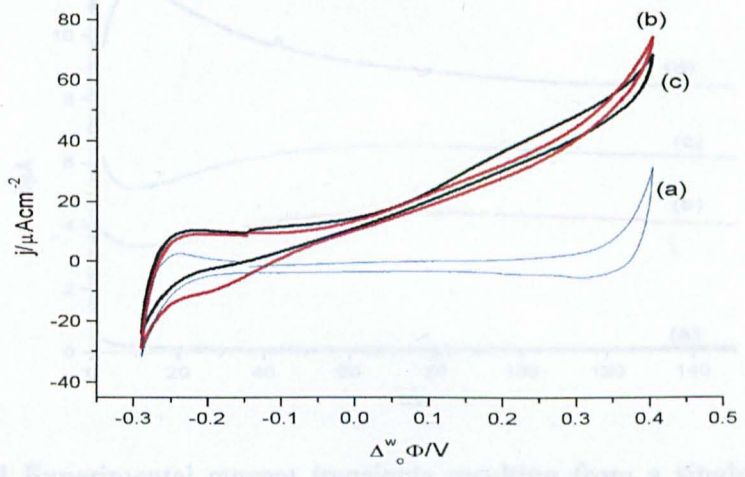

Figure 5.4.2 Cyclic voltammograms for the interfacial ET between Ag^+ and DCMFc at a sweep rate of 25 mV s^{-1}. All conditions as described in Cell 5.4(ii). (a) Baseline with 1 mM Ag^+ added to the aqueous phase, (b) and (c) as (a) but with the addition of 1.5 mM DCMFc to the organic phase, first and second scans respectively.

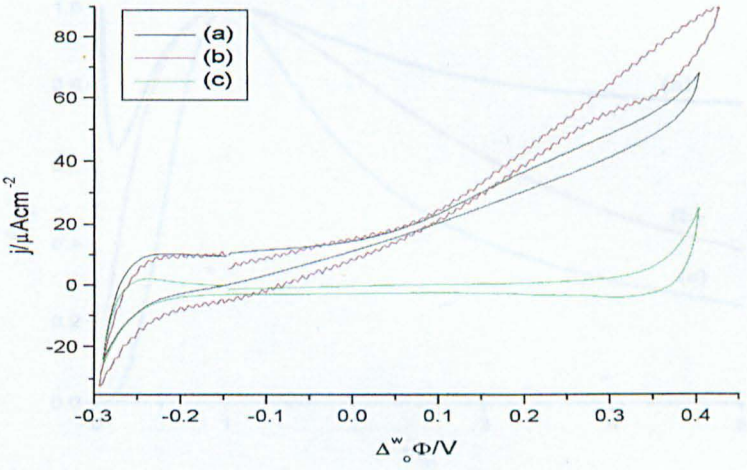

Figure 5.4.3 Cyclic voltammograms for the interfacial ET between Ag^+ and DCMFc at a sweep rate of 25 mV s^{-1}, conditions as described in Cell 5.4. (a) Baseline with 1 mM Ag^+ in the aqueous phase, (b) and (c) as (a) but with the addition of 1.5 and 3.5 mM DCMFc respectively to the organic phase.

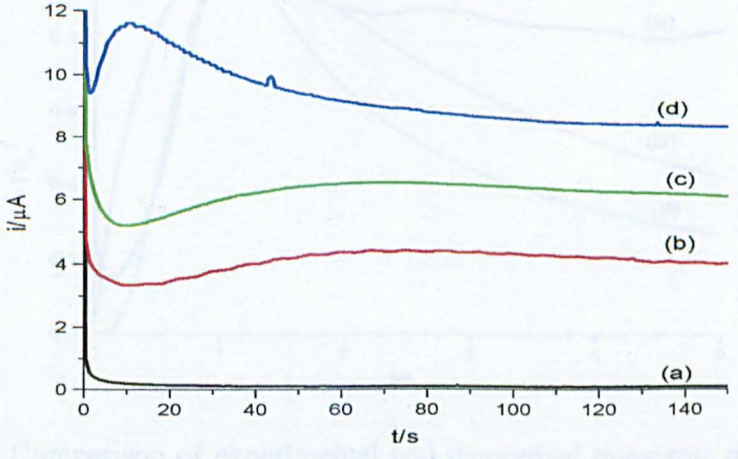

Figure 5.4.4 Experimental current transients resulting from a single potential step applied to the system described by Cell 5.4(ii). The potential was stepped from 360 mV to the following potentials (a) baseline, (b) 150, (c) 250 and (d) 350 mV.

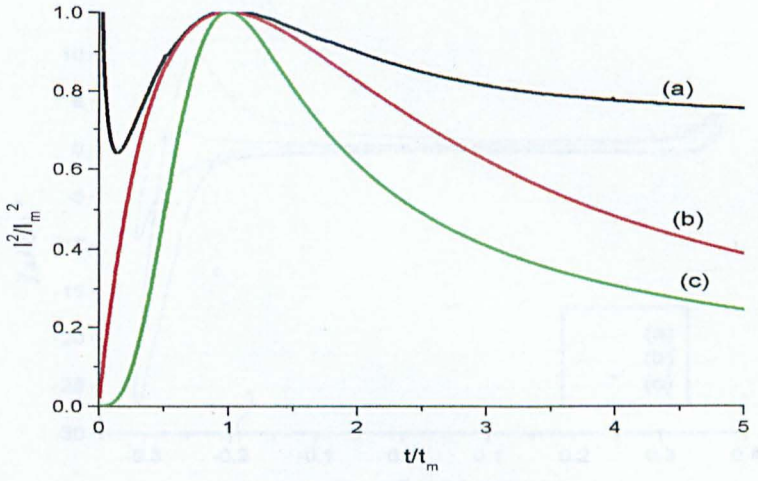

Figure 5.4.5 Comparison of experimental and theoretical transients resulting from a single potential step from -150 mV to 250 mV, for the system described in Cell 5.4. (a) experimental, (b) instantaneous and (c) progressive.

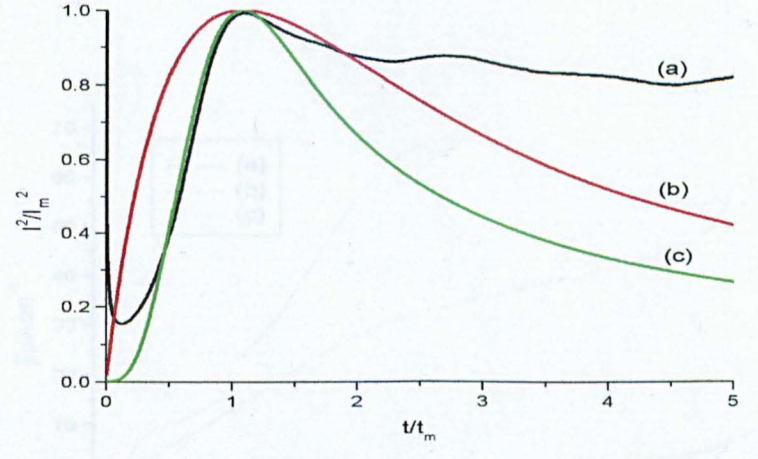

Figure 5.4.6 Comparison of experimental and theoretical transients resulting from a single potential step from -150 mV to 300 mV, for the system described in Cell 5.4. (a) experimental, (b) instantaneous and (c) progressive.

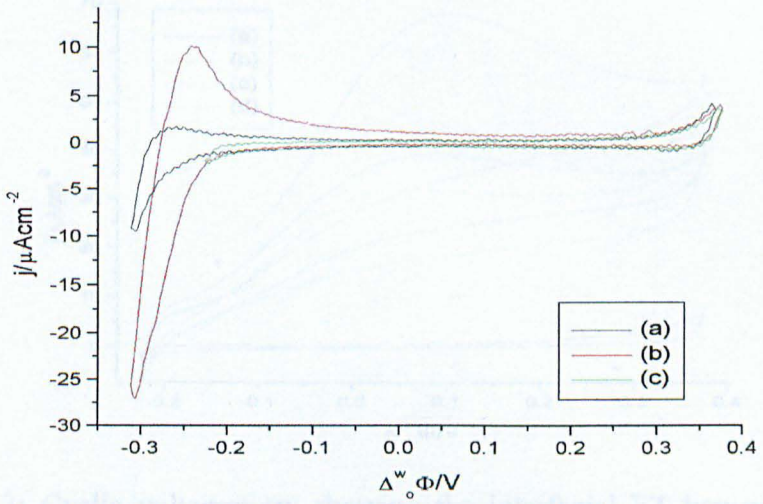

Figure 5.5.1: Cyclic voltammetry showing the transfer of $PtCl_4^{2-}$ from the aqueous to organic phase at a sweep rate 50 $mVs^{-1}$of. Cell 5.5. (a) baseline, (b) 1 mM $PtCl_4^{2}$ added to base electrolyte system and (c) shows the available the potential window for the interfacial nucleation reaction.

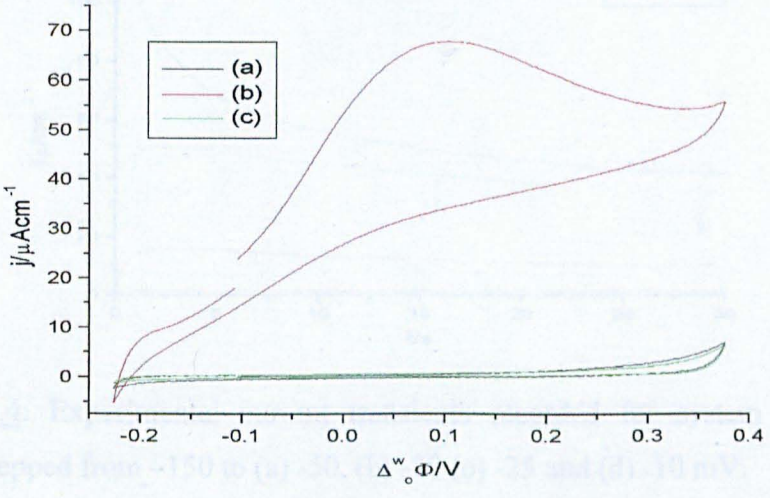

Figure 5.5.2: ET between $PtCl_4^{2-}$ and DCMFc,. at a sweep rate of 50 mVs^{-1}(a) baseline, (b) 5 mM DCMFc added to base electrolyte system (c) both redox couples present in Cell 5.5.

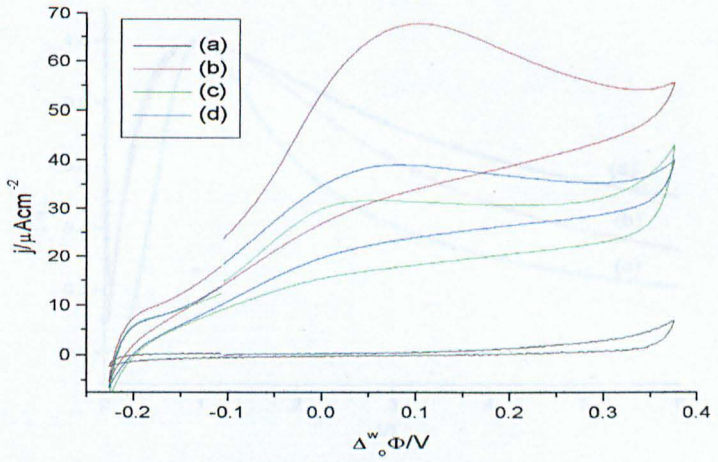

Figure 5.5.3: Cyclic voltammetry showing the interfacial ET between $PtCl_4^{2-}$ and DCMFc., at a sweep rate of 50 mVs^{-1} (system as described in Cell 5.5). (a) baseline, (b) (c) and (d) 1st, 2nd and 3rd scans respectively upon addition of DCMFc to the organic phase.

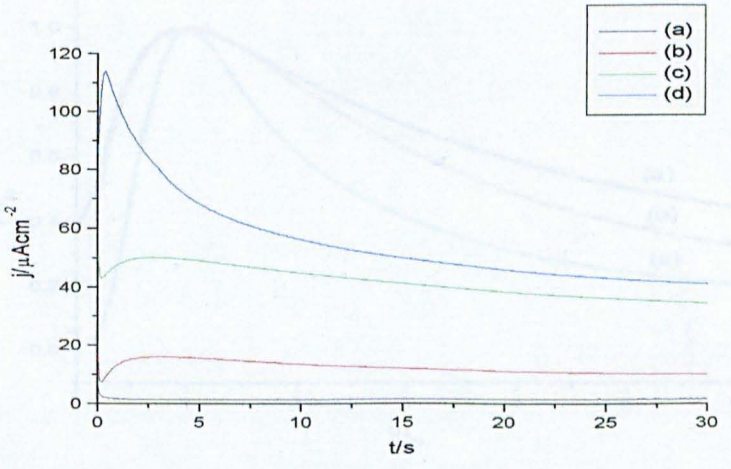

Figure 5.5.4: Experimental current transients recorded for system in Cell 5.5, potential stepped from –150 to (a) -50, (b) -30 (c) -25 and (d) -10 mV.

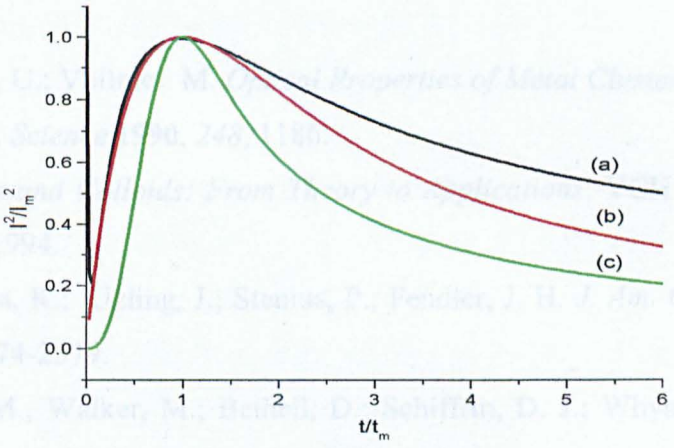

Figure 5.5.5 Comparison of experimental and theoretical transients resulting from a single potential step transients from -150 mV to 30 mV. Experimental conditions as in Cell 5.5. (a) experimental, (b) and (c) theoretical transients calculated for instantaneous and progressive nucleation respectively.

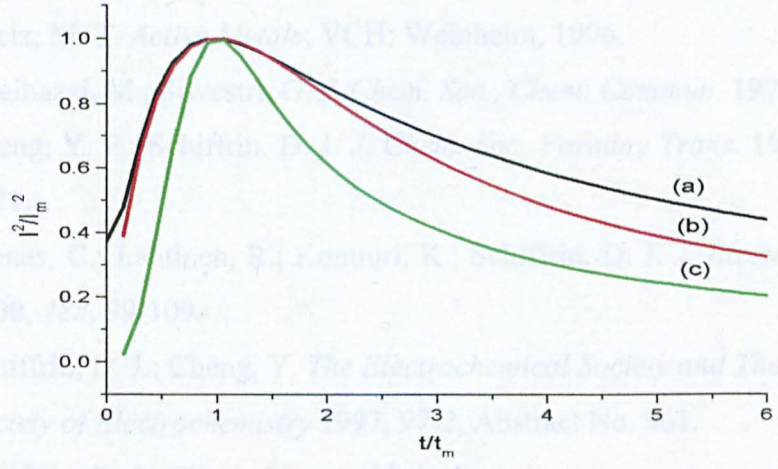

Figure 5.5.6 Comparison of experimental and theoretical transients resulting from a single potential step transients from -150 mV to 50 mV. Experimental conditions as in Cell 5.5. (a) experimental, (b) and (c) theoretical transients calculated for instantaneous and progressive nucleation respectively.

5.5. References

(1) Kreibig, U.; Vollmer. M. *Optical Properties of Metal Clusters*, 1995.

(2) Pool, R. *Science* **1990**, *248*, 1186.

(3) *Clusters and Colloids: From Theory to Applications*; VCH Publishers: New York,, 1994.

(4) Kurihara, K.; Kizling, J.; Stenius, P.; Fendler, J. H. *J. Am. Chem. Soc.* **1983**, *105*, 2574-2579.

(5) Brust, M.; Walker, M.; Bethell, D.; Schiffrin, D. J.; Whyman, R. *J. Chem. Soc.-Chem. Commun.* **1994**, 801-802.

(6) Meguro, K.; Torizuka, M.; Esumi, K. *Bull. Chem. Soc. Jpn.* **1988**, *61*, 341-345.

(7) Bonnemann, H.; Braun, G.; Brijoux, W.; Brinkmann, R.; Schulze Tilling, A.; Seevogel, K.; Siepen, K. U. *J. Organometallic Chem.* **1996**, *520*, 143-162.

(8) Reetz, M. T.; Lohmer, G. *Chem. Commun.* **1996**, 1921-1922.

(9) Reetz, M. T. *Active Metals*; VCH: Weinheim, 1996.

(10) Guainazzi, M., Silvestri, G. *J. Chem. Soc., Chem. Commun.* **1975**, 201.

(11) Cheng, Y. F.; Schiffrin, D. J. *J. Chem. Soc.-Faraday Trans.* **1996**, *92*, 3865-3871.

(12) Johans, C.; Lahtinen, R.; Kontturi, K.; Schiffrin, D. J. *J. Electroanal. Chem.* **2000**, *488*, 99-109.

(13) Schiffrin, D. J.; Cheng, Y. *The Electrochemical Society and The International Society of Electrochemistry* **1997**, *97-2*, Abstract No. 961.

(14) Schiffrin, D. J.; Cheng, Y. *unpublished results* .

(15) Scharifker, B.; Hills, G. *Electrochim. Acta* **1983**, *28*, 879-889.

(16) Gunawardena, G.; Hills, G.; Montenegro, I.; Scharifker, B. *J. Electroanal. Chem.* **1982**, *138*, 225-239.

(17) Samec, Z.; Maracek, J.; Weber, J. *J. Electroanal. Chem.* **1977**, *96*, 245.

(18) Geblewicz, G.; Schiffrin, D. J. *J. Electroanal. Chem.* **1988**, *244*, 27-37.

(19) Cunnane, V. J.; Schiffrin, D. J.; Beltran, C.; Geblewicz, G.; Solomon, T. *J. Electroanal. Chem.* **1988**, *247*, 203-214.

(20) Cunnane, V. J.; Geblewicz, G.; Schiffrin, D. J. **1995**, *40*, 3005-3014.

(21) Cheng, Y. F.; Schiffrin, D. J. *J. Electroanal. Chem.* **1991**, *314*, 153-163.

(22) Stewart, A. A.; Campbell, J. A.; Girault, H. H.; Edddowes, M. *Ber. Bunsen-Ges. Phys. Chem. Chem. Phys.* **1990**, *94*, 83-87.

(23) Czapkiewicz, J., Czapkiewicz-Tutaj, B. *J. Chem. Soc. Faraday Trans. I* **1980**, *76*, 1663.

(24) Turkevich, J.; Kim, G. *Science* **1970**, 873-879.

(25) Furlong, D. N.; Launikonis, A.; Sasse, W. H. F.; Sanders, J. V. *J. Chem. Soc. Faraday Trans. I* **1984**, *80*, 571.

(26) Turkevich, J.; Cooper Stevenson, P.; Hillier, J. *Disc. of the Faraday Society* **1951**, *11*, 55-75.

(27) *CRC Handbook of Chemistry and Physics*; 76th ed., 1995.

(28) Gunawardena, G.; Hills, G.; Montenegro, I.; Scharifker, B. *J. Electroanal. Chem.* **1982**, *138*, 225-271.

(29) Hailstone, R. K. *J. Phys. Chem.* **1995**, *99*, 4414-4428.

(30) Lewis, M.; Tarlov, M.; Carron, K. *J. Am. Chem. Soc.* **1995**, *117*, 9574-9575.

(31) Sun, T., Seff, K. *Chem. Rev.* **1994**, *94*, 857.

(32) Vlkova, B., Gu, X., Tsai, D., **1996**, *100*, 3169.

(33) Pal, T. *J. Chem. Educ.* **1994**, *71*, 679-681.

(34) Henglein, A. *J. Phys. Chem.* **1993**, *97*, 5457-5471.

(35) Cooley, A. C., Dagon, T. J. *J Appl. Phptogr. Eng.* **1976**, *2*, 36.

(36) Cooley, A.; Vacco, D. *J. Imaging Sci. Technol.* **1993**, *37*, 603-606.

(37) Vandeputte, S.; Verboom, E.; Hubin, A.; Vereecken, J. *J. Electroanal. Chem.* **1995**, *397*, 249-260.

(38) Gonnissen, D.; Vandeputte, S.; Hubin, A.; Vereecken, J. *Electrochim. Acta* **1996**, *41*, 1051-1056.

(39) Simons, W.; Gonnissen, D.; Hubin, A. *J. Electroanal. Chem.* **1997**, *433*, 141-151.

(40) Gonnissen, D.; Simons, W.; Hubin, A. *J. Electroanal. Chem.* **1997**, *435*, 149-155.

(41) Scharifker, B. R.; Mostany, J. *J. Electroanal. Chem.* **1984**, *177*, 13-23.

(42) Palomar Pardave, M.; Ramirez, M. T.; Gonzalez, I.; Serruya, A.; Scharifker, B. R. *J. Electrochem. Soc.* **1996**, *143*, 1551-1558.

(43) Mostany, J.; Mozota, J.; Scharifker, B. R. *J. Electroanal. Chem.* **1984**, *177*, 25-37.

(44) Kontturi, A. K.; Kontturi, K.; Murtomaki, L.; Schiffrin, D. J. *J. Chem. Soc.-Faraday Trans.* **1995**, *91*, 3433-3439.

(45) Ye, S. Y.; Vijh, A. K.; Dao, L. H. *J. Electrochem. Soc.* **1997**, *144*, 90-95.

(46) Takasu, Y.; Ohashi, N.; Zhang, X. G.; Murakami, Y.; Minagawa, H.; Sato, S.; Yahikozawa, K. *Electrochim. Acta* **1996**, *41*, 2595-2600.

(47) Radmilovic, V.; Gasteiger, H. A.; Ross, P. N. *J. Catal.* **1995**, *154*, 98-106.

(48) Yahikozawa, K.; Fujii, Y.; Matsuda, Y.; Nishimura, K.; Takasu, Y. *Electrochim. Acta* **1991**, *36*, 973-978.

(49) Barker, M. H. Ph.D., The University of Liverpool, U.K., 1999.

CHAPTER SIX

SPECTROELECTROCHEMISTRY

6.1. Introduction

Particles in the nanometer size range are considered as a new physico-chemical dimension between that of molecules and the bulk material. The particles have an extremely large surface-to-volume ratio and exhibit unusual chemical and physical properties. Given that factors including size, shape, symmetry and how close the particles are to each other all affect their optical properties,[1,2] optical methods can be used for the direct determination of these parameters.[3] Many transition metal particles absorb in the visible region,[4] but due to the excitation of surface plasmon resonances Ag and Au have been the most widely studied metals.[5-10] A brief description of how UV-visible spectroscopy can be used to monitor such changes is given below.

(a) Size: It is generally accepted, that as particle size decreases, the maximum in the plasmon resonance band shifts to shorter wavelengths (blue shift) due to an increase in the band gap of the smaller particle. Conversely as the average particle size increases, the plasmon band shifts to longer wavelengths (red shift).[11,12] Also small particles exhibit a broader absorption band than larger particles.[13,14]

(b) Shape: The effect of shape on the position of plasmon resonance band of colloidal particles is not well understood, but recently it was found that specific geometrical shapes give distinct spectral responses.[15] It was shown that altering the shape of Ag particles led to an obvious spectral shift from blue to red.

(c) Symmetry: A strong dependence of the spectral response on the symmetry of the particle has been predicted; 2-d nanoparticles of constant size but with non-regular cross-section, exhibit absorption spectra of varying complexity; the higher the particles' symmetry, the simpler the spectrum.[16]

(d) Aggregation: Aggregation of particles leads to the emergence of an absorbance band at longer wavelengths with respect to the plasmon band of individual particles. Thus a Ag particle of cylindrical geometry exhibits an absorbance at 550-580 nm[17] while the plasmon absorbance band of a spherical particle occurs at 380-400 nm.

Another important optical characteristic of these particles is their ability to scatter light. Plasmon resonant particles (PRP) are sub-micron (d=40-100 nm) metallic nanoparticles that scatter light upon illumination with white light. This effect is well-established for nanometer sized particles of Ag[18] and Au.[19] The collective surface plasmon resonance of the particles is responsible for the efficient scattering of incident light. The characteristics of the scattering (i.e. magnitude, peak wavelength and the bandwidth of the plasmon resonance) are dependent on the particle's size, shape, composition, and local environment.[18] The formation of individual PRP's which scatter in different regions of the visible range of the spectrum, and their use as a convenient, non-radioactive probe in highly sensitive biological analysis has been reported.[18,19]

The ability to tune the optical properties of a system by changing, for example, particle size and degree of aggregation holds potential for many practical applications. However, the ultimate usefulness of this concept relies on the

development of improved techniques to prepare particles of a predetermined geometry and composition, and this requires a detailed understanding of the particle formation reaction.

As was clearly demonstrated in the previous chapter, metal clusters can the generated electrochemically at the liquid | liquid interface when a metal ion present in one phase is reduced by a suitable electron donor in the opposite phase. It is essential that neither the metal ion nor the reducing agent transfer within the potential window so that the electron transfer reaction is truly heterogeneous. The nucleation and growth characteristics of this system have been studied using simple voltammetric and potential step techniques. However, since the optical properties of small metal particles are dependent on their size, interfacial nucleation and growth can conveniently be followed by non-invasive, in-situ optical techniques. The incorporation of in-situ spectroscopic techniques in traditional electrochemical experiments[20-22] and at the ITIES[23] has proven both a popular and effective means of monitoring solution phase reactions. It has previously been demonstrated that the growth of a metal film at the liquid | liquid interface can be followed by spectroscopic techniques using transmission UV-VIS spectroscopy[24] and ellipsometry for Au.[25]

The system investigated in the present study concerns the nucleation of Ag. This metal offers an ideal substrate for UV-visible spectroscopic investigation, since Ag particles absorb strongly in the visible region due to surface plasmon resonance.[5] Its suitability was discussed in Chapter 5 (Section 5.3.4) and typical voltammetric and chronoamperometric responses for Ag nucleation were also given there.

It is expected that the use of in-situ optical techniques in combination with conventional electrochemical methods would supplement information obtained from electrochemical measurements on the preparation and behaviour of metallic particles at a polarised liquid | liquid interface. In the next chapter, the potential dependent adsorption of a charged metal colloid at the interface is studied. The results of these studies, in conjunction with the previously obtained electrochemical measurements, allow important conclusions to be drawn on the formation and behaviour of transition metals at the interface of two-phase liquid | liquid systems.

6.2. Experimental

The aim of this section is to follow the nucleation and growth of silver particles at the interface between two immiscible solutions using in-situ, potential modulated UV-visible spectroscopy. A prerequisite for this type of study is that the wavelengths of the absorption maxima of the various species are sufficiently different. Table 6.1 summarises information obtained from UV-visible spectroscopy of the species involved in the present study. The supporting electrolyte used for all previous experiments involving the nucleation of silver at the ITIES was tetraphenylarsonium tetrakis[4-chlorophenyl]borate (TPAsTPBCl). While the TPBCl anion was shown to be problematic when studying the nucleation of mercury (Section 5.3.1) since this anion acts as a reducing agent for the Hg_2^{2+} ion, no such complications were seen for silver nucleation in any of the electrochemical experiments. However, voltammetric scans run simultaneously with spectroscopic measurements revealed that the system was unstable. Oscillations were observed at the positive edge of the potential window due to the irreversible transfer of supporting electrolyte. It has previously been reported that TPAsTPBCl is prone to photodecomposition,[26] and Cheng reported a slight drift in the absorbance of the UV-visible absorption baseline using this anion.[24] Voltammetry recorded using the anion tetrakis[pentafluorophenyl]borate ($TPBF_5$) showed none of these complications. The available potential window was also extended by changing the cation from TPAs to bis[triphosphoranylidene] ammonium (BTPPA).

For the above reasons, $BTPPATPBF_5$ was adopted as the supporting electrolyte for the remainder of the spectroscopic work on silver nucleation.

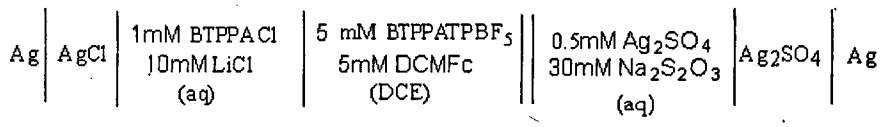

Cell 6

Cell 6 was used for all potential modulated UV-visible spectroscopic studies of silver nucleation. Due to the low solubility of BTPPACl, 10 mM LiCl was added to the aqueous reference phase to increase the conductivity of this solution. Commercially available SCE electrodes could not be used as reference electrodes for voltammetric experiments due to the dimensional constraints of the electrodes and of the cell used. Homemade Ag/AgX wire electrodes were prepared as described in Chapter 3. A silver/silver chloride reference electrode (Ag/AgCl) was used in the organic reference phase when lithium chloride was present. However, the electrode could not be used in the aqueous phase as the presence of any trace of chloride would cause precipitation of silver chloride and therefore a silver/silver sulphate (Ag/Ag_2SO_4) was used instead. SO_4^- was present in this phase as the counterion of the silver salt. The organic soluble electron donor was present in excess (5 : 1) to avoid diffusion control in the organic phase.

Cyclic voltammetry and chronoamperometry had already been used to investigate the initial stages of electrodeposition of silver thiosulphate at the liquid-liquid interface (Section 5.3.4). Both techniques showed that the system exhibited nucleation characteristics similar to those observed at a metal electrode/electrolyte solution interface.[27,28] A nucleation loop was observed in the voltammogramms and current maximum at short times was observed in potential step experiments. From this information, it was expected that the generation and dissolution of silver particles could be monitored as a change in the intensity of the collected light while varying

the potential of the system. Specifically, the presence of an absorption peak at ca. 400 nm, corresponding to the plasmon band of colloidal silver[4] was anticipated. The potential modulated behaviour of this band should yield information regarding the nucleation process.

The experimental set-up and cell used for the potentially modulated UV-visible spectroscopic experiments was described in Chapter 3. It was important that the interface was both small and supported for these measurements. When using a cell with a large, unsupported interface it was possible to observe the movement of the interface as the potential was changed, leading to an unstable baseline. Two types of experiment were carried out, firstly a sinusoidally varying potential was applied to the system (Cell 6) and the intensity of the transmitted light recorded. Prior to potential scanning, the system was held at a potential negative of where nucleation occurs ($\Delta_o^w\phi$ = -250 mV) for 30 seconds and scanned positively at a slow sweep rate of typically 5 mVs^{-1}.

The second experiment was carried out in three steps. It involved the application of a potential step to pre-determined values and again recording the intensity of the collected light over long periods (up to 80 minutes). The interfacial potential was first held at a value negative to where any reaction takes place ($\Delta_o^w\phi$ = -250 mV) and held there to confirm that no nucleation occurs even after prolonged times. The potential was then stepped positively to a value where nucleation occurs ($\Delta_o^w\phi$ =+215 mV) and the current-time transient was recorded. The potential was finally stepped back to a negative value ($\Delta_o^w\phi$ =-250 mV) to determine whether it was possible re-

oxidise the particles. This experiment considered the effect on the system of a large potential perturbation, while the previous experiment investigated the effect of small potential changes. Also, the combination of the two approaches enabled the system to be studied at both short and long times. In order to determine the degree of reversibility of the reaction, the effect of reversing the potential was considered in both experiments, directly after nucleation and growth had occurred. The reactions were monitored by recording the absorbance in single scans, for a wide range of wavelengths, at various time intervals during the reaction. For all experiments, a fresh interface, free of preferential nucleation sites was used. Identical experiments were run in the presence of each redox couple in turn so that conclusions could be drawn as to which spectral features were due to the base system and which were due to the nucleation reaction.

The same experiments were carried out in the reflectance and scattering arrangements. Information concerning the size, size dispersion and concentration-of the resulting particles, was obtained. One other point of interest was to try to ascertain whether the particles remain at the interface or dissolve in one of the two phases. In the next chapter, chemically prepared, aqueous surfactant-stabilised, nanoparticles are studied in a two-phase system.

Table 6.1 Wavelength of the maximum absorption (λ_{max}) for complexes used in this study

Complex	λ_{max}/nm
Ag_2SO_4	225
$Ag(S_2O_3)^{2-}$	230
DCMFc	238
$DCMFc^+$	778

6.2.1 UV-Visible Transmission Spectroscopy

Experiments carried out in transmission mode allow changes in each phase as well as the interface itself to be studied. A schematic diagram of the experimental arrangement used is shown in Figure 6.2.1. Perpendicularly incident light was used. It has been shown that the changing equilibrium concentrations of redox species due to heterogeneous electron transfer (HET) reactions in the two-phase liquid-liquid systems can be monitored by transmission UV-visible spectroscopy at different interfacial potentials.[29] More recently this method has been used to monitor the interfacial formation and growth of Au particles.[24] By this method, the concentration of the oxidised form of the redox organic couple could also be studied, assuming that the absorption maxima wavelengths for the oxidised and reduced forms are sufficiently well separated.

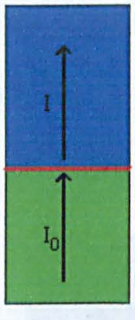

Figure 6.2.1 Schematic representation of experimental arrangement for measurements made in the transmission mode, showing the relationship of the incident (I_0) and transmitted light (I) intensities to the interface under investigation (δ, shown in red). The organic phase is shown in green and the aqueous phase in blue.

The intensity of the transmitted beam (I) corresponds to the light intensity at each wavelength and was converted to absorbance (A) by the relationship:

$$A = \log \frac{I_0}{I} \qquad (6.1)$$

where I_0 is the incident light intensity or the signal detected prior to any electrochemical process taking place. The normalised Absorbance was then plotted against the wavelength at various times of electrolysis.

The presence of a plasmon absorption band at 400nm,[1] was expected. It is important to remember, however, that the resonance spectrum strongly depends on particle size and shape. The presence of a sharp plasmon band can be expected only for a solution of particles of uniform sizes; agglomeration drastically broadens the plasmon band via dipole coupling.[6,30] Also growing particles exhibit a characteristic behaviour of the plasmon band. As the average particle size increases the plasmon band shifts to longer wavelengths.[24,31,32]

6.2.2. UV-Visible Reflectance Spectroscopy

In contrast to the transmission absorbance method described previously, experiments carried out in total internal reflection mode consider only the properties of the interface (See Figure 6.2.2).

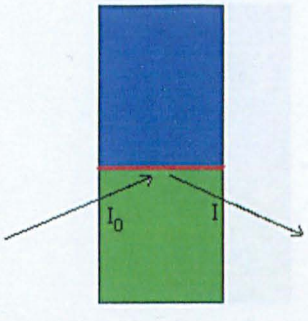

Figure 6.2.2 Schematic representation of the experimental arrangement for measurements made in the reflectance mode, showing the relationship of the incident (I_0) and reflected light (I) intensities at the interface under investigation (δ red). The organic phase is shown in green and the aqueous phase in blue.

In this approach, the excitation beam is confined to one phase and consequently, the changes in reflected light intensity are related to the growth of particles at the interface and/or to their transfer to the organic phase. Previous application of this technique were investigated by Kakiuchi who studied ion transfer kinetics by recording the fluorescence transient in a total internal reflection (TIR) arrangement.[33,34] Using the same principle, Girault introduced differential cyclic volt-absorptometry (DCV), where changes in the absorbance in TIR mode are related to the faradaic current as a function of the applied potential.[35-38]

6.2.3. UV-Visible Scattering Spectroscopy

Experiments carried out in scattering mode allow the measurement of changes occurring only at the interface and in the organic solution to be considered. The experimental arrangement is shown in Figure 6.2.3. Perpendicularly incident light was used.

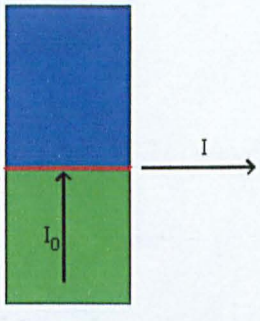

Figure 6.2.3 Schematic representation of experimental arrangement for measurements made in the scattering mode, showing the relationship of the incident (I_0) and scattered light (I) intensities to the interface under investigation (δ red). The organic phase is shown in green and the aqueous phase in blue.

Experimental spectra for both scattering and reflectance mode measurements were plotted as difference spectra, in the form of $\frac{\Delta I}{I} = \frac{I_2 - I_1}{I_1}$, where I_2 is the light intensity recorded for the sample and I_1 that corresponding to the reference spectrum.

6.3. Results and Discussion

Silver thiosulphate is reduced at positive potentials according to the following two-step reaction:[39,40]

$$Ag(S_2O_3)_2^{3-} \rightarrow Ag(S_2O_3)^- + S_2O_3^{2-} \quad (6.2)$$

$$Ag(S_2O_3)^- + e^- \rightarrow Ag + S_2O_3^{2-} \quad (6.3)$$

Experiments in each of the three modes consider slightly different aspects of the system and a combination of all three should allow differentiation between changes that occur at the interface and in the solutions. For example, a decrease in the recorded signal at positive potentials with time is common to experiments in reflectance and scattering modes. This is likely to be due to the migration of particles into the aqueous phase on formation and not due to their dissolution since neither technique accesses the aqueous phase. The transmission signal due to silver particles at positive potentials, on the other hand, increases. This is because, in the transmission mode, despite migration of particles from the interface to the aqueous phase, they are still observable.

Stability of the system upon application of potential and light is an essential prerequisite for this work. From blank potential scan measurements it is clear that no side reactions occur within the potential range. Potential step measurements showed this to be the case even after long times (up to 80 minutes) and in addition, it showed that no nucleation occurred without the application of a suitable interfacial Galvani potential. The results obtained from these basic experiments together with observations from simple electrochemical measurements (i.e. that no nucleation

reaction occurs in the absence of the reducing agent) allow further important conclusions to be made. Firstly, the silver system is suitable for nucleation studies since it is free of spontaneous and adventitious reactions of the base electrolyte system and secondly, that the reaction observed in the presence of both redox couples is the HET between silver thiosulphate and DCMFc.

A colour change in the organic phase from yellow to green was observed at long times along with the formation of a metallic grey precipitate at the interface while in absence of DCMFc, under otherwise identical experimental conditions, no such changes occurred. The transmission UV-visible spectrum of $DCMFc^{+}$ shows an absorption maximum at 778nm.[41] However, this band is masked by the resonant light scattering of the incident light by the particles at longer wavelengths (as discussed later in this section).

In the wavelength range 540-610 nm a spike in the spectra was sometimes recorded; this is an artefact of the spectrometer and not related to nucleation of Ag at the interface. A broad plasmon absorption band centred at 400nm, due to the presence of colloidal silver,[4] was visible immediately after the application of a positive interfacial potential in both scan and step experiments. The effects on the absorbance of the plasmon signal of Ag observed at positive potentials are identical; while the position of the peak did not vary significantly with time or potential (Figure 6.1.1), the absorbance of the peak did vary (Figure 6.1.2). These observations are very important and can be interpreted in the following way. Since no red shift is observed in the plasmon band, it can be concluded that the average particle size does not increase as a function of time (or potential). It is most likely that adsorption of ions

($BTPPA^+$, $TPBF_5^-$ or $S_2O_3^{2-}$) from solution onto the particles' surface occurs, preventing growth and increasing the particles' solubility in the aqueous phase. For this reason, it is likely that the particles migrate into the aqueous phase, once formed. This was also suggested from the analysis of the results of the electrochemical measurements (Chapter 5).

The absorbance due to the plasmon band varied throughout the scan and step experiments. The absorbance corresponds to the integrated charge in a potential step experiment and its value is linearly dependent on $t^{1/2}$ (Figure 6.1.1) as expected for a diffusionally controlled process. Therefore, the nucleation process is limited by the diffusion of the Ag salt to the interface. These observations also suggest that as particles are formed, they diffuse into the aqueous phase and new particles of similar size and shape are formed at the interface. This plot could be used to estimate the total number of particles formed at a given time provided information on the scattering properties is available.

The spectra shown in Figures 6.1.3-6.1.9 are unusual in that a "bipolar" band is observed. The absorbance at ca. 400 nm corresponds to the expected plasmon absorbance of Ag particles.[18,19] The negative absorbance clearly indicates that actual emission of light is taking place in the wavelength range 500-700 nm. This is a very interesting observation and it is proposed that this is due to resonant light scattering of aggregated Ag particles. In the present case, plasmon excitation occurs efficiently as white light is used as the excitation signal. This is particularly important when considering that the unfiltered output of the Xe-Hg lamp was employed.

Transmission and scattering are complementary modes and experimental results obtained from each should be considered in association with the other. The spectral response recorded in transmission mode is the result of the sum of two effects, absorbance of light and resonant light scattering. In the scattering mode only the resonance light scattering effect was observable. Comparison of the two experimental modes allows the individual effects to be seen. Spectra recorded in the scattering mode (Figures 6.2.1 and 6.2.2) show an optical response in the wavelengths range 300-650 nm, due to the resonant light scattering by the aggregated particles.

Spectra recorded in the reflectance mode (Figures 6.3.1 and 6.3.2) show a complex behaviour. It should be stressed that the results presented in this Figures correspond to the relative changes in light intensity of the reflected beam. A positive value of $\Delta I/I$ means that the reflected light intensity is greater than that of the incident beam. The experiments at longer times show a second signal, in the wavelength range 650-750 nm, besides the signal observed at 400-480 nm.

The resonant light scattering (RLS) by nanoparticles can account for these observations. RLS results from excitation of the particles plasmon band in the 400-800 nm range. The low wavelength emission is related to spherical particles present at the boundary or within the depth of the evanescent field at the interface. The origin of the signal observed at longer wavelengths is the same but corresponds to the aggregated particles. The plasmon band of these particles is known to be red shifted.

Figure 6.2.2 shows that the re-oxidation and dissolution of the Ag aggregates formed is a very slow process. The reason for this is the absence of an electron acceptor in the organic phase and applying a water negative potential cannot result in an ET reaction. These results complement the lateral scattering experiments previously discussed and reflect the same phenomena. The results presented in this chapter confirm the conclusions made in Chapter 5, regarding the formation of particles at the ITIES under potential control.

6.4. Conclusions

Analysis of the spectroscopic response in combination with electrochemical results yields an unambiguous result— the application of a suitable interfacial Galvani potential leads to the nucleation of silver metal at the interface. Also it was clearly observed that the particles formed at the interface absorb and scatter the incident light.

It is clear that Ag nucleation occurs via a complex and irreversible reaction, the irreversibility being due to the presence of the stabilising ligand that also increases the solubility of the particles in the aqueous phase.

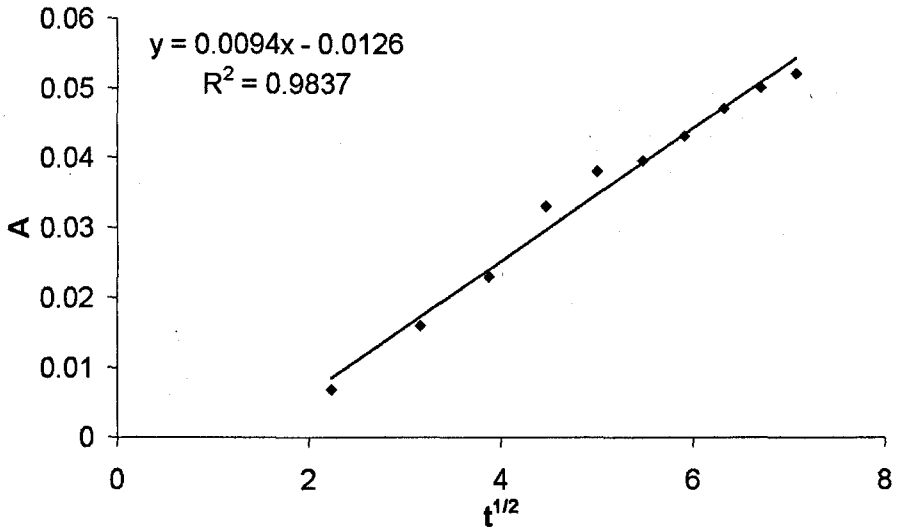

Figure 6.1.1 Time dependence of the absorbance for potential step experiment to +215 mV. The concentrations refer to Cell 6.

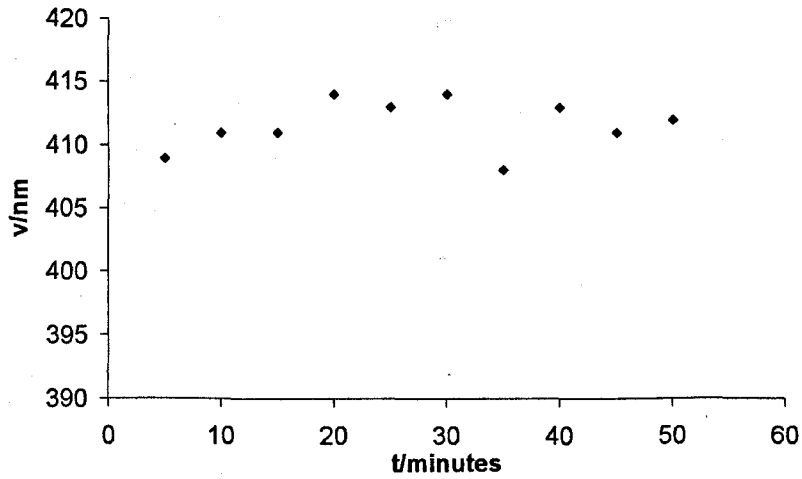

Figure 6.1.2 Variations of wavelength of the Ag plasmon absorption band with time for a potential step to +215 mV. Experimental conditions as described in Cell 6.

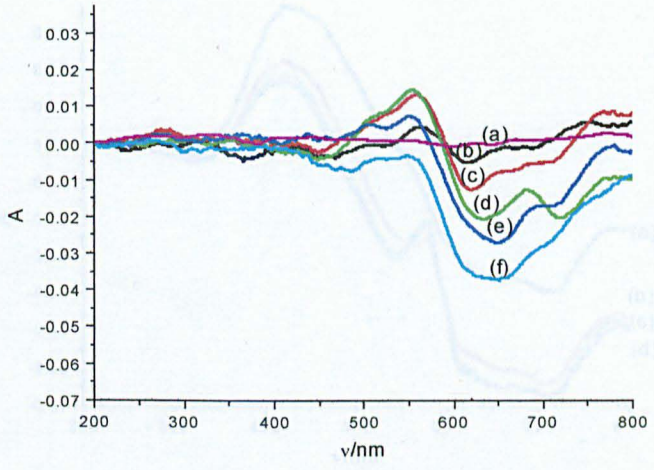

Figure 6.1.3 The optical response resulting from the application of a potential scan to the system described in Cell 6. The optical signal was recorded in transmission mode. The signals were recorded on the forward scan at applied potentials of (a) –250 (b) –200 (c) –150 (d) –100 (e) –50 and (f) 0 mV.

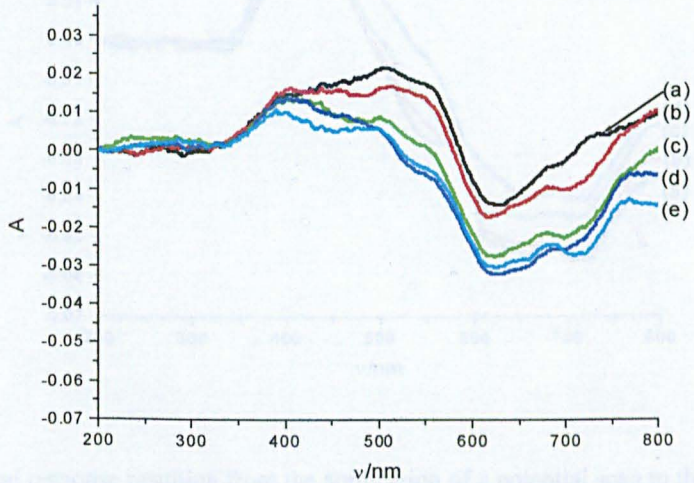

Figure 6.1.4 Optical response resulting from the application of a potential scan to the system described in Cell 6. The optical signal was recorded in transmission mode. The signals were recorded on the forward scan at applied potentials of (a) 50, (b) 100, (c) 150, (d) 200 and (e) 250 mV.

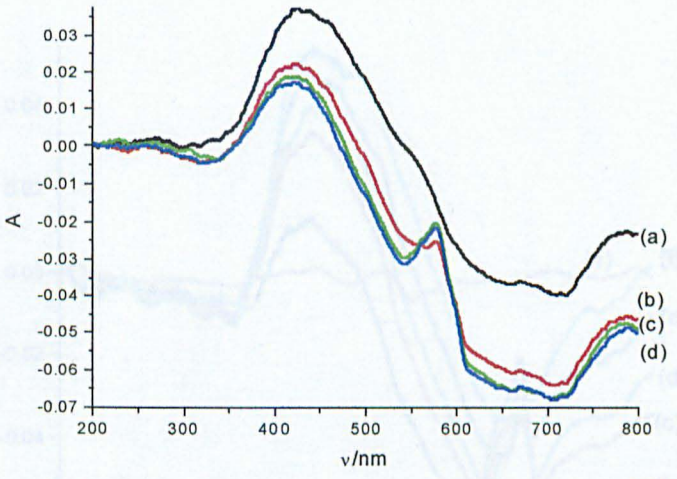

Figure 6.1.5 Optical response resulting from the application of a potential scan to the system described in Cell 6. The optical signal was recorded in transmission mode. The signals were recorded on the reverse scan at applied potentials of (a) 50, (b) 0, (c) –50 and (d) -100 mV.

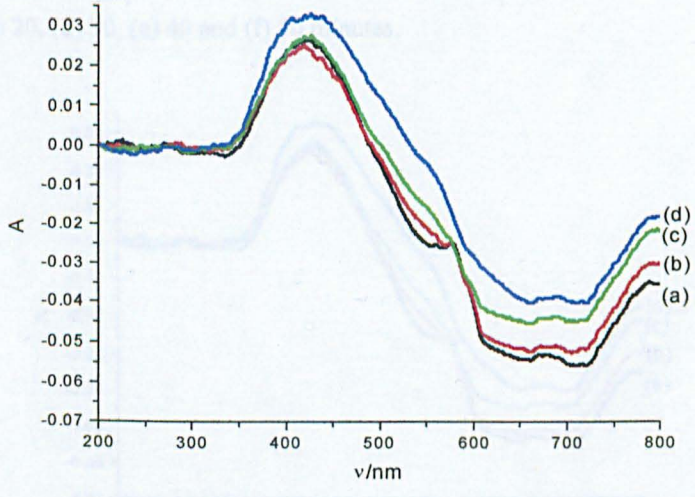

Figure 6.1.6 Optical response resulting from the application of a potential scan to the system described in Cell 6. The optical signal was recorded in transmission mode. The signals were recorded on the reverse scan at applied potentials of (a) -200, (b) -250, (c) –300 and (d) -350 mV.

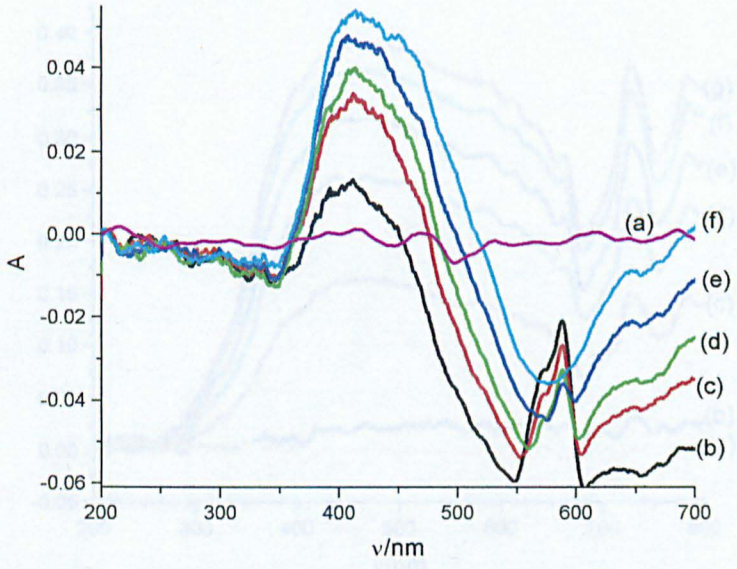

Figure 6.1.7 Optical response resulting from the application of a potential of +215 mV to the system described in Cell 6. The optical signal was recorded in transmission mode. The signals were recorded at (a) 0, (b) 10, (c) 20, (d) 30, (e) 40 and (f) 50 minutes.

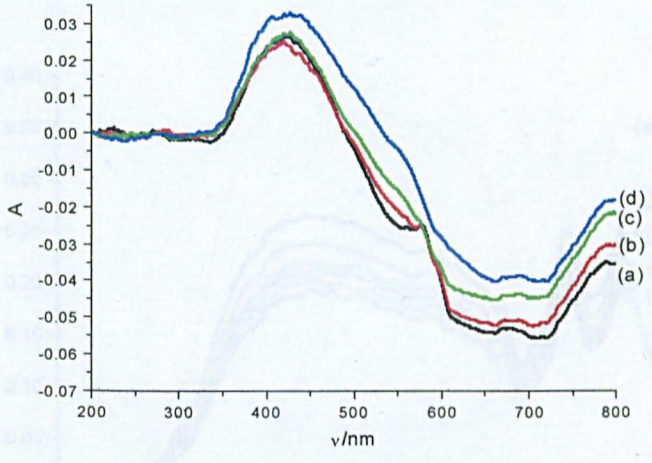

Figure 6.1.8 Optical response resulting from the application of a potential of –250 mV to the system described in Cell 6. The optical signal was recorded in transmission mode. The signals were recorded at (a) 0, (b) 10, (c) 20, (d) 30, (e) 40 and (f) 50 minutes.

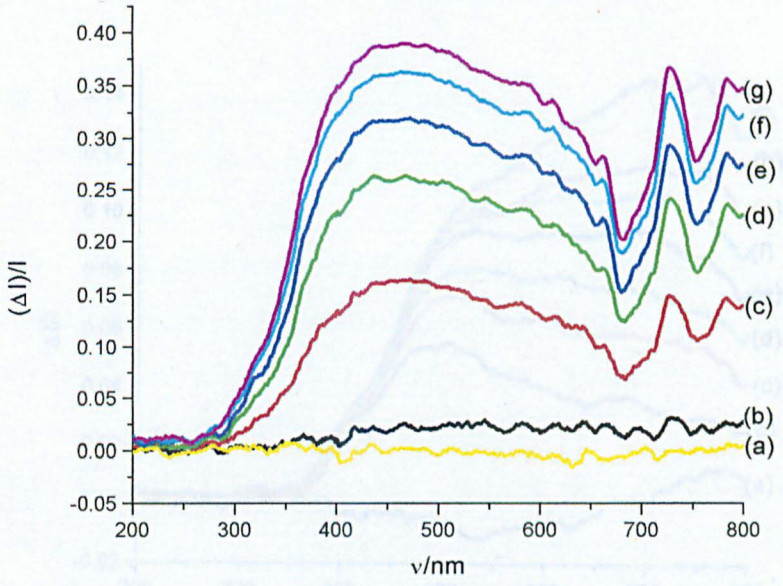

Figure 6.2.1 Optical response resulting from the application of a potential of +215 mV to the system described in Cell 6. The optical signal was recorded in scattering mode. The signals were recorded at (a) 0, (b) 5, (c) 10, (d) 15, (e) 20, (f) 25 and (g) 30 minutes.

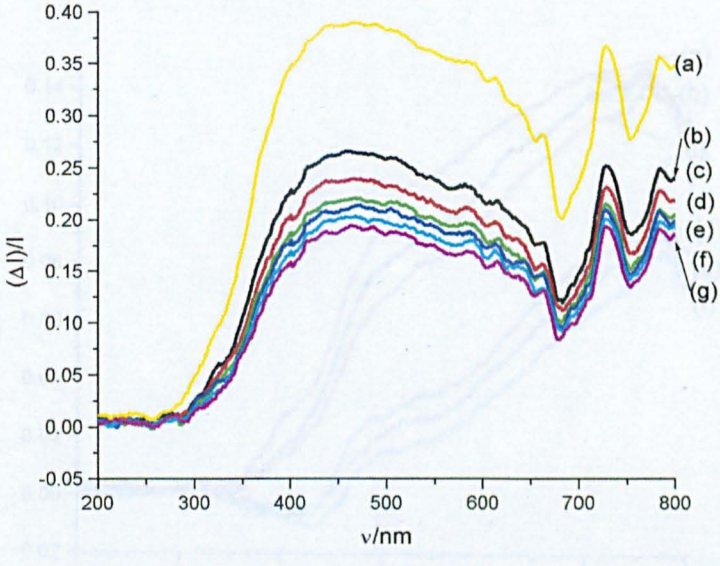

Figure 6.2.2 Optical response resulting from the application of a potential of –250 mV to the system described in Cell 6. The optical signal was recorded in scattering mode. The signals were recorded at (a) 0, (b) 5, (c) 10, (d) 15, (e) 20, (f) 25 and (g) 30 minutes.

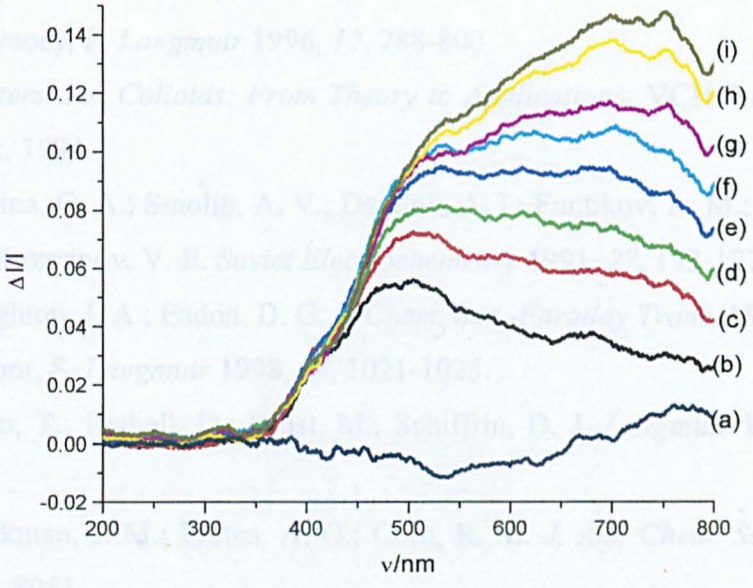

Figure 6.3.1 Optical response resulting from the application of a potential of +215 mV to the system described in Cell 6. The optical signal was recorded in reflectance mode. The signals were recorded at (a) 0, (b) 5, (c) 10, (d) 15, (e) 20, (f) 25, (g) 30, (h) 35, and (i) 40 minutes.

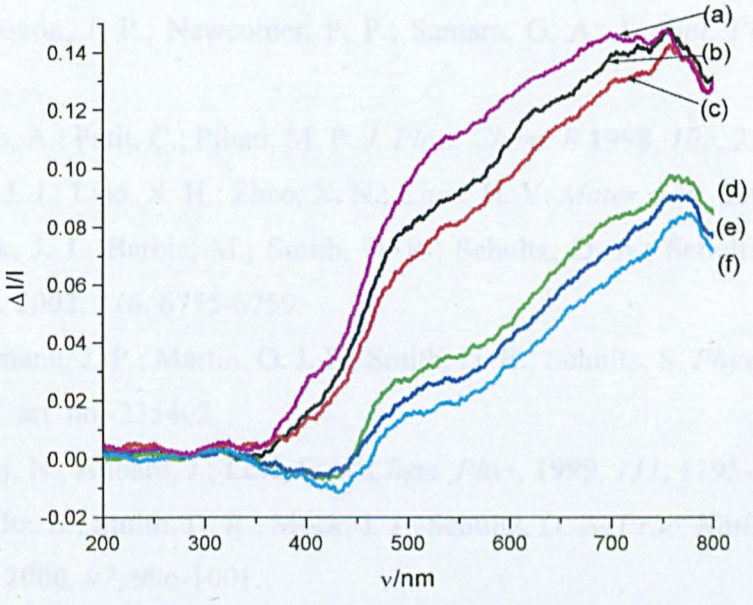

Figure 6.3.2 Optical response resulting from the application of a potential of –250 mV to the system described in Cell 6. The optical signal was recorded in reflectance mode. The signals were recorded at (a) 0, (b) 5, (c) 10, (d) 15, (e) 20 and (f) 25 minutes.

6.5. References

(1) Mulvaney, P. *Langmuir* **1996**, *12*, 788-800.

(2) *Clusters and Colloids: From Theory to Applications*; VCH Publishers: New York, 1994.

(3) Tsirlina, G. A.; Smolin, A. V.; Danilov, A. I.; Funtikov, A. M.; Polukarov, Y. M.; Kazarinov, V. E. *Soviet Electrochemistry* **1991**, *27*, 173-177.

(4) Creighton, J. A.; Eadon, D. G. *J. Chem. Soc.-Faraday Trans.* **1991**, *87*, 3881.

(5) Kapoor, S. *Langmuir* **1998**, *14*, 1021-1025.

(6) Baum, T.; Bethell, D.; Brust, M.; Schiffrin, D. J. *Langmuir* **1999**, *15*, 866-871.

(7) Brockman, J. M.; Frutos, A. G.; Corn, R. M. *J. Am. Chem. Soc.* **1999**, *121*, 8044-8051.

(8) Link, S.; El-Sayed, M. A. *J. Phys. Chem. B* **1999**, *103*, 8410-8426.

(9) Link, S.; Mohamed, M. B.; El-Sayed, M. A. *J. Phys. Chem. B* **1999**, *103*, 3073-3077.

(10) Link, S.; El-Sayed, M. A. *J. Phys. Chem. B* **1999**, *103*, 4212-4217.

(11) Wilcoxon, J. P.; Williamson, R. L.; R., B. *J. Chem. Phys.* **1998**, *93*, 9933.

(12) Wilcoxon, J. P.; Newcomer, P. P.; Samara, G. A. *J. Appl. Phys.* **1997**, *81*, 7934.

(13) Taleb, A.; Petit, C.; Pileni, M. P. *J. Phys. Chem. B* **1998**, *102*, 2214-2220.

(14) Zhu, J. J.; Liao, X. H.; Zhao, X. N.; Chen, H. Y. *Mater. Lett.* **2001**, *49*, 91-95.

(15) Mock, J. J.; Barbic, M.; Smith, D. R.; Schultz, D. A.; Schultz, S. *J. Chem. Phys.* **2002**, *116*, 6755-6759.

(16) Kottmann, J. P.; Martin, O. J. F.; Smith, D. R.; Schultz, S. *Phys. Rev. B* **2001**, *6423*, art. no.-235402.

(17) Felidj, N.; Aubard, J.; Levi, G. *J. Chem. Phys.* **1999**, *111*, 1195-1208.

(18) Schultz, S.; Smith, D. R.; Mock, J. J.; Schultz, D. A. *Proc. Natl. Acad. Sci. U. S. A.* **2000**, *97*, 996-1001.

(19) Elghanian, R.; Storhoff, J. J.; Mucic, R. C.; Letsinger, R. L.; Mirkin, C. A. *Science* **1997**, *277*, 1078-1081.

(20) Kuwana, T.; Heineman, W. R. *Acc. Chem. Res.* **1976**, *9*, 241.

(21) Bancroft, E. E. *Anal. Chem.* **1981**, *53*, 1862.

(22) Sailausa, N. *J. Am. Chem. Soc.* **1979**, *101*, 455.

(23) Webster, R. D.; Dryfe, R. A. W.; Coles, B. A.; Compton, R. G. *Anal. Chem.* **1998**, *70*, 792-800.

(24) Cheng, Y. F.; Schiffrin, D. J. *J. Chem. Soc.-Faraday Trans.* **1996**, *92*, 3865-3871.

(25) Gomis-Bas, C.; Schiffrin, D. J. *unpublished results*.

(26) Samec, Z.; Brown, A. R.; Yellowlees, L. J.; Girault, H. H. *J. Electroanal. Chem.* **1990**, *288*, 245-261.

(27) Bard, A. J., Faulkner, L. R., *Electrochemical Methods*; John Wiley: New York, 1980.

(28) Greef, R.; Peat, R.; Peter, L. M. *Instrumental Methods in Electrochemistry*; Ellis Horwood Limited: Chichester, 1985.

(29) Cunnane, V. J.; Schiffrin, D. J.; Beltran, C.; Geblewicz, G.; Solomon, T. *J. Electroanal. Chem.* **1988**, *247*, 203-214.

(30) Ung, T.; Liz-Marzan, L. M.; Mulvaney, P. *J. Phys. Chem. B* **2001**, *105*, 3441-3452.

(31) Mosseri, S.; Henglein, A.; Janata, E. *J. Phys. Chem.* **1989**, *93*, 6791-6795.

(32) Kurihara, K.; Kizling, J.; Stenius, P.; Fendler, J. H. *J. Am. Chem. Soc.* **1983**, *105*, 2574-2579.

(33) Kakiuchi, T.; Takasu, Y. *J. Electroanal. Chem.* **1994**, *365*, 293-297.

(34) Kakiuchi, T.; Takasu, Y. *J. Electroanal. Chem.* **1995**, *381*, 5-9.

(35) Ding, Z. F.; Brevet, P. F.; Girault, H. H. *Chem. Commun.* **1997**, 2059-2060.

(36) Ding, Z. F.; Reymond, F.; Baumgartner, P.; Fermin, D. J.; Brevet, P. F.; Carrupt, P. A.; Girault, H. H. *Electrochim. Acta* **1998**, *44*, 3-13.

(37) Ding, Z. F.; Wellington, R. G.; Brevet, P. F.; Girault, H. H. *J. Electroanal. Chem.* **1997**, *420*, 35-41.

(38) Kakiuchi, T.; Takasu, Y.; Senda, M. *Anal. Chem.* **1992**, *64*, 3096-3100.

(39) Simons, W.; Gonnissen, D.; Hubin, A. *J. Electroanal. Chem.* **1997**, *433*, 141-151.

(40) Cooley, A. C., Dagon, T. J. *J. Appl. Photogr. Eng.* **1976**, *2*, 36.

(41) Carney, M. J.; Lesniak, J. S.; Likar, M. D.; Pladziewicz, J. R. *J. Am. Chem. Soc.* **1984**, *106*, 2565-2569.

CHAPTER SEVEN

ELECTROCATALYSIS

7.1. Introduction

Electrocatalysis (mediated electron transfer)[1] at the liquid | liquid interfaces involves modifying the rate of the heterogeneous charge transfer process, by the application of an interfacial Galvani potential difference, so that the selectivity, yield and efficiency of the reaction are maximised. A chemical reaction at the liquid | liquid interface is more favourable than that in the homogenous system when the reactant and product have greatly different resolvation energies. Appropriate choice of solvent further accelerates the reaction by altering the redox properties of the reacting species.[2] The presence of the adsorbed species also facilitates the redox reaction between species in adjacent phases by reducing the distance between the redox species.

Electrocatalysis in the two-phase system has been demonstrated for redox reactions catalysed by species that are absorbed at the interface.[3-5] For the study of the reactivity of membrane-bound biological compounds the liquid | liquid interface offers one important advantage over the traditional metal electrode | electrolyte solution interface, in that the inherent mobility of the complex is not affected, whereas proteins irreversibly adsorbed onto bare metal electrodes are prone to denaturation. [6]

Transition metals and their complexes catalyse a wide variety of commercially important reactions and nanometer-sized catalysts not only act with increased activity and selectivity, but also catalyse reactions that are not successful with supported metal clusters. It has previously been shown that metallic colloids can act as a catalyst in a two-phase dehalogenation reaction of an organic substrate.[7]

Monolayer protected clusters (MPC) consist of a nanometer sized core of metal atoms coated with a monolayer of ligand that passivates the particle against aggregation. The electrochemistry of these clusters has been extensively investigated and quantized capactatance charging has been widely observed for monodisperse solutions.[8-12] Electrocatalysis experiments involving MPC's bound to redox active species has revealed that protected metal clusters can accept electron from a suitable electron donor[13,14] and that these charged solutions are stable for several hours.[13,15]

Using well-established electrochemical techniques, charge transfer reactions at a liquid | liquid interface can be studied. The electrochemical generation of transition metal particles has been discussed in Chapters 5 and 6. Electrochemical measurements were carried out in order to examine the behaviour of transition metal particles at the ITIES. Capacitance measurements were made in order to determine whether or not the aqueous colloids are charged. The possibility of carrying out heterogenous electron transfer (HET) reactions in the two-phase system was also considered.

Oxidation of the MPC prior to electrochemical measurements by electrolysis[13] and chemical[16] methods is possible and electrochemical studies of these charged clusters in the two-phase system found ET to be slow due to the increased distance between the reacting centres.[12]

7.2. Experimental

7.2.1. Preparation of colloids

Citrate stabilised colloids of Au, Pd, Pt and Ag were prepared by the classical, single-phase, Turkevich method with citrate acting as both reductant and stabilising agent.[17-19] $PdCl_2$, Na_2PtCl_4, Ag_2SO_4, $HAuCl_4$ and sodium citrate were used as the starting materials for the colloids. The exact mechanism of this synthesis is unclear, but the formation of particles results from the reduction of the metal ion by citrate and the particles are stabilised by excess citrate or reaction intermediates. Table 7.1 summarises the concentrations of metal to reductant in each preparation.

Table 7.1 Concentrations of metal and citrate used in the preparation of citrate stabilised particles.

Metal	[Metal] /μM	[Citrate] /mM
Au	126.9	1.7
Ag	129.9	1.7
Pt	19.2	3.6
Pd	211.0	22.7

7.2.2. Characterisation of colloids

The particles were characterised using UV-visible spectroscopy. UV-visible spectra were recorded using a Hewlett Packard 8452A Diode array spectrophotometer with a 450 nm by 125 mm quartz cell. The instrument parameters were set to an integration time of 10 seconds and a wavelength range of 200 to 820 nm. A background scan for the pure solvent (water) was run prior to each measurement.

7.2.3.Capacitance measurements of colloids

Ac voltammetry measurements were made using a homemade 4-electrode potentiostat, PPR1 waveform generator, and a Stanford SR830 lock-in amplifier. The internal waveform generator of the latter was used to generate the sinusoidal potential perturbation. Data acquisition was carried out using LabView software.

The pH of all citrate particle solutions was approximately 7; the addition of supporting electrolyte (5 mM) caused no appreciable change in the solution pH.

$$\mathrm{Ag}\,|\,\mathrm{AgCl}\,|\,\begin{matrix}1\ \mathrm{mM\ BTPPACl}\\ 10\mathrm{mM\ LiCl}\\ (\mathrm{aq})\end{matrix}\,|\,\begin{matrix}3\mathrm{mM\ BTPPATPBF_5}\\ (\mathrm{DCE})\end{matrix}\,|\,\sigma\,|\,\begin{matrix}5\ \mathrm{mM\ LiCl}\\ (\mathrm{aq})\end{matrix}\,|\,\mathrm{AgCl}\,|\,\mathrm{Ag}$$

Cell 7.1

7.2.4. Electrochemical charging of colloid

The electrochemical cell 7.2 was used for liquid | liquid voltammetric experiments with the aqueous soluble colloid. Electrochemical experiments were carried out using an Autolab potentiostat (PGSTAT 20, Eco Chemie) in the four-electrode mode. A SCE and Pt coil were the aqueous reference and counter electrodes respectively while a Pt coil and SCE dipped in a 10 mM TPAsCl aqueous solution served as the organic counter and reference electrodes respectively. A schematic representation of the cell used for these experiments is given in Chapter 3.

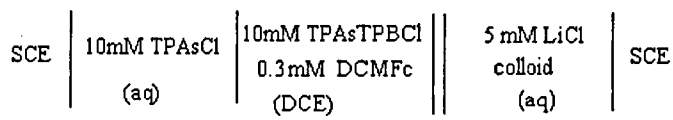

Cell 7.2

7.3. Results and Discussion

7.3.1. Preparation of colloids

The colloids were used in the voltammetric, charging and catalytic experiments as-prepared. Figure 7.1.1 shows a comparison between the absorbance spectra of the starting materials and the colloidal solution for the Au preparation. The characteristic plasmon absorbance band is observed.

The solutions were stable in the timescale of the experiment. However, particle aggregation was detected in the presence of a high concentration of ionic salt (e.g. LiCl). There was a striking colour change, from red to purple/blue, associated with this reaction for the Au colloid. Figure 7.1.2 shows the effect of particle aggregation on the UV-visible spectrum of the Au citrate colloid when the pH was increased from 7.8 to 12.2. The plasmon absorption band for spherical particles at 520 nm can still be observed but the aggregated cylindrical particles exhibit a band at 715 nm.[15] The particles were found to be stable in a 5 mM LiCl solution.

7.3.2. Characterisation of colloids

The UV-visible spectra of the colloidal solutions (Figures 7.1.1-7.1.5) were in good agreement with those obtained previously.[17-20] The absorbance spectra of the Pt particles (Figures 7.1.3) exhibit no spectral peaks in the wavelength range 200 to 800 nm, where the absorbance increases as the wavelength decreases. The dependence of the absorbance, A, on wavelength, λ, is a useful indication of particle size.[21] Based

upon the calculations made by Furlong[19] for Pt, the average particle size was estimated from a plot of -d(logA)/d (logυ) (Figure 7.1.4) for the Pt particles. It can be seen that the slope (S) is approximately constant in the spectral range 250-800 nm. For Pt particles, it has been estimated that the value of S decreases with increasing particle size and the presence of even a small fraction of larger particles results in a decrease in S.[19] A slope (S) of 1.9 corresponds to an average particle size of 2-8 nm.[19]

The plasmon band of the Ag particles (Figure 7.1.5) is quite broad indicating a large size distribution. The shoulder that can be seen at approximately 350 nm probably corresponds to a smaller particle size.

The parameters obtained from absorbance spectra are summarised in Table 7.2.

Table 7.2 Values for the maximum plasmon absorption (λ_{max}) for citrate stabilised particles and the theoretical particle radii (r_{av}) based upon the experimental conditions used.

Metal	r_{av} /nm	Colour	λ_{max} /nm
Au	20	wine/red	540
Pt	2-8	clear	<200
Pd	15	yellow	240
Ag	-	grey	380

7.3.3. Capacitance measurements of colloids

The interfacial capacitance between the metal colloidal solutions and a solution of the organic supporting electrolyte salt ($BTPPATPBF_5$) in 1,2-DCE was measured in an attempt to characterise the interfacial properties of these colloids. As described in Chapter 2, in the region where no transfer of the supporting electrolyte occurs, the differential capacitance can be calculated from the admittance using an equivalent circuit composed of a resistance (uncompensated iR drop, R) and a capacitance (interfacial capacitance, C) in series.

The purpose of these experiments was to determine the changes to interfacial properties that could result from the presence of metal nanoparticles at the water-1,2-DCE interface. In particular, it was of interest to determine whether the large negative charge carried by the colloidal solution would result in a strong asymmetry in the capacitance curves due to metal cluster adsorption at water negative potentials. It was hoped that these experiments would be correlated with the electrocatalytic properties of these systems.

Figures 7.2.1(a)–(d) show the potential dependence of the interfacial capacitance of the colloidal metal solutions investigated in contact with 3 mM $BTPPATPBF_5$ in 1,2-DCE. As described in Chapter 2, the limits of the polarisation window result from transfer of the ionic components of the supporting electrolyte across the interface. In the case of the base system, when the Galvani potential difference is made more negative, the transfer of $BTPPA^+$ (or Cl^- or citrate in the opposite direction) from the organic to the aqueous phase occurs, while at the positive limit $TPBF_5^-$ (or Li^+ or

Na^+) will transfer from water to organic phase. In the presence of the colloids, it was anticipated that specific adsorption of the colloid at the interface, would occur at water negative potentials. At negative potentials, in the presence of the Au and Ag colloids, a lower capacitance was observed as compared with the base system. For the Pd and Pt colloids, the opposite effect was observed.

The main difference in the capacitance behaviour in the presence of the four metals is the position of the capacitance minimum. In the absence of the colloid, the capacitance minimum is located at 380 mV. Addition of Au or Ag colloids to the system resulted in the potential of the minimum being shifted to a more negative potential. Again, the Pd and Pt colloids show the opposite effect. The origin of the shift is unclear, however for three of the metals considered (Au, Pt and Pd), it follows the variation in electronegativies of the metal atom (Table 7.2). If this were to reflect the order of specific adsorption of a negatively charged species, the order would be Ag<Au<Pt<Pd. Since TEM images of the preparations were not obtained at the time of the experiment, we can only speculate on the possible origin of this behaviour. Since a strong dependence of the capacitance mimima on base electrolyte concentration exists, in the absence of any specific absorption,[22] this shift alone cannot be assumed to indicate the adsorption of colloid at the interface. Also since no asymmetry in the $C/\Delta^{w}_{o}\Phi$ dependence is in evidence, it must be concluded that the citrate stabilised particles do not approach the interfacial region to the point where coagulation can occur. Considering the hydrophilic nature of citrate, and the fact that the hydration energy of the colloid must be very negative, this is not unexpected. In consequence, penetration of the interfacial mixed solvent layer[23] is strongly inhibited and the charged colloidal particle is always present in the aqueous side of

the interface. This is also borne out by the observed irreversibility of ET to the metal core from the electron donor in the organic phase (see Section 7.3.4).

From the experimental results, it is unlikely that specific adsorption does occur, as a large deviation in the capacitance behaviour was not observed.[24] Furthermore, the formation of a monolayer of metal nanoparticles would result in a sudden increase in capacitance, as the interface would behave as two metal-solution interfaces which is not observed for any of the metal colloids investigated.

There are two major contributions to the Gibbs Energy of adsorption of species at the ITIES, electrostatic and non-electrostatic contributions. The potential of the capacitance minimum reflects the potential of zero charge of the interface. Also, the strong hydration of the particle would result in its approach to the interface being strongly inhibited. These two effects rule out specific electrostatic contributions to explain the different capacitance curves obtained.

It can be concluded that the main polar interaction that can be considered is due to the polarisability of the nanoparticles. The metallic cores have a classical polarisability (α) given by:[25]

$$\alpha = R^3 \qquad (7.1)$$

where R is the core radius. Equation 7.1 regards the metallic core as having a density of electrons equal to that of a bulk metal. This is observed for particles of radius greater than 2 nm[26] which is the case here.

Thus it would be expected that charge induced dipole and dispersion forces[27] would determine the Gibbs energy of interaction of the metal particles and the organic phase. The position of the minimum observed in Figures 7.2.1(a) –(d) will be determined by the size distribution in a particular preparation. Although a quantitative description cannot be given at present, the particles effect on the capacitance curves is interesting and warrants further study, the ideas discussed should serve as a guideline for understanding the structure of the interface.

Table 7.1 Table of Minimum in the capacitance curve (E_{min}) and Electonegativies on the Pauling scale (E) of the metals.

Colloid	E_{min}/mV	E
Ag	300	1.93
Pd	420	2.20
Pt	390	2.28
Au	350	2.54

7.3.4. Electrochemical charging of colloid

The colloids considered were those of the aqueous soluble, citrate stabilised Au and Pd particles. The colloids were used as-prepared and no size separation was carried out. The voltammetric response of an aqueous colloid in contact with an electron donor in the organic phase was studied by cyclic voltammetry using Cell 7.2. Prior to performing an electrochemical measurement, the aqueous particle colloid and the 1,2-DCE solution containing the electron donor were contacted in the absence of an applied potential for prolonged periods to determine the stabilities of the systems

under investigation. In all cases there was no evidence of either spontaneous reaction or decomposition.

For each of the colloids studied, an irreversible response was obtained as the potential of the aqueous phase was swept to more positive values (Figures 7.3.1 and 7.3.2). This response was detected only when the electron donor, DCMFc, and the colloid were both present in the cell; in the absence of either, the response followed the baseline. The peak current is linearly dependent on the square root of the sweep rate and the peak potential shifts to more positive values with increasing sweep rate. A representative plot is shown for Au in Figure 7.3.3.

The colloids were used as prepared, hence the possibility that residual metal salt was present in the solutions had to be considered. Citrate was present in excess in each of the preparations (see Table 7.1) and it is expected that complete reduction of the metal ion occurred in each case. This was confirmed by several observations. Firstly, the electrochemical response would be more complex if a significant concentration of metal ion were left in the solution. The characteristic behaviour of these Au, Pd, Ag and Pt salts at the ITIES was described in Chapter 5. The Au, Pt and Ag salts undergo ion transfer (IT) from the aqueous to the organic phase within the potential window and this behaviour was not observed for the particle solutions. Four-electrode voltammetry for $AuCl_4^-$, and $AuCl_4^-$ /sodium citrate solutions each show the characteristic ion transfer waves, i.e. citrate does not prevent transfer of the ion by forming a hydrophilic complex with $AuCl_4^-$. This behaviour was not observed for Au citrate. Secondly, in the case of the Pd salt a visible reaction occurred between the salt and DCMFc when the two phases were placed in contact but no reaction was

detected for a solution of the Pd colloid. Also, the concentration of DCMFc used with the colloid studies were lower than those required to cause nucleation (typically 0.3 and 5 mM respectively see Chapter 5). Thirdly, the polarisation curve for the metal ions at a Pt microelectrode show obvious reduction, but the voltammogram of the colloid followed the baseline scan. Representative results are shown in Figure 7.3.4 for Au. Finally, a comparison of the UV-visible spectra of the starting material and of the colloid is a good indication of the degree of reaction. UV-visible spectra of the colloids showed no evidence of the presence of starting material. This is illustrated for Au in Figure 7.1.1.

Thus, it can be concluded, that the colloidal solutions did not contain significant amounts of unreacted starting materials and therefore, the electrochemical response observed with the 4-electrode system is not due to trace contamination by the metal complexes.

The possibility that the voltammetric response was due to redox reactions with the stabilising agent/reductant was also considered. Voltammetry scans were run under identical conditions with citrate instead of the colloidal metal solutions. At the ITIES, the addition of citrate produced a slight increase in capacitance over the baseline but no reduction process associated with this anion was observed. In addition, the fact that a similar voltammetric response was observed using a Pd colloid stabilised by the ligand sodium sulfanilate (p-$H_2NC_6H_4SO_3Na$) in the same two-phase system[28] confirms that the response is characteristic of the colloid and not the stabilising ligand.

From a comparison of Figures 7.3.1 and 7.3.2 it can be seen that the response for both systems was very similar. The occurrence of an irreversible reaction is common to all the particles investigated, indicating that the behaviour is characteristic of the particles and not of the particular metal. One possibility is that the voltammetric behaviour corresponds to an electrocatalytic process, for example that the particles act as nanoelectrodes at the interface catalysing either the reduction of dissolved oxygen or the hydrogen evolution reaction. In order to ascertain the origin of the observed voltammetric wave, the concentration of the reacting species was calculated from the dependence of the peak current on the sweep rate according to the Randles-Sevcik equation

$$j_p = 2.69 \times 10^5 n^{3/2} D^{1/2} c \nu^{1/2} \qquad (7.2)$$

If the reacting species are the particles this concentration can be estimated from Equation 7.1 provided that the diffusion coefficient is known. An estimate of the diffusion coefficient for the Au particles can be obtained from the Stokes-Einstein Equation.[27,29]

$$r = \frac{kT}{6\pi\eta D} \qquad (7.3)$$

where k is the Boltzmann constant, T the absolute temperature, η the viscosity of water (0.89 mPa s at 25 ^{0}C),[30] and r is the particle radius. From equation (7.2), for a particle of 20 nm radius the diffusion coefficient in water at 25 ^{0}C is 0.25 $\times$ 10^{-6} cm^2 s^{-1}. From the results in Figure 7.3.2 $dj_p/d(\nu^{-1/2})$ is 8.71 $\times$ 10^{-5} cm^{-2}V$^{-1/2}$s$^{1/2}$ and the equivalent concentration for a one ET reaction is 6.48 $\times$ 10^{-4} M. This calculation shows that the ET reaction must involve a number of electrons much greater than one since the molar concentration of particles was very small compared with the original

concentration of Au(III). The main conclusion of these experiments is that a multi-electron transfer reaction takes place.

The possibility that the voltammetric waves observed were due to oxygen reduction catalysed by the particles was further investigated by comparing voltammetric experiments of air and oxygen saturated solutions. Oxygen saturation should result in a five-fold increase in peak current. The results are shown in Figure 7.3.5. These show a slight increase in current upon saturation with oxygen clearly showing O_2 is not responsible for the voltammetric wave. Experiments carried out in deoxygenated solutions also showed an irreversible response at positive potentials.

In conclusion, it is proposed that the responses observed in Figures 7.3.1 and 7.3.2 are the result of the heterogeneous charging of the aqueous colloid, which is adsorbed at the interface, with electrons from DCMFc. This reaction can be described as follows:

$$M_{ads}\,(aq) + DCMFc\,(org) \rightarrow M^{-}(aq) + DCMFc^{+} \qquad (7.4)$$

where M_{ads} is the citrate stabilised metal colloidal particle adsorbed at the interface. The ET reaction is facilitated by the ability of the uncharged particles to approach the interface, since the distance of closest approach between the reacting species is reduced.

The ET reaction observed at positive potentials appears to be irreversible even at low scan rates. This irreversibility is likely to be related to the charge on the particle. The strong negative charge carried by the colloidal particles results in their repulsion from the interface at positive potentials and in consequence, a decrease of the

transfer coefficient. As discussed in Chapter 4, ET occurs via tunnelling of the electron between states in the electrode (or in this case, an electron donor in the organic phase) and those in the reactant. The rate of electron tunnelling decreases exponentially with increasing distance as follows.

$$k^0 \propto \exp[-\beta(x - x_0)] \qquad (7.5)$$

where k^0 is the standard rate constants for the heterogeneous electron transfer (HET) reaction at the distance x from the electrode surface; x_0 is the distance of closest approach and the meaning of β has been discussed in Chapter 4. The overall negative charge on the particle makes its approach to the interface unfavourable at water positive potentials, where ET from the organic phase to the particles occurs. This is because a charge exclusion zone is created in the vicinity of the interface at positive potentials. Both the particle and the reducing agent are separated from the interface by a large distance, due to their respective hydrophilic and hydrophobic natures. In other words, the ET reaction is largely irreversible due to the large distance separating the two redox centres. This is probably the main factor determining the low rate constant value observed for the ET. The probability of ET occurring to the charged particle is even lower, since the net negative charge on the particle is increased with the initial ET, which results in a further increase in the distance between the two redox couples.

At higher sweep rates however, a peak due to the de-charging of the particles, was observed at negative potentials. In this case the reaction occurs before the particles diffuse from the interface.

A recent SECM investigation of the interfacial charge transfer between a monodisperse solution of charged MCP's and a redox couple in the adjacent phase also found the reaction to be extremely slow.[12] This worker noted that the ET reaction at the ITIES was dependent on the charge of the colloid, while the reaction at the metal electrode | electrolytic solution did not depend on core charge.

The results obtained here support the suggestion that the metallic colloidal particles could be used as an electro-mediator in a two-phase redox reaction by virtue of their ability to store charge. Figure 7.1 shows a schematic representation of the generalised interfacial reaction mechanism involved in an electrocatalytic reaction. The use of the stored charge on the particles to initiate ET process in the adjacent phase was previously considered.[7,31]

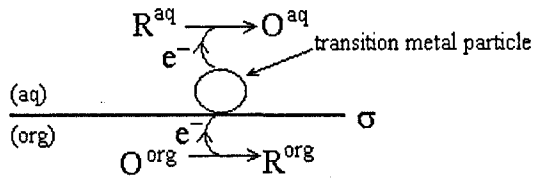

Figure 7.1 Schematic representation of use of aqueous soluble transition metal particles as an electro-mediators in a two phase redox reaction. O and R represent the oxidised and reduced forms of the redox couple; (aq) and (org) refer to the immiscible water and organic phases respectively and σ is the interface between the two phases.

These results show that colloidal particles are capable of acting in a manner that is analogous to a simple redox couple, in the two-phase system. The results are supported by suggestions made previously. Lahtinen[32] suggested that Pd colloids

became negatively charged in the two-phase system and in a separate work[31] that Pd particles electrogenerated at the ITIES act as electron transfer (ET) mediators for reactions in the water phase. Interestingly this author also noted that the stored charge is stable for several hours.[32]

7.4. Conclusions

It has been shown that the particles are capable of undergoing a multiple electron transfer step with an electron donor in the adjacent phase, when a suitable interfacial potential is applied across the ITIES. In the present work, it was found that the voltammetric response of the two metals (Pd and Au) was similar. The particles act as tiny capacitors capable of giving and receiving electrons. In this sense citrate stabilised colloidal particles may be seen as a suitable substrate for heterogeneous catalysis or electrocatalytic processes. From capacitance measurements, it was determined that specific adsorption of the colloids at the ITIES does not occur. Due to the large distance between the redox centres at the ITIES the charging appears irreversible. The capacitance behaviour of the colloids at the ITIES showed interesting features, however, without further investigation it is not possible to determine the exact meaning of this behaviour.

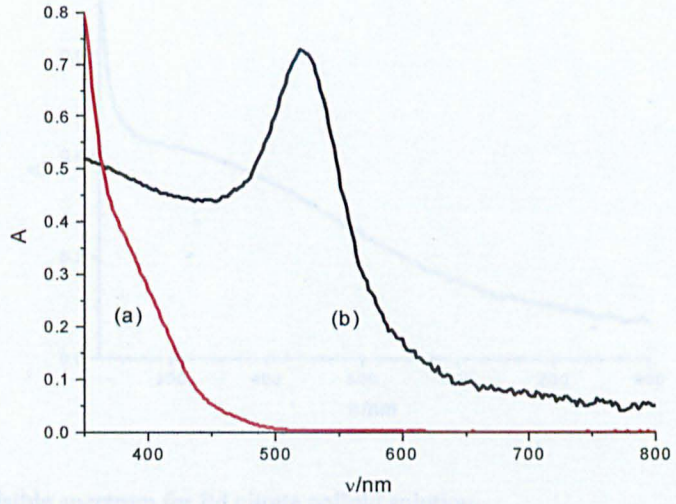

Figure 7.1.1 UV-visible spectra for (a) $AuCl_4^-$ and (b) Au citrate stabilised particles.

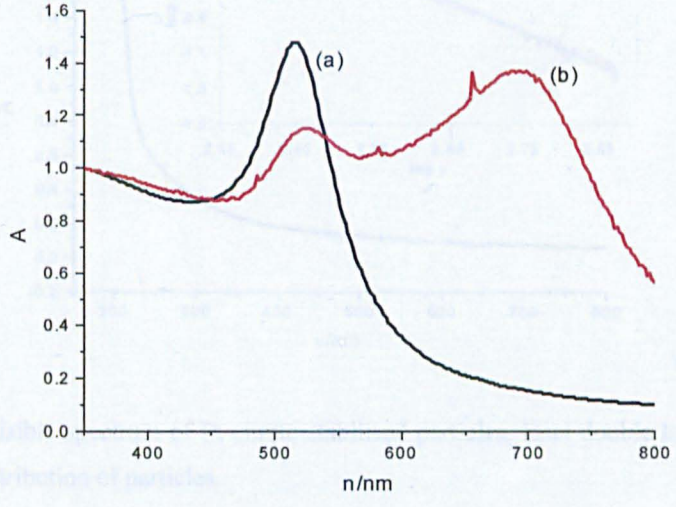

Figure 7.1.2 UV-visible spectra showing the effect of pH on Au citrate stabilised particles (a) 7.8 and (b) 12.2.

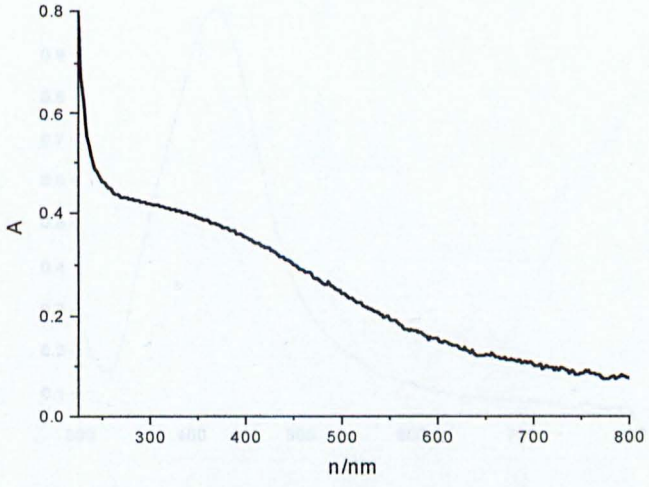

Figure 7.1.3 UV-visible spectrum for Pd citrate colloid solution.

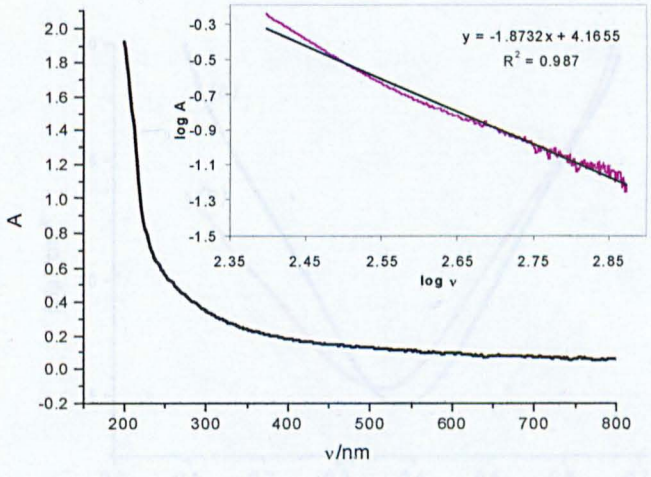

Figure 7.1.4 UV-visible spectrum of Pt citrate stabilised particles, inset double logarithmic plot used to estimate size distribution of particles.

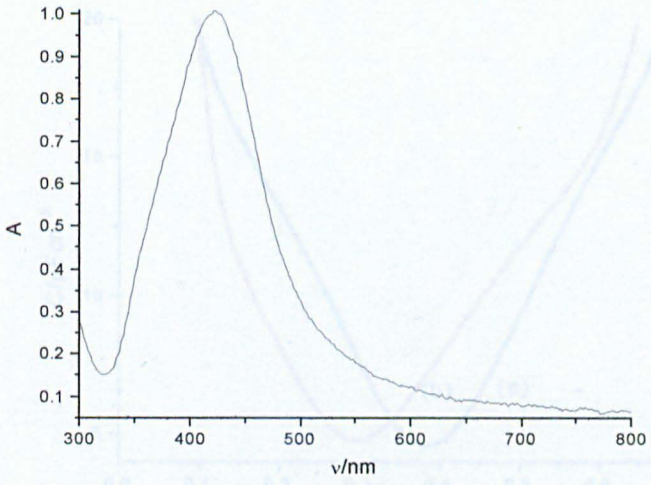

Figure 7.1.5 UV-visible spectrum of Ag citrate stabilised particles

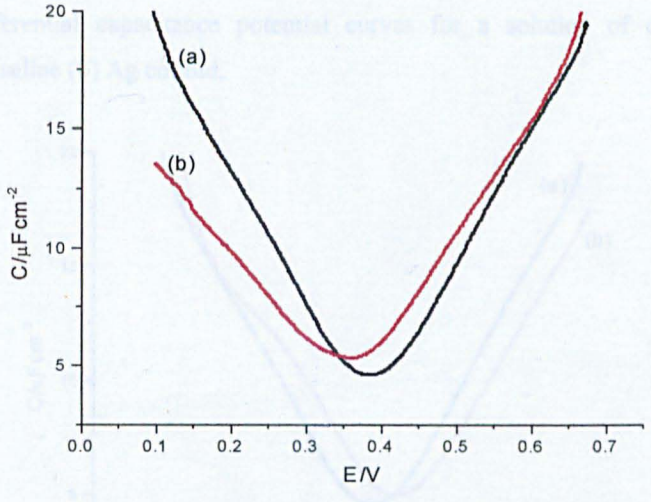

Figure 7.2.(a) Differential capacitance potential curves for a solution of citrate stabilised Au nanoparticles. (a) baseline (b) Au colloid.

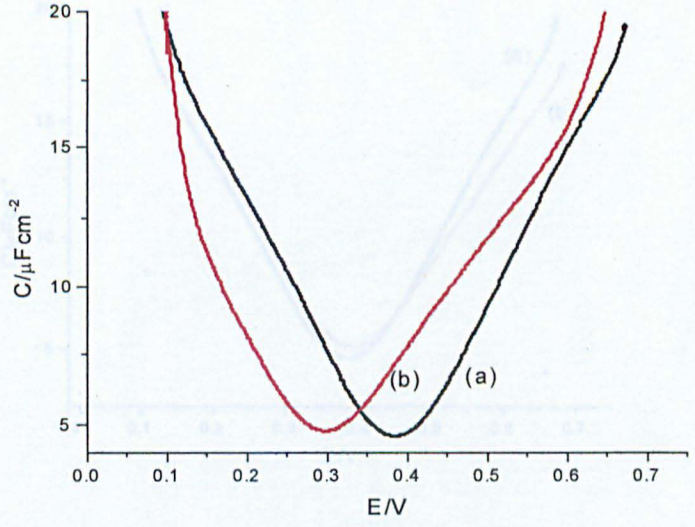

Figure 7.2.(b) Differential capacitance potential curves for a solution of citrate stabilised Ag nanoparticles. (a) baseline (b) Ag colloid.

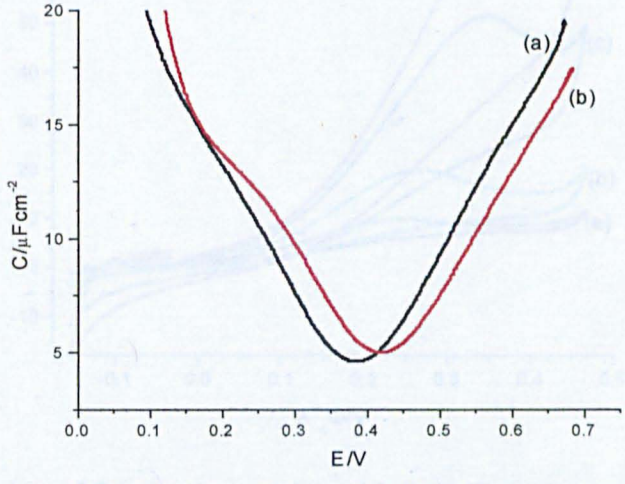

Figure 7.2.(c) Differential capacitance potential curves for a solution of citrate stabilised Pd nanoparticles. (a) baseline (b) Pd colloid.

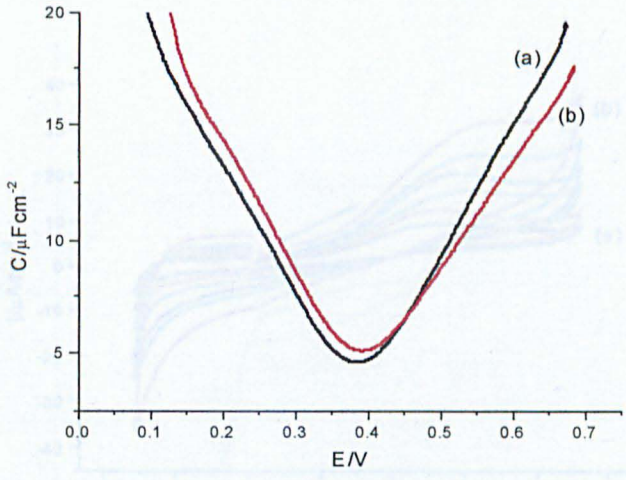

Figure 7.2.(d) Differential capacitance potential curves for a solution of citrate stabilised Pt nanoparticles. (a) baseline (b) Pt colloid.

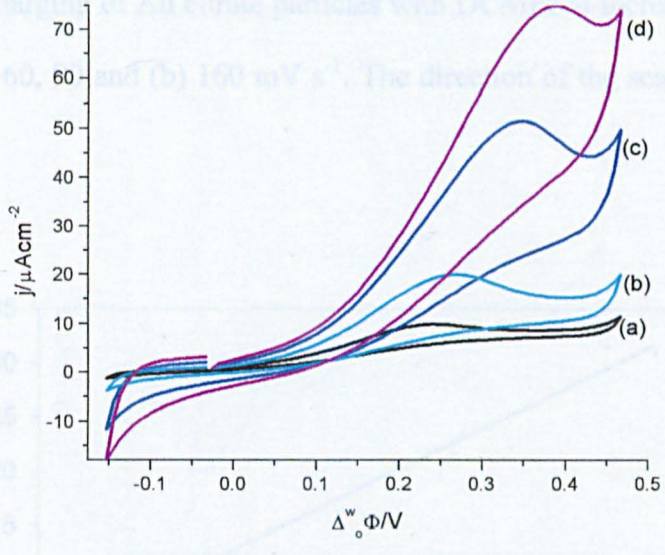

Figure 7.3.1 Charging of Pd citrate particles with DCMFc at increasing scan rates of (a) 10, (b) 40 (c) 90 and (b) 160 mV s^{-1}.

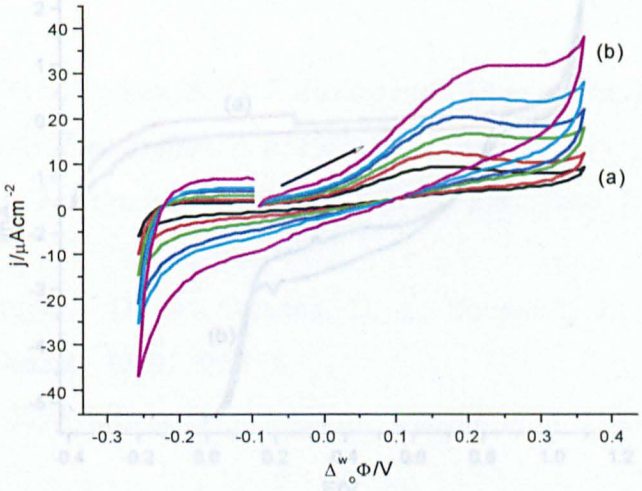

Figure 7.3.2 Charging of Au citrate particles with DCMFc at increasing scan rates of (a) 10, 20, 40, 60, 90 and (b) 160 mV s^{-1}. The direction of the scan is marked by an arrow.

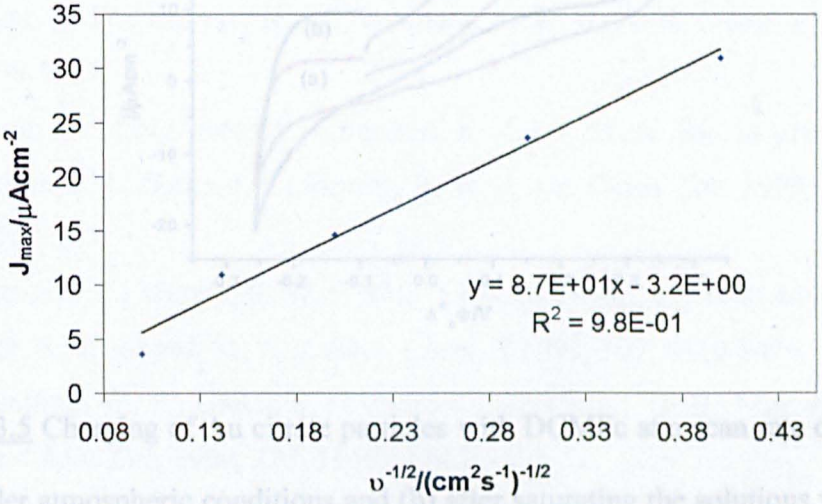

Figure 7.3.3 Dependence of maximum peak current density (J_{max}) on the sweep rate for charging of Au citrate particles with DCMFc. Conditions as in Figure 7.3.2.

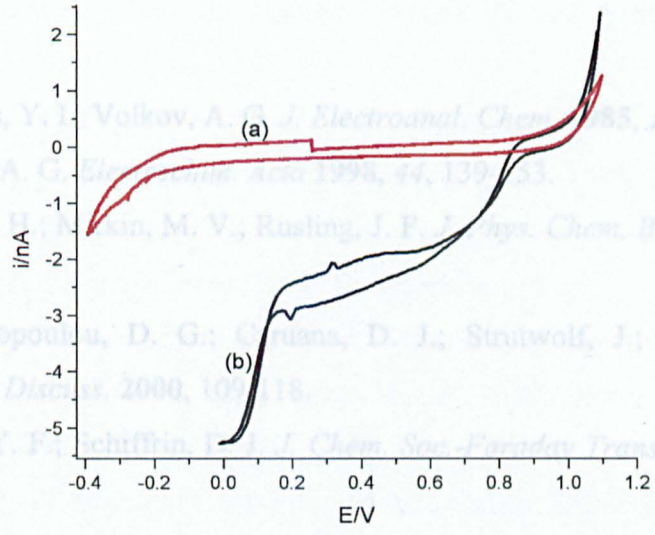

Figure 7.3.4 Polarisation curve for (a) Au citrate derivitised particles and (b) 0.5 mM $AuCl_4^-$ at a Pt microelectrode/electrolyte interface at a sweep rate of 50 mVs^{-1}.

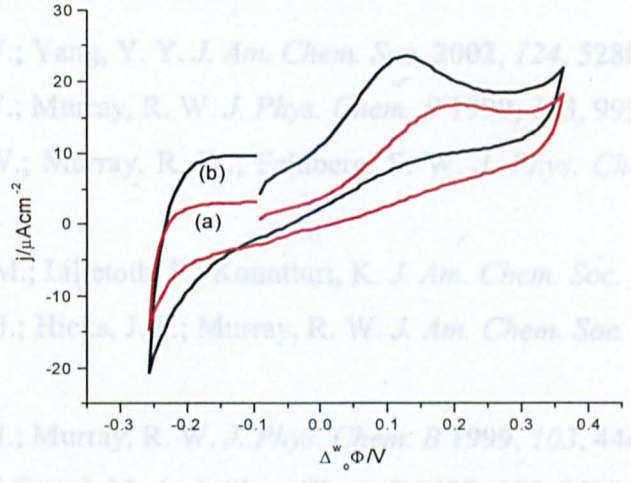

Figure 7.3.5 Charging of Au citrate particles with DCMFc at a scan rate of 40 mV s^{-1}, (a) Under atmospheric conditions and (b) after saturating the solutions with O_2. all other conditions as in Figure 7.3.2.

7.5. References

(1) Kharkats, Y. I.; Volkov, A. G. *J. Electroanal. Chem.* **1985**, *184*, 435-442.

(2) Volkov, A. G. *Electrochim. Acta* **1998**, *44*, 139-153.

(3) Shao, Y. H.; Mirkin, M. V.; Rusling, J. F. *J. Phys. Chem. B* **1997**, *101*, 3202-3208.

(4) Georganopoulou, D. G.; Caruana, D. J.; Strutwolf, J.; Williams, D. E. *Faraday Discuss.* **2000**, 109-118.

(5) Cheng, Y. F.; Schiffrin, D. J. *J. Chem. Soc.-Faraday Trans.* **1994**, *90*, 2517-2523.

(6) Hickel, A.; Radke, C. J.; Blanch, H. W. *J. Mol. Catal. B-Enzym.* **1998**, *5*, 349-354.

(7) Schiffrin, D. J.; Cheng, Y. *The Electrochemical Society and The International Society of Electrochemistry* **1997**, *97-2*, Abstract No. 961.

(8) Cheng, W. L.; Dong, S. J.; Wang, E. K. *Electrochem. Commun.* **2002**, *4*, 412-416.

(9) Chen, S. W.; Yang, Y. Y. *J. Am. Chem. Soc.* **2002**, *124*, 5280-5281.

(10) Chen, S. W.; Murray, R. W. *J. Phys. Chem. B* **1999**, *103*, 9996-10000.

(11) Chen, S. W.; Murray, R. W.; Feldberg, S. W. *J. Phys. Chem. B* **1998**, *102*, 9898-9907.

(12) Quinn, B. M.; Liljetoth, P.; Konntturi, K. *J. Am. Chem. Soc.* **in press**.

(13) Pietron, J. J.; Hicks, J. F.; Murray, R. W. *J. Am. Chem. Soc.* **1999**, *121*, 5565-5570.

(14) Pietron, J. J.; Murray, R. W. *J. Phys. Chem. B* **1999**, *103*, 4440-4446.

(15) Link, S.; El-Sayed, M. A. *J. Phys. Chem. B* **1999**, *103*, 8410-8426.

(16) Wuelfing, W. P.; Green, S. J.; Pietron, J. J.; Cliffel, D. E.; Murray, R. W. *J. Am. Chem. Soc.* **2000**, *122*, 11465-11472.

(17) Turkevich, J.; Kim, G. *Science* **1970**, 873-879.

(18) Turkevich, J.; Cooper Stevenson, P.; Hillier, J. *Disc. of the Faraday Society* **1951**, *11*, 55-75.

(19) Furlong, D. N.; Launikonis, A.; Sasse, W. H. F.; Sanders, J. V. *J. Chem. Soc. Faraday Trans. I* **1984**, *80*, 571-&.

(20) Creighton, J. A.; Eadon, D. G. *J. Chem. Soc.-Faraday Trans.* **1991**, *87*, 3881.

(21) Busser, G. W.; vanOmmen J.G.; Lercher, J. A. In *Advanced Catalysis and Nanostructured Materials, Modern Synthetic Methods.*; Moser, W. K., Ed.; Academic Press: U.S.A., 1996.

(22) Volkov, A. G. *Langmuir* **1996**, *12*, 3315-3319.

(23) Girault, H. H.; Schiffrin, D. J. *J. Electroanal. Chem.* **1983**, *150*, 43-49.

(24) Cheng, Y.; Cunnane, V. J.; Schiffrin, D. J.; Mutomaki, L.; Kontturi, K. *J. Chem. Soc.-Faraday Trans.* **1991**, *87*, 107-114.

(25) Blottcher, C. J. F. *Theeory of Electric Polarisation*: Amsterdam, 1973.

(26) Clarke, N. Z.; Waters, C.; Johnson, K. A.; Satherley, J.; Schiffrin, D. J. *Langmuir* **2001**, *17*, 6048-6050.

(27) Atkins, P. W. *Physical Chemistry*; 4th ed.; Oxford University Press: Suffolk, 1990.

(28) Lahtinen, R. Ph.D. Thesis, Helsinki University of Technology, 2000.

(29) Robinson, R. A.; Stokes, R. H. *Electrolytic Solutions*: London, 1959.

(30) *CRC Handbook of Chemistry and Physics*; 76th ed., 1995.

(31) Lahtinen, R. M.; Fermin, D. J.; Jensen, H.; Kontturi, K.; Girault, H. H. *Electrochem. Commun.* **2000**, *2*, 230-234.

(32) Lahtinen, R.; Fermin, D. J.; Kontturi, K.; Girault, H. H. *J. Electroanal. Chem.* **2000**, *483*, 81-87.

CHAPTER EIGHT

CONCLUSIONS

8.1. Conclusions

Only a limited number of electron transfer systems have been investigated at the interface between two immiscible solutions (ITIES). Three Ru(II) based redox couples soluble in the organic phase were proposed for this purpose. Using electrochemical techniques, it was found that these complexes were suitable for this purpose. Simple, quasi-reversible, heterogeneous ET was observed between these complexes and the hexacyanoferrate couple in the aqueous phase, the rate of which was much slower than at the metal electrode-electrolyte interface. This is related to the increased distance between the redox species at the ITIES. Kinetic and thermodynamic parameters were related to the degree of accessibility of the redox centre.

Metal clusters were prepared at the ITIES via a heterogeneous electron transfer reaction. The nucleation and growth of transition metal clusters was investigated using both electrochemical and spectroelectrochemical techniques. It was shown that, with careful choice of the experimental conditions, the potential controlled deposition of Hg, Au, Pt and Ag clusters at the interface is possible. The potential step and voltammetric responses obtained show behaviour characteristic of nucleation at a solid electrode. Thus, a model derived for nucleation at a solid electrode was applied to Ag and Pt nucleation at the ITIES in order to determine particle size. The dimensions of the particles deposited are in the nanometer size range. The presence of a passivating ligand in the case of Ag nucleation caused its low reaction rate.

The nucleation of Ag nanoclusters at the ITIES was followed using in situ spectroelectrochemical techniques and it was found that these nanoclusters absorb and scatter incident light strongly in the visible region of the spectrum.

The behaviour of these clusters at the ITIES was examined using electrochemical techniques. It was shown that metal nanoclusters are capable of undergoing a multiple electron transfer step with an electron donor in the adjacent phase, when a suitable interfacial potential is applied across the interface between two immiscible solutions. The particles act as tiny capacitors capable of giving and receiving electrons. In this sense citrate stabilised colloidal particles may be seen as a suitable substrate for heterogeneous catalysis or electrocatalytic processes. From capacitance measurements, it was determined that specific adsorption of the colloids at the ITIES does not occur. Due to the large distance between the redox centres at the ITIES the charging appears irreversible.